INFORMATION TO USERS

This was produced from a copy of a document sent to us for microfilming. While the most advanced technological means to photograph and reproduce this document have been used, the quality is heavily dependent upon the quality of the material submitted.

The following explanation of techniques is provided to help you understand markings or notations which may appear on this reproduction.

1. The sign or "target" for pages apparently lacking from the document photographed is "Missing Page(s)". If it was possible to obtain the missing page(s) or section, they are spliced into the film along with adjacent pages. This may have necessitated cutting through an image and duplicating adjacent pages to assure you of complete continuity.

2. When an image on the film is obliterated with a round black mark it is an indication that the film inspector noticed either blurred copy because of movement during exposure, or duplicate copy. Unless we meant to delete copyrighted materials that should not have been filmed, you will find a good image of the page in the adjacent frame. If copyrighted materials were deleted you will find a target note listing the pages in the adjacent frame.

3. When a map, drawing or chart, etc., is part of the material being photographed the photographer has followed a definite method in "sectioning" the material. It is customary to begin filming at the upper left hand corner of a large sheet and to continue from left to right in equal sections with small overlaps. If necessary, sectioning is continued again—beginning below the first row and continuing on until complete.

4. For any illustrations that cannot be reproduced satisfactorily by xerography, photographic prints can be purchased at additional cost and tipped into your xerographic copy. Requests can be made to our Dissertations Customer Services Department.

5. Some pages in any document may have indistinct print. In all cases we have filmed the best available copy.

University
Microfilms
International

300 N. ZEEB RD., ANN ARBOR, MI 48106

8203292

JOHNSON, ANTHONY MICHAEL

CARRIER TRANSPORT IN AMORPHOUS SILICON UTILIZING PICOSECOND PHOTOCONDUCTIVITY

City University of New York PH.D. 1981

University Microfilms International 300 N. Zeeb Road, Ann Arbor, MI 48106

Copyright 1981

by

Johnson, Anthony Michael

All Rights Reserved

CARRIER TRANSPORT IN AMORPHOUS SILICON UTILIZING PICOSECOND PHOTOCONDUCTIVITY

By

ANTHONY MICHAEL JOHNSON

A dissertation submitted to the Graduate Faculty in Physics in partial fulfillment of the requirements for the degree of Doctor of Philosophy, The City University of New York.

1981

Copyright by

ANTHONY M. JOHNSON

1981

This manuscript has been read and accepted for the Graduate Faculty in Physics in satisfaction of the dissertation requirement for the degree of Doctor of Philosophy.

9/17/81
Date

Robert R Alfano
Chairman of Examining Committee

9/17/81
Date

Executive Officer

D. H. Auston

H. Z. Cummins

M. Lax

F. H. Pollak

F. W. Smith

Supervisory Committee

The City University of New York

Abstract

Carrier Transport in Amorphous Silicon Utilizing Picosecond Photoconductivity

By

Anthony M. Johnson

Advisors: Dr. David H. Auston
(Bell Laboratories, Murray Hill, NJ 07974)

Prof. Robert R. Alfano
(C.C.N.Y.)

The development of a new, high-speed electronic measurement capability has permitted the direct observation of the transient photoresponse of amorphous silicon (a-Si) with a time resolution of approximately 10ps. We have used this technique to measure the initial mobility of photogenerated (2.1eV) free carriers in three types of a-Si having widely different densities of structural defects (i.e., as prepared by: (1) rf glow discharge (a-Si:H), (2) chemical vapor deposition, and (3) evaporation in ultra-high vacuum). In all three types of a-Si, we find the same initial mobility of approximately 1 cm^2/Vs at room temperature. This result tends to confirm the often-made suggestion that the free carrier mobility is determined by the influence of shallow states associated with the disorder in the random atomic network, and is an intrinsic property of a-Si which is unaffected by the method of preparation. The rate of decay of the photocurrent correlates with the density of structural defects and varies from 4ps to 200ps for the three types of a-Si investigated. The initial mobility of a-Si:H was found to be thermally activated with an activation energy of approximately 58 meV and a preexponential factor of 8 cm^2/Vs consistent with theoretical estimates of the free carrier mobility above the mobility edge. We discuss the possible application of extended state transport controlled by multiple trapping and small polaron formation.

To Adrienne, the Johnsons,

and the Steplights.

ACKNOWLEDGEMENTS

To Dr. David Auston, whose patient instruction, enthusiasm, and personable style stimulated and developed my initial interest in picosecond spectroscopy, I would like to express my deepest appreciation. As my mentor, not only did he offer his knowledge, expertise, and laboratory for use in compiling this thesis, but also the friendship and the warm hospitality of the entire Auston family, and I am forever grateful.

To Professor Robert Alfano, I give very special thanks for serving as my Thesis Advisor and Chairman of the Doctoral Committee. His cooperation and assistance contributed invaluably to the organization, documentation, and presentation of the thesis.

Special thanks to colleague Peter R. Smith for fruitful discussions and expert technical assistance. Special thanks also go to Dr. Shirley Jackson and Dr. Morris Washington for inspiration and moral support.

I would like to acknowledge Bell Laboratories for financing my graduate studies under the Cooperative Research Fellowship Program for Minorities. I am especially thankful to Dr. P. M. Platzman of Dept. 11115, who offered additional financial support and encouragement.

Finally, there are no words to express my appreciation for the love and support of my wife and our family throughout my graduate school experience.

TABLE OF CONTENTS

LIST OF TABLES

LIST OF FIGURES

LIST OF PUBLICATIONS

A. M. Johnson and D. H. Auston, "Microwave Switching by Picosecond Photoconductivity," *IEEE J. Quantum Electron.* **QE-11**, 283 (1975).

D. H. Auston, A. M. Johnson, P. LeFur, C. V. Shank, E. P. Ippen, and O. Teschke, *Digest of IX International Quantum Electronics Conference,* Amsterdam, June 1976.

A. M. Johnson, D. H. Auston, J. P. Harbison, J. C. Bean, D. Kaplan, and P. R. Smith, "Carrier Transport in a-Si Utilizing Picosecond Photoconductivity," *Bull. Am. Phys. Soc.* **25**, 384 (1980).

D. H. Auston, P. R. Smith, A. M. Johnson, W. M. Augustyniak, J. C. Bean, and D. B. Fraser, "Recent Advances in Picosecond Optoelectronics," *Picosecond Phenomena II*, ed. by R. Hochstrasser, W. Kaiser, and C. V. Shank (Springer-Verlag, Berlin), p. 71 (1980).

A. M. Johnson, D. H. Auston, P. R. Smith, J. C. Bean, J. P. Harbison, and D. Kaplan, "Picosecond Photoconductivity in Amorphous Silicon, "*Picosecond Phenomena II*, W. Kaiser, and C. V. Shank (Springer-Verlag, Berlin), p. 285 (1980).

D. H. Auston, A. M. Johnson, P. R. Smith, W. M. Augustyniak, J. C. Bean, J. P. Harbison, and D. Kaplan, "Picosecond Optoelectronics with Amorphous Semiconductors," *Digest of XI International Quantum Electronics Conference*, Boston, p. 605 (June 1980).

D. H. Auston, A. M. Johnson, P. R. Smith, and J. C. Bean, "Picosecond Optoelectronic Detection, Sampling, and Correlation Measurements in Amorphous Semiconductors, "*Appl. Phys. Lett.* **37**, 371 (1980).

P. R. Smith, D. H. Auston, A. M. Johnson, and W. M. Augustyniak, "Picosecond Photoconductivity in Radiation-Damaged Silicon-On-Sapphire Films," *Appl. Phys. Lett.* **38**, 47 (1981).

P. R. Smith, D. H. Auston, and A. M. Johnson, "Thin Film Photoconductor Mounting Schemes for Picosecond Optical Detectors," *Rev. Sci. Instrum.* **52**, 138 (1981).

A. M. Johnson, D. H. Auston, P. R. Smith, and J. P. Harbison, "Temperature-Dependence of the Picosecond Time-Resolved Photoconductivity of a-Si:H," *Bull. Am. Phys. Soc.* **26**, 454 (1981).

A. M. Johnson, D. H. Auston, P. R. Smith, J. C. Bean, J. P. Harbison, and A. C. Adams, "Picosecond Time-Resolved Photoconductivity in Amorphous Silicon," A.I.P. Conference Proceedings, *Tetrahedrally Bonded Amorphous Semiconductors*, ed. by R. A. Street, D. K. Biegelsen, and J. C. Knights (A.I.P. No. 73, N.Y.) p. 248 (1981).

A. M. Johnson, D. H. Auston, P. R. Smith, J. C. Bean, J. P. Harbison, and A. C. Adams, "Picosecond Transient Photocurrents in Amorphous Silicon," *Phys. Rev. B* **23**, 6816 (1981).

A. M. Johnson, "Carrier Transport in Amorphous Silicon Utilizing Picosecond

Photoconductivity," Proceedings of the *VIII Annual Day of Scientific Lectures and Meeting of the National Society of Black Physicists*, ed. by H. B. White, Jr., Fermilab, Batavia, Illinois, May 1981 (to be published).

I. INTRODUCTION

In the last few decades we have seen a revolution in the field of electronics and a tremendous increase in the number of applications of crystalline semiconductors such as silicon (LeComber, 1979). These developments are possible because the electrical conductivity of crystalline silicon (or germanium) can be controlled over many orders of magnitude by the addition, during the growth of the crystal, of small concentrations of impurities. However, there are a number of areas where the expense of preparing these crystals and where the limited size to which they can be grown (at present about 15 cm diameter) have prevented any large-scale applications. For example, crystalline silicon solar cells are widely used in space vehicles for converting sunlight into electrical power, but the economics of their production is such that their use here on earth is relatively limited.

Silicon can be prepared very cheaply in large areas by vacuum evaporation or by sputtering, but the material is then amorphous rather than crystalline (LeComber, 1979). In an amorphous solid the periodic structure of the crystal is replaced by a random network of atoms or molecules. A widely accepted structure of an amorphous solid is a continuous random network (CRN) (Polk, 1971). Figure (1-1) depicts both an ideal (defect-free) CRN and a more realistic structure that includes extrinsic disorder due to the presence of structural defects (dangling bonds, microvoids, etc.) which depends heavily upon the method of preparation. This difference in the atomic arrangement in the crystalline and amorphous phases can influence many of the properties of the material. In particular, all the earlier attempts to control the electrical conductivity of amorphous silicon (a-Si) and amorphous germanium (a-Ge) by doping with impurities, an essential requirement for the majority of device applications, failed because the effect of these impurities was counterbalanced by the disorganized amorphous structure. Recently, it has been shown that if a-Si is prepared by the glow discharge decomposition of silane gas (SiH_4) then its electrical conductivity can be

controlled reproducibly over about ten orders of magnitude by adding small concentrations of phosphine (PH_3) or diborane (B_2H_6) as impurities to the silane (Spear and LeComber, 1975).

From the beginning, the economic advantages of amorphous solids was well recognized (Adler, 1980). However, many speculated that these materials could never perform as specialized electronic devices because of the difficulty in preparing well-characterized, reproducible films, the low carrier mobilities, and the inability to dope the semiconductors. Recent work has shown that most of the problems can be overcome. In addition, amorphous materials have proven to be stronger and less corrosive than the corresponding crystals. Hydrogenated a-Si (a-Si:H) has been utilized to produce p-n junctions (Spear et al., 1976a), 5.5% efficiency Schottky barrier solar cells (Carlson, 1977), photo-receptors for xerography (Shimizu et al., 1980), metal-oxide-semiconductor field-effect transistors (Hayama and Matsumura, 1980) and other devices. Because of its tremendous applied potential, this work has stimulated a lot of additional interest in the amorphous phase. Fundamental to any large-scale applications is an understanding of electrical conductivity in amorphous materials.

It has generally been accepted that in amorphous semiconductors, states lie in bands separated by energy gaps, as in crystals. It has been suggested that the lack of long-range order is responsible for the tailing of the density of states into the gap in contrast to the sharp edges observed in crystals. In an effort to explain some of the differences between the amorphous and crystalline phases, Anderson (1958) has proposed that the spatial randomness of the atomic potential, due to the intrinsic disorder of the lattice, gives rise to states localized to within a few lattice sites - localized states. Anderson uses a tight-binding approximation (interaction between nearest neighbors only), in which a crystalline array of potential wells of depth H produces a narrow band of levels of bandwidth B (Mott and Davis, 1979). Anderson maintains the positions of the atoms in the point lattice, but introduces disorder by the addition of a random potential

$V/2$ to each potential well; and supposes that V takes on all values at random between $\pm V_0$, so that Anderson's theorem says that if the ratio V_0/B is greater than some critical value (that depends on the coordination number), a particle placed at time $t=0$ on a given well will not, at zero temperature, diffuse away. It does not stay on its original well, but the chance as $t \rightarrow \infty$ that it has diffused a distance r decays exponentially as $e^{-\alpha r}$, where α depends on V_0/B. In terms of the solution of the Schrödinger equation, the absence of diffusion means that the states are localized; each eigenstate has a quantized energy value and the envelope falls off exponentially as $e^{-\alpha r}$. In amorphous semiconductors the randomness of the atomic potential introduces a range of localized states at the band tail. The disorder is not large enough to produce an Anderson transition (all the states in the band are localized).

These localized band tail states are generally associated with electronic mobilities in the range $10^{-3} - 10^{-2}$ cm^2/Vs (Fig. (1-2)). The relatively high-mobility valence and conduction band states are called extended states. There is also preparation-dependent extrinsic disorder due to the presence of structural defects (dangling bonds, microvoids, etc.). Amorphous silicon when nominally pure (i.e., ultra-high vacuum evaporated a-Si) is permeated with dangling bonds as evidenced by a detectable electron spin resonance (ESR) signal from about 5×10^{19} spin cm^{-3} (Brodsky, 1979). The electron energy levels of the dangling bonds form states within the energy gap which contribute to optical absorption and electrical conduction processes. There is a large density of gap states which act as fast traps and nonradiative recombination centers, with the result that photoconductivity and photoluminescence is very small in pure a-Si. In Fig. (1-2) E_c and E_v indicate the postulated existence of a sharp transition between extended and localized states called "mobility edges," in which the mobility discontinuously drops two to three orders of magnitude (Mott and Davis, 1979). Above the mobility edges conduction is believed to occur by a diffusive type motion with a mobility in the range 1-10 cm^2/Vs. Below the mobility edge the wave functions are localized and conduction

occurs by thermally activated hopping with a mobility in the range 10^{-3}–10^{-2} cm^2/Vs.

The relaxation of non-equilibrium carriers in amorphous semiconductors spans a time scale which extends from picoseconds to seconds and involves many different processes including thermalization, capture and emission by localized states, and recombination. The early time history is especially interesting since it relates more closely to the transport properties of the extended and localized states associated with the intrinsic disorder of the random atomic network, whereas the slower events tend to be influenced by the deeper states associated with structural defects and depend on the method of preparation. It is especially important to have more detailed information about the magnitude and temperature dependence of the mobility of carriers in extended states and to determine the magnitude and energy distribution of the shallow localized states.

In order to obtain an estimate of the time resolution required to investigate the initial capture of photoexcited free carriers by the distribution of localized states in the gap we utilize a widely used expression for the capture rate (by traps) in crystals:

$$\tau^{-1} = N_t \langle v \rangle \sigma$$

where N_t is the trap density, $\langle v \rangle$ is an average electronic thermal velocity, and σ is the capture cross-section. We will utilize a trap density equal to the dangling bond density given above for nominally pure a-Si ($N_t \sim 5 \times 10^{19}$ cm^{-3}) and a thermal velocity $((3kT/m)^{1/2})$ $\langle v \rangle \sim 10^7$ cm/s. For a state whose electronic wavefunction is localized to a few angstroms ($\sim$ lattice constant) a reasonable order of magnitude capture cross-section would be a few square angstroms -- $\sigma \sim 10^{-15}$ cm^2. This is a reasonable cross-section for a neutral center (Lax, 1959, 1960). The result is a capture time of approximately $\tau \sim$ 2ps. This order of magnitude calculation indicates that *direct* measurements of free carrier transport in amorphous semiconductors requires picosecond time resolution.

The use of time-resolved photoconductivity to measure trap-free microscopic mobilities was first demonstrated by Smith and Rose (1955) who were able to directly time resolve the initial photocurrent of free carriers in single-crystal CdS prior to their capture at defect sites. In amorphous semiconductors, this approach allows the direct observation of electronic transport near the mobility edge. The high-defect density of these materials, however, requires exacting time resolution in the subnanosecond to picosecond range. Consequently, most transient photoconductivity measurements thus far reported measure a mobility-relaxation time product, $\mu\tau$ and fail to individually resolve μ and τ (Loveland et al., 1973; Spear et al., 1974). Although time-of-flight measurements provide direct mobility information, these experiments measure a trap-limited mobility whose interpretation is complicated by the dispersive nature of the transport (LeComber and Spear, 1970; LeComber et al., 1972). An exception is the recent experiment by Tiedje et al., (1980), who observed non-dispersive, high-mobility (0.8 cm^2/Vs) transport in certain plasma deposited a-Si:H samples. From the temperature dependence of the trap-limited mobility and an estimate of the densities of extended and localized states, LeComber and Spear (1970) and LeComber et al. (1972) were able to extrapolate their time-of-flight measurements (0.003-0.1 cm^2/Vs) to estimate an extended state mobility in the range of 1-10 cm^2/Vs, a result that has been the most frequently cited evidence for a mobility edge.

Recently, we have developed a measurement technique which enables us to directly observe transient photocurrents with a time resolution of approximately 10ps (Auston et al., 1980b,c,d). Three different types of a-Si, prepared by rf glow discharge (a-Si:H), chemical vapor deposition, and ultra-high vacuum evaporation, were found to have the same initial mobility of ~1 cm^2/Vs at room temperature and different carrier relaxation times ranging from 200 to 4ps. (Auston, et al., 1980a,d; Johnson et al., 1980a,b). The initial mobility of a-Si:H is thermally activated with an activation energy of approximately 58meV and a preexponential factor of 8 cm^2/Vs (Johnson et al.,

1981a,b,c). These results give strong support to the existence of a mode of conduction in extended states which is an intrinsic property of a-Si.

The major differences and similarities in the structure of amorphous and crystalline silicon is discussed in Chapter II. We were also interested in some of the structural properties that are intrinsic to the various forms of a-Si. The second section of this chapter is concerned with the major aspects of electronic conduction in the presence of disorder.

In Chapter III, we have a description of the methods of preparation utilized in the three forms of a-Si studied. We also describe the photodetector geometry and measurement technique required to investigate picosecond photocurrent transients. In order to produce these electrical transients a picosecond optical source is required -- a synchronously mode-locked cw Rh 6G dye laser.

Chapter IV contains the results of picosecond photoconductivity experiments, performed at room temperature, on the three forms of a-Si. In addition, the temperature dependence of the photoconductivity in a-Si:H was investigated.

Chapter V discusses the possible application of several models of electronic transport in disordered semiconductors, with emphasis upon extended state transport controlled by multiple trapping.

Chapter VI summarizes the major conclusions drawn from the thesis and discusses some possibilities for future research.

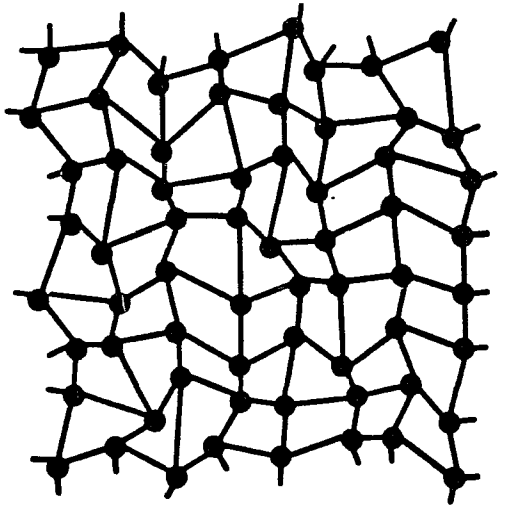

AMORPHOUS SOLID
(IDEAL CRN)

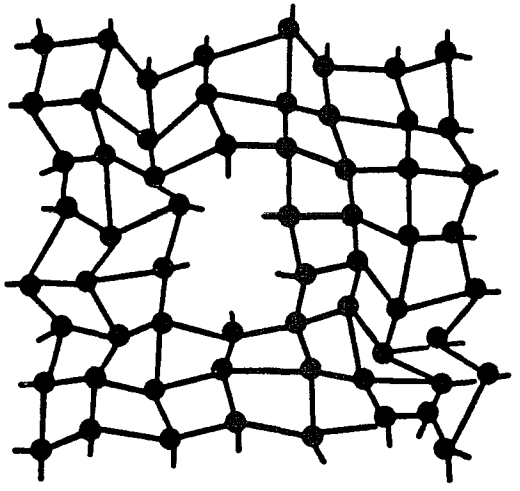

AMORPHOUS SOLID WITH
STRUCTURAL DEFECTS

Fig. (1-1): Continuous Random Network

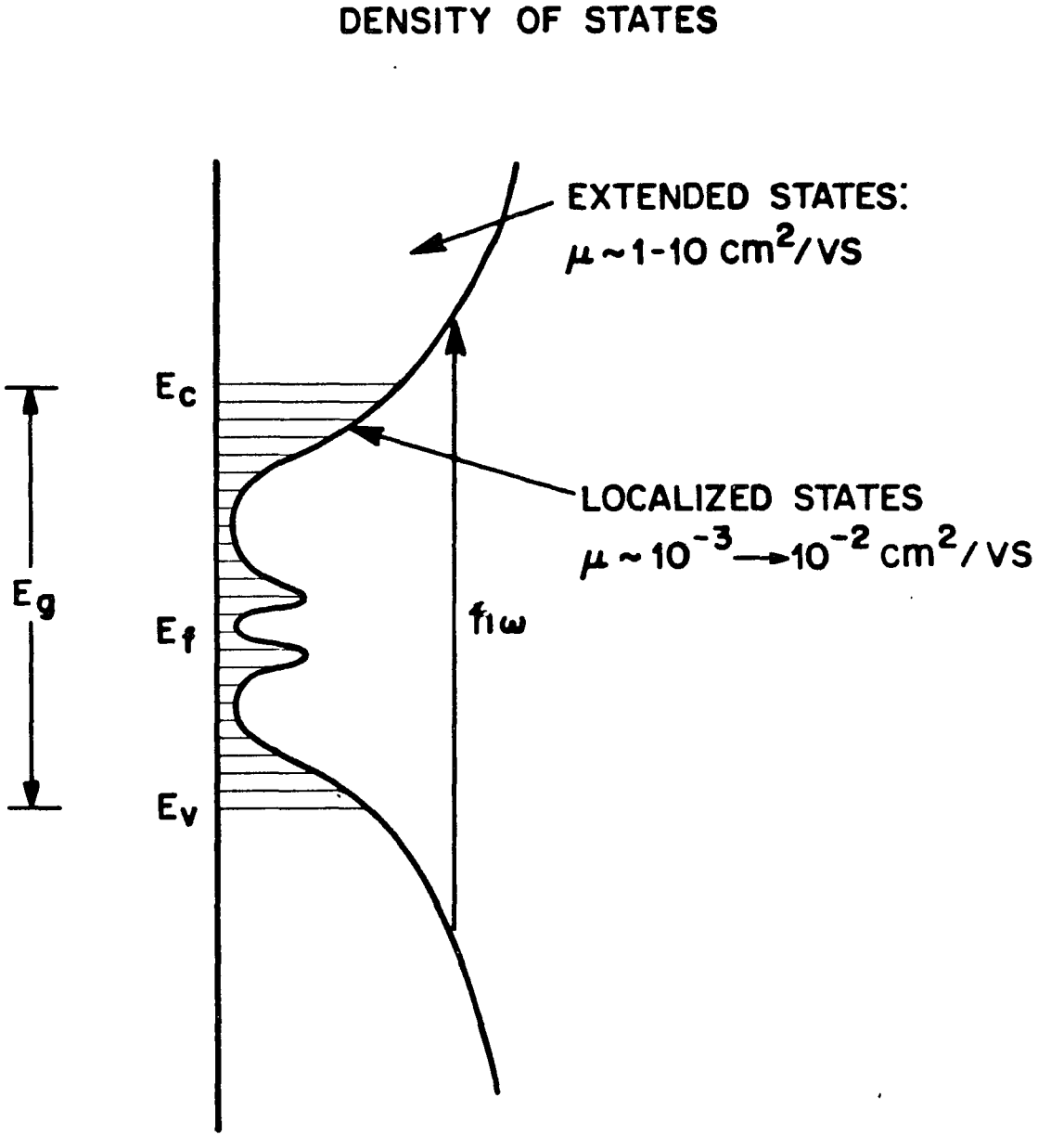

Fig. (1-2): Density of States of an Amorphous Semiconductor

II. AMORPHOUS SILICON

This chapter is a brief synopsis of the consensus of thought on the nature of the salient properties of amorphous silicon ($a-Si$).

2.1 Structure

In describing the amorphous state it is customary to explain what it isn't as opposed to specifying precisely what it is (Brodsky, 1979). A crystal is defined as a substance consisting of atoms arranged in a pattern that repeats periodically in three dimensions. Amorphous semiconductors are noncrystalline. They lack long-range periodic ordering of their constituent atoms. The diffraction pattern of an amorphous solid consists of diffuse rings or halos rather than the sharp Bragg rings and spots characteristic of polycrystalline and single crystal solids, respectively.

There are "positive" definitions of disorder. Cellular disorder is found in substitutional alloys and mixed crystals, where a crystal lattice is still present but we can no longer say with precision which type of atom is to be found on each lattice site [Yonezawa and Cohen, 1981]. In structural disorder, found in liquid and amorphous metals, 'no ghost of a crystal lattice' remains. The positions of atoms are no longer regular in these systems.

Amorphous silicon cannot be prepared by the rapid cooling (quenching) of the melt (glasses). In the case of the tetrahedrally bonded semiconductors, this generally results in polycrystallinity. Amorphous silicon is usually produced in the form of a thin film by an atomic deposition procedure such as evaporation, sputtering, chemical vapor deposition, plasma decomposition of gases, or electroplating. Ion bombardment of crystalline silicon ($c-Si$) can also result in producing $a-Si$. The emphasis of this thesis is on three of the above methods of preparation: ultra-high vacuum evaporated $a-Si$ (EV), chemical vapor deposition (CVD), and rf plasma decomposition of siliane (SiH_4) or rf glow discharge deposited $a-Si:H$ (GD).

X-ray, neutron, and electron diffraction are the structural probes of choice for most solids (Lucovsky and Hayes, 1979). In a single crystal they yield the equilibrium positions of the atoms as well as the averaged distributions about those sites. This precise information is reduced substantially in a liquid or amorphous solid. The disorder eliminates all of the angular information, leaving only the radial distribution function (RDF). The RDF is a one-dimensional description of the short-range order which yields the atom density as a function of the distance from an arbitrarily chosen atom (Grigorovici, 1974). Peaks in the RDF indicate by their position and area the radius of and the number of atoms in a given coordination sphere.

The RDF of evaporated *a—Si* and *c—Si* were determined from the analysis of electron diffraction data (Moss and Graczyk, 1970). From the RDF it is clear that the short-range order of the two phases is very similar. The position of the first peak, which gives the nearest neighbor separation, is the same within a few percent in both phases. The area under the first peak indicates that the coordination number is four in both *c—Si* and *a—Si*. The averaged position of the second neighbors is essentially the same except that the increased width in the peak of the *a—Si* reflects bond-angle distortions of approximately $\pm$ 10°. The virtual disappearance of the third peak in *a—Si* indicates the spread in third-neighbor separations resulting from the bond-angle distribution.

The generally accepted structural model for *a—Si* is the continuous random network (CRN) due to Polk (1971). In this model the amorphous solid is supposed to consist of an infinite, non-periodical, three-dimensional array of interlinked atoms in which the short-range order about each atom is imposed by the same characteristics of the chemical bond as in the crystal. Each atom has four immediate neighbors arranged in a tetrahedral geometry. Bond angle deviations are allowed, so that the tetrahedra are generally distorted from an idealized geometry. The random character of the network results from a statistical distribution of dihedral angles. (The relative orientation of

triads of bonds emanating from two nearest neighbors is known as the dihedral angle (Mott and Davis, 1979)). This CRN model represents the structure of "ideal" *a—Si* which is free of voids, impurities, and other defects, and contains no unsatisfied bonds.

Films of *a—Si* and *a—Ge* have densities ranging from 3-15 percent below that of the crystals (Mott and Davis, 1979). CRN models are normally associated with density deficits of 1-3 per cent. Taken in conjunction with the bond length and the coordination number deduced from the RDF, measurements of the density of films can provide information about the presence of voids in the structure. Small-angle scattering of electrons or X-rays estimate that spherical voids ranging in diameter from 3-250 angstroms can be detected.

There is strong evidence that evaporated layers of *a—Ge* or *a—Si* contain an internal network of microvoids (Fritzsche and Tsai, 1979). Direct evidence was found in evaporated *a—Ge* by transmission electron microscopy and porosity measurements. Recent porosity measurements by Fritzsche and Tsai (1979) reveal that when *a—Si* films, deposited by electron beam evaporation, are exposed to the atmosphere they absorb a considerable amount of water which cannot be removed by drying. Complimentary measurements by Bean and Poate (1980a) report on a series of epitaxial crystallization experiments which indicate that UHV-evaporated *a—Si* absorbs ambient gases at room temperature and atmospheric pressure. Indirect evidence suggests that gases penetrate to depths greater than 1000 Å. In contrast, *a—Si:H* films prepared by sputtering in a gas mixture of *Ar* and H_2 or by *rf* plasma decomposition of SiH_4 are impervious to moisture. These results agree with the electron-micrograph studies of Barna et al. (1977) who observed a coarse surface texture on evaporated films and a very smooth surface on plasma deposited films.

There is experimental information that supports a model of *a—Si* which is independent of sample preparation. Barna et al. (1977) noted that in spite of the drastic structural difference revealed by phase contrast electron microscopy, the RDF's

(from electron diffraction) of both evaporated *a—Si* and *a—Si:H* were rather similar. There was an apparent difference near the third coordination distance of the crystal, from which they concluded that the degree of local order was higher in *a—Si:H*. D'Antonio and Konnert (1979), in a study of small-angle X-ray scattering (SAXS), reported that *a—Si:H* produced a large amount of small-angle scattering very similar to that observed in evaporated *a—Si*. This implied that the samples produced from glow discharge of silane contain a distribution of voids or holes containing an undetermined amount of hydrogen similar to that found in evaporated samples. Postol et al. (1980) made an extensive structural study of *a—Si* (sputtered) and of hydrogenated and deuterated *a—Si* (reactive sputtering), using neutron scattering. They observed very intense small-angle scattering indicative of the existence of large voids. A comparison of both small- and large-angle scattering from pure *a—Si* with hydrogenated and deuterated *a—Si* indicated that the microscopic structure of the silicon was not modified by the incorporation of large amounts (14%) of hydrogen or deuterium. Thus RDF, SAXS, and neutron scattering studies suggest that the intrinsic structures of pure *a—Si* (i.e. EV) and *a—Si:H* (i.e. GD) are similar.

A recent model by Phillips (1979; 1980) suggests that infinite continuous covalent networks are strain-free only for an average coordination number of $\bar{N}_{cn} \lesssim 6^{1/2}$, and with $N_{cn} = 4$ (a-Si) in order to be strain-free such a network would have to be embedded in an $N_d = 8$ (eight-dimensional) space. Thus the strain-energy in a-Si is very large and Phillips (1979; 1980) invokes a model of strain-relieving clusters connected by bridges. Transmission (TEM) and scanning (SEM) electron microscopy have shown that deposition proceeds via nucleation and growth of island structures, imperfect coalescence of which results in interstitial regions of low density whose presence has been correlated with the observation of electronically active defects (Knights, 1980). Within the range of thickness accessible to TEM, the island dimensions do not change substantially suggesting columnar or rod-like growth with

diameters ~ 100Å. This suggestion has been confirmed directly by Leadbetter et al. (1980) using small angle X-ray and neutron scattering. This situation can be visualized initially in the absence of hydrogen as being the coalescence of a series of continuous random network structures of diameter ~ 100Å (Knights, 1980). This will on an average create partly bridged interfaces with large numbers (~ 50%) of dangling and strained bonds. Hydrogenation of these interfaces will result in the removal of the dangling bonds and probably scission of some of the more strained bonds but will still leave stress in the structure and an inhomogeneous distribution of both defects and hydrogen. It is important to recognize that this behavior can lead naturally to, (1) a higher average density of hydrogen than required to satisfy dangling bonds by a single random network structure, and (2) a non-unique relationship between hydrogen content and defect densities, biased in favor of lower hydrogen content in the least defective material.

2.2 Electronic Transport

Ioffe and Regel (1960) stated the empirical rule that a molten or amorphous semiconductor retains its semiconducting properties in spite of the destruction of the long-range order if the non-crystalline phase conserves the short-range order present in the related semiconducting crystal. The short range order was characterized by the number of atoms in and the radius of the first coordination sphere. There is at present not a single exception to this rule (Grigorovici, 1974).

In crystalline materials each electron is described by a Bloch wave function. In non-crystalline materials the wave functions do not necessarily have this form (Mott and Davis, 1979). Nevertheless, solutions of the Schrodinger equation must exist, and therefore a concept that can be carried over from the theory of crystals to the theory of non-crystalline materials is the density of states. The density of states can in principle be determined experimentally, for instance by photoemission. In general, the available evidence suggests that the form of the density of states in a liquid or non-crystalline material does not differ greatly from the corresponding form in the crystal, except that the finer features may be smeared out, and some localized states may appear in the forbidden energy range in semiconductors.

In defining a localized state it is appropriate to define what is meant by an extended or delocalized state. In the free particle case the eigenstates are extended in the sense that the particle can be found anywhere in space with equal probability (Economou et al., 1974). In the periodic case the particle can also be found in any unit cell with equal probability. Finally, in the more general case of disordered systems we call a wave function extended if there are paths extending to infinity in both directions lying entirely in regions where the wave function is not negligible. Thus, in an extended state, an electron can travel through the system from one end to the other and consequently make a non-zero contribution to the conductivity of the system.

There is nothing unfamiliar about the concept of localized states; they are simply 'traps,' and the most direct evidence for their existence in amorphous materials is provided by measurements of the transit time for injected carriers; if this shows an activation energy, a trap-limited mobility can be inferred (Mott and Davis, 1979). By a localized state, we mean one with probability amplitude decreasing exponentially with distance from the center of localization for sufficiently large distance (Cohen et al., 1969).

In the absence of long-range order, i.e., without the translational symmetry of the lattice, $\vec{k}$ is not a good quantum number any more; one cannot define an energy band structure $E(\vec{k})$ as in the crystalline case and the momentum conservation selection rule, for optical transitions, has to be relaxed (Theye, 1976). It is not difficult to see why the energy band theory, which has been so successful in elucidating the properties of high-mobility semiconductors fails when the mobility is less than about $1 cm^2/Vs$ (Smith, 1978). If we use the relationship $\mu = e\tau/m_e$, which does not depend on crystal structure or band theory, we find that if we take m_e equal to the electron mass and $\mu = 1\ cm^2/Vs$ then $\tau = 5.7\times10^{-16}s$. Since there will be an uncertainty in the electron's state in a time of order τ, we can express the uncertainty δE in energy through the Uncertainty Principle as $\delta E\tau \sim \hbar$. Inserting the value of τ we find that $\delta E \sim 1.2eV$. An uncertainty of energy of this amount makes band structure meaningless. Ioffe and Regel drew particular attention to the fact that band structure theory based on Bloch waves is inapplicable when the mobility is less than $10 cm^2/Vs$ and not likely to be very good if it falls below $100 cm^2/Vs$.

In amorphous semiconductors, the atomic potential is strong enough that even slight distortions of the nearest neighbor bond length and bond angle distributions, within otherwise identical molecular units, lead to strong electronic scattering and a short coherence length of the wave functions (Connell, 1979). Indeed the coherence length is of the order of the lattice spacing and the resulting uncertainty in the wave vector is

of the order of the wave vector itself (i.e. $\Delta k/k \sim 1$). Under these circumstances, the momentum selection rule breaks down in optical transitions, creating perhaps the single most important difference between the responses of the crystalline and amorphous phases.

Studies of optical absorption and electrical conduction have revealed much about the nature of amorphous semiconductors (Fritzsche, 1971). The transparency in the infrared indicates the existence of a gap between valence and conduction bands. The temperature dependence of the electrical conductivity seems to support this picture: the conductivity increases exponentially with temperature as

$$\sigma = \sigma_o \exp(-\Delta E/kT) \tag{2.2-1}$$

similar to the behavior of intrinsic semiconductors. The magnitude of ΔE is roughly one-half of the optical gap. This behavior seems to be in accord with the general rule of Ioffe and Regel, that is it is the short-range order of a material which determines whether it is metallic, semiconducting, or insulating. When there is no long-range order the structure in the optical spectra characteristic of the translational symmetry of the crystal are absent. Furthermore, the band edges cease to be well defined and one expects the densities of states to tail into the gap, since the gap is a forbidden gap only when there is perfect order.

In disordered materials localized states are associated with fluctuations in atomic configuration always present in such materials (Economou et al., 1974). Within a region in which the configuration differs from an average or typical configuration, so does the potential acting on the electron differ from its average or typical set of values. When the fluctuation is strong enough, or large enough in spatial extent, the associated potential change can bind, or localizes, one or more states. The associated energy levels depend on the details of the fluctuation, and the density of states can be determined from the probability distribution of fluctuations: The states furthest from the center of the band are associated with the widest or deepest, and thus least likely

fluctuations. The result is a band tail.

A simple model for the density of states, due to Mott (1967), uses a perfect crystal possessing a single isolated band as the starting point, and introduces randomness continuously through some disordering process (Economou et al., 1974). A sketch of the density of states is displayed in Fig. (2.2-1). As the randomness increases, the band becomes broader and the nature of the wave functions changes. For $E_c < E < E_c'$, the states remain extended with a finite phase coherence length. At the energies E_c, E_c' the character of the states is assumed to change abruptly from extended to localized so that for $E < E_c$ and $E_c' < E$ there are tails of localized states. For the states in the middle of the band, the long-range phase order is lost, but the states remain extended. Localized and extended states cannot belong to the same energy except accidentally; any infinitesimally small perturbation would mix the two states, transforming both of them to extended. There should therefore be two characteristic energies E_c, E_c' separating the regions of localized states from that of extended states. Such energies E_c, E_c' are called mobility edges. As the randomness increases, more and more localized states are created, and the mobility edges E_c, E_c' move inward into the band. At the same time, the mean free paths of the extended states are reduced. When the randomness reaches a certain critical value, the two mobility edges merge, and, for any randomness greater than this critical one, all the states in the band are localized. This is the Anderson (1958) transition.

As to the nature of the disorder which produces mobility edges it is supposed that it is *intrinsic*, i.e. arising from the presence of short-range disorder rather than from random fields due to point defects (*extrinsic*) (Mott and Davis, 1979). For elements such as *Si* local variations in bond angle are likely to be the principal source, but in some materials a spread in bond lengths or alternatively a variation in density or composition over distances of a few bond lengths may contribute. It is generally considered that any form of disorder will lead to a range of *intrinsic* localized states at

the band edges. The conjecture that they exist goes back a long way (Frohlich, 1947), and they are indeed little different from the electron or hole traps found in many crystalline semiconductors. What is new for amorphous semiconductors are the concepts of a continuous range or band of *intrinsic* localized states and of charge transport by activated hopping between them.

Figure (2.2-2) illustrates the major differences in the structure of the density of states of crystalline and amorphous semiconductors (Le Comber, 1979). In crystalline semiconductors $g(\epsilon)$ is finite in the allowed energy bands and, in the absence of impurities and crystalline defects, zero in the forbidden energy ranges (Fig. 2.2-2(a)). Although the details may vary, the form of $g(\epsilon)$ shown in Fig. (2.2-2 (b)) is believed typical of elemental amorphous solids such as $a-Si$ and $a-Ge$. Above ϵ_C and below ϵ_V the electron wave functions extend throughout the material so that these states, denoted by E, are extended states. The states between ϵ_C and ϵ_V shown shaded in the figure, are localized states. Those marked T between ϵ_C and ϵ_A and between ϵ_B and ϵ_V are thought to arise because of the lack of long-range order and are called tail states. The states denoted by D arise from defects in the material and the density of these depends critically on the method used to prepare the amorphous film.

The electron density at a particular energy can be written in terms of the density of states at that energy and the Fermi-Dirac probability $f(\epsilon)$ of those states being occupied:

$$n(\epsilon) = g(\epsilon)\, f(\epsilon) \tag{2.2-2}$$

where

$$f(\epsilon) = \left[1 + \exp(\epsilon - \epsilon_F)/kT\right]^{-1} \tag{2.2-3}$$

and ϵ_F is the Fermi energy. Provided we restrict ourselves to energies more than a few kT away from ϵ_F, we can use Boltzmann statistics to describe the occupancy of states, so that $n(\epsilon)$ becomes

$$n(\epsilon) = g(\epsilon)\ \exp[-(\epsilon-\epsilon_F)/kT] \qquad (2.2\text{-}4)$$

In materials with mobilities of the order $1-10\ cm^2/Vs$, the mean free path is comparable to a lattice constant - the Boltzmann equation is no longer suited to the description of transport properties (Madelung, 1978). The generalized expression for the conductivity is the Kubo-Greenwood formula, from which the Boltzmann equation can be derived in the limit of long mean-free path. When the states involved in the conductivity are several kT above the Fermi energy, the Kubo-Greenwood formula takes the form

$$\sigma = \int e\,\mu(\epsilon)\ n(\epsilon)\ d\epsilon\ .$$

The contribution to the conductivity from the electrons at any particular energy is given by:

$$\sigma(\epsilon) = e\,\mu(\epsilon) n(\epsilon)$$

$$\sigma(\epsilon) = e\,\mu(\epsilon) g(\epsilon)\ \exp[-(\epsilon-\epsilon_F)/kT] \qquad (2.2\text{-}5)$$

A similar expression can be written for the hole contribution, but we shall restrict the discussion to electrons. In a pure crystal, $g(\epsilon)$ is zero within the energy gap (Fig. 2.2-2 (a)) so that $\sigma(\epsilon)$ will also be zero in this energy range. In the amorphous case $g(\epsilon)$ is finite throughout the whole energy range shown in Fig. (2.2-2 (b)) so that we can expect contributions to the conductivity from each of these energies. From Eqn. (2.2-5) it is clear that the details of the mobility in the various energy ranges is as important as the density of states and the occupancy of those states in determining the magnitude of the conductivity.

At energies well into the conduction band, i.e. $\epsilon \gg \epsilon_C$, electrons are thought to propagate more or less freely between occasional scatterings (Brenig, 1974). The conductivity is believed to obey the well known relation

$$\sigma = ne^2\tau/m \qquad (2.2\text{-}5)$$

Band conduction with long mean free path will occur and the normal formula for the

mobility

$$\mu = e\tau/m \tag{2.2-6}$$

can be used (Davis and Shaw, 1970). As long as the mean-free path is large compared with the lattice constant, the Boltzmann equation formalism can be used (Madelung, 1978). The mobility is expected to be similar to that in the crystal, but because of the small probability of the states being occupied they do not make any significant contribution to σ (Le Comber, 1979).

As we decrease ϵ and approach ϵ_C, the disorder in the lattice increases the scattering more and more, until just above ϵ_C the mean free path between scattering events has decreased from its crystalline value (of several hundred atomic distances) to a value of the order of the interatomic spacing (Le Comber, 1979). Under these conditions the electron transport may no longer be considered as band motion with occasional scattering, as in crystalline theory. In this case, Cohen (1970) suggests that charge transport proceeds via diffusion or Brownian motion (Fritzsche, 1974). Adopting this classical picture for estimating the mobility one considers fast jumps between neighboring sites and obtains

$$\mu_C = \frac{1}{6}\frac{ea^2}{kT}\nu_{el} \tag{2.2-7}$$

where the interatomic spacing is a and the jump frequency $\nu_{el} \sim 10^{15}s^{-1}$ is an electronic hopping frequency associated with the electronic transfer integral between nearest neighbors $J = h\nu$. A more detailed analysis of this problem is based on the random phase model which assumes that the extended state wave functions can be represented as a linear combination of atomic wave functions with coefficients which have no phase relation from one site to the next. The conductivity was calculated by Mott (1967, 1970), Hindley (1970) and Friedman (1971). The mobility in the extended states near ϵ_C or ϵ_V is according to Friedman:

$$\mu_C = \frac{2\pi}{3} \frac{ea^2}{\hbar} z \frac{J}{kT} a^3 J g(\epsilon_c) \tag{2.2-8}$$

where z is the coordination number and J is the two site transfer integral ($J \sim 1eV$). With a=2.5Å, $z = 4$, $g(\epsilon_C) = 10^{21} cm^{-3} eV^{-1}$, and T=300°K Eqn. (2.2-8) yields $\mu_C \sim 5cm^2/Vs$. Cohen's classical expression (Eqn. 2.2-7) yields $\mu_C \sim 4cm^2/Vs$ ($\nu_{el} \sim 10^{15} s^{-1}$).

The region between ϵ_C and ϵ_V, i.e. the tail states T and the defect states D in Fig. (2.2-2 (b)), are localized and they can contribute to transport only with the assistance of phonons (Le Comber, 1979, Nagels, 1979; Adler 1980). This type of transport is ordinarily called hopping conduction, to distinguish it from the band-like propagation of free carriers in extend states. Below the mobility edge, the localized electronic states do not overlap sufficiently for band-like propagation. Instead, an electron above ϵ_F typically needs an additional energy to reach a neighboring empty state, and this energy can be obtained only from the thermal vibrations of the atoms around their equilibrium positions. If the nearest-neighboring localized states are an average distance R apart at the energy of the electron but are separated by an average energy W, then the probability of hopping must be proportional to the product of the overlap of the electronic wave functions on nearest-neighboring sites, (i.e., tunnelling)

$$\exp(-2\alpha R),$$

and the probability of finding a phonon with an excitation energy equal to W, given by a Boltzmann expression,

$$\exp(-W/kT).$$

The expression for the hopping mobility is of the Miller and Abrahams (1960) form for impurity conduction at low temperatures in semiconductors:

$$\mu_H = \frac{1}{6} \frac{eR^2}{kT} \nu_{ph} \exp(-2\alpha R)\exp(-W/kT) \tag{2.2-9}$$

where R is the jumping distance, which at high temperatures equals the interatomic

spacing (a), α is a quantity which is representative of the rate of fall-off of the wave function at a site, and ν_{ph} is an attempt frequency which is on the order of a phonon frequency ($\sim 10^{12}s^{-1}$). For a plausible choice of parameters one finds that

$$\mu_H \lesssim 10^{-2}\text{–}10^{-3}cm^2/Vs.$$

Mott (1969) points out that, as the temperature is lowered the number and energy of phonons decrease, and the more energetic phonon-assisted hops will progressively become less favorable. Carriers will tend to hop to larger distances in order to find sites which lie energetically closer than the nearest neighbors. This mechanism is the so-called variable range hopping. The factor $\exp(-2\alpha R - W/kT)$ in Eqn. (2.2-9) will not have its maximum value for the nearest neighbors. Mott's treatment of variable range hopping leads to a temperature dependence for the conductivity of the form

$$\sigma(\epsilon_F) = \frac{1}{6} e^2 R^2 \nu_{ph}\, g(\epsilon_F) \exp(-A/T^{1/4})$$

or

$$\sigma(\epsilon_F) = \sigma_o exp[-(T_o/T)^{1/4}] \qquad (2.2\text{-}10)$$

where σ_o and T_o are constants. When Eqn. (2.2-10) is obeyed, a log σ vs. T^{-1} plot is concave upward, but a log σ vs. $T^{-1/4}$ plot should be linear.

Thus there is an abrupt change in the value of the mobility, by approximately three orders of magnitude, as we pass through the energies ϵ_C and ϵ_V - the mobility edge. This mobility edge is depicted in Fig. (2.2-2 (c)). In an amorphous semiconductor we have a mobility gap, defined by $\epsilon_C - \epsilon_V$, rather than the forbidden energy gap ϵ_g in the crystalline density of states (Fig. 2.2-2 (a)).

The transport properties of amorphous semiconductors are dominated by carriers within kT of the transition energy ϵ_C where the states are uniquely characteristic of disordered materials (Economou et al., 1974). Thus, the localized states in the band tails and the deeper states make a very substantial contribution to electronic conduction

processes in amorphous semiconductors.

Another type of electronic transport can possibly occur by the formation of small-polarons (Emin, 1976). To define what is meant by a polaron, consider the two-dimensional array of atoms illustrated in Fig. (2.2-3a). As schematically depicted in Fig. (2.2-3b), if a stationary electron is added to this system the atoms will generally be displaced in response to its presence. These atomic displacements will be such as to produce an additional potential well for the added electron. If this carrier - induced potential well is sufficiently deep, the carrier may occupy a bound state, being unable to move without an alteration of the positions of the surrounding atoms. The unit comprising the bound carrier and its induced lattice deformation is termed a polaron. Alternatively, since the potential well results from the carrier it is often referred to as being "self-trapped." In addition, the adjective "small" in the term small-polaron indicates that the "self-trapped" carrier is essentially confined to a "small region" which is typically associated with a single atomic site.

The energetic situation which prevails in the case of an excess electron forming a small-polaron follows the usual procedure of assuming that the energy of the electron is a linear function of the displacements of the atoms from their equilibrium positions (Emin, 1976). One finds that as a result of a carrier displacing the atoms surrounding it, its energy is reduced by an amount $2E_b$ while the strain energy of the lattice associated with producing this distortion is increased by an amount E_b. This yields a net reduction of the energy of the system comprising a stationary electron and a deformed lattice, relative to that of a stationary electron in an undeformed lattice, by an amount E_b; this energy is termed the small-polaron binding energy. Furthermore, since the small-polaron may equally well reside on any one of the geometrically equivalent sites in the crystal, we may expect the formation of a small-polaron band analogous to an electronic band of a rigid lattice (Fig. (2.2-4)). In a crystal the small-polaron band is usually extremely narrow, its width being very small compared with

even vibrational energies. This is because the motion of the carrier requires the concomitant transport of both an electron and its associated atomic displacement pattern.

There are essentially two models of the intrinsic equilibrium states of an amorphous semiconductor (Emin, 1980a). The rigid (non polaronic) model envisions the disorder simply as introducing a fractionally small number of localized states at the band edges while leaving states in the bulk of the band extended. In this picture the mobility edge plays the role of the band edge in a crystalline semiconductor, with high mobilities being ascribed to charge transport in the extended states. On the other hand, the small-polaron model views charge carriers as relaxing into "self-trapped" states which lie within the absorption gap. Small-polaron motion in disordered solids is always described as phonon-assisted hopping motion (Emin, 1973). Thus charge transport is characterized in terms of hopping motion with rather low mobilities which increase with increasing temperature.

When the small-polaron state exists, an energy barrier also exists which separates it from the nonpolaronic solution (Emin, 1980a). Surmounting or tunneling through this barrier corresponds to the atoms classically or quantum mechanically undergoing rearrangements that correspond to the change of state. The height of this barrier tends to diminish with an increase in the strength of the electron-lattice interaction. Furthermore, if the particle experiences an additional potential (associated with defects or disorder) which tends to confine it, the barrier may be reduced or eliminated. The presence of a significant barrier manifests itself in a time delay for small-polaron formation. For an injected carrier to form a small-polaron, the atoms of the material must assume an appropriate displacement pattern. In the absence of a barrier, the requisite time is of the order of a vibrational period ($\sim 10^{-12} s$). However, when a barrier is present, the time interval can be very much longer. In such instances the delay time associated with atomic rearrangements decreases with increasing

temperature. While there is limited information about the delay time for small-polaron formation in amorphous semiconductors, the available evidence suggests that it is near the (minimal) time of a picosecond in $a-SiO_2$ (Hughs and Emin, 1978) and chalcogenide glasses (Emin, 1980b).

Typically the electron-lattice interaction is sufficiently large so that severely localized states (radii $\sim$ lattice constant) are accompanied by substantial lattice deformations; they form localized small-polarons (Emin, 1976). However, for localized states of rather large radii the effect of the electron-lattice interaction may be sufficiently small so as to justify adopting a rigid-atom approach to studies of the ground-state of these systems. The large-radii ($\sim 10^2$ Å) shallow dopants in silicon and germanium are examples of this circumstance. Thus, as a carrier finds itself increasingly confined, the likelihood of its ground-state being small-polaronic is enhanced. Since the presence of disorder acts to impede the motion of a carrier through a noncrystalline semiconductor both by creating regions in which an electron is confined (localized) and by reducing the rate that characterizes the real intersite motion of a particle, it is reasonable to anticipate that at least some of the states which a carrier can occupy will be small-polaronic.

Figure (2.2-5) illustrates some of the ramifications of rigid-atom and small-polaronic states in a disordered solid (Emin, 1976). Figure (2.2-5a) is a hypothetical rigid-atom density of states consisting of a conduction band, band-tail states, and a set of defect levels for a noncrystalline solid. Permitting the atoms to adjust to the presence of a charge carrier, making the system deformable, may yield one of the two stable-state situations illustrated in Figs. (2.2-5b) and (2.2-5c). With a finite electron-lattice interaction both the band-tail states and the defect states of the rigid-atom model (Fig. 2.2-5a) are energetically unstable with respect to small-polaron formation in Fig. (2.2-5b). Instead, these unstable rigid atom states result in lower-lying small-polaron counterparts. The energy spread of the polaronic levels is assumed to be relatively

narrow, consistent with the assumption of the presence of substantial short-range order. In Fig. (2.2-5c) all of the rigid-atom states are unstable with respect to small-polaron formation. In this case the narrow band of small-polaron states is associated with a very high density of states. Small-polaron formation may be an important aspect of electronic transport in a-Si.

Though the elemental and compound amorphous semiconductors are translationally disordered, the short-range order is in general so well defined that structural defects can occur (Cohen, 1970). Examples would be broken bonds in a covalently bonded network, vacancies, nonbridging atoms, chain ends, etc. Being structurally well defined, these defects can be expected to have well defined energy levels associated with them. These would not be sharp as in a crystal, but varying somewhat with local environment would give rise to peaks in the density of states.

A very large amount of data has been accumulated on group-IV tetrahedrally coordinated amorphous semiconductors since the first discovery of a large electronic spin resonance (ESR) by Brodsky and Title (1969) in *Ge*, *Si*, and *SiC* (Solomon, 1979). The unpaired electrons of the broken bonds are quite stable, and give a strong ESR signal. It appears that the ideal continuous random network where all the normal covalent bonds are satisfied is not stable, and that paramagnetic dangling bonds are necessary to stabilize the disordered structure. The magnetic resonance signal, directly proportional to the number of the localized centers, provides a powerful tool for the experimental study of the local microstructure of these materials.

The amorphous films produced by evaporation (i.e. EV) or sputtering generally contain a large number of defects which give rise to electronically active states in the energy gap (Lucovsky and Hayes, 1979). These films display densities lower than those of the corresponding crystalline phases, and also below those estimated from idealized random network models. The density of paramagnetic centers observed by ESR is 10^{19}–$10^{20} cm^{-3}$ (Davis, 1979). The density deficiency implies that a substantial fraction

of these defect states may reside on the internal void surfaces.

Amorphous silicon films produced by the thermal decomposition of silane (CVD) have an ESR intensity which corresponds typically to 10^{19} *spins* cm^{-3} (Hirose et al., 1977). This is 3 to 10 times less than in evaporated specimens (Sol et al., 1980). This low value may be the result of a combination of two effects: better structural coordination due to the high temperatures of deposition (from 500 to 650 C) and/or passivation by hydrogen residues. The hydrogen content, inferred from IR absorption, is smaller than 0.5%.

Lewis et al., (1974) were the first to demonstrate that hydrogen could compensate dangling bonds in tetrahedrally bonded amorphous semiconductors (Carlson, 1980). They showed that the density of gap states in sputtered $a-Ge$ was reduced when H_2 was added to the Ar sputtering atmosphere. Sakurai and Hagstrum (1975) showed that atomic hydrogen could compensate dangling bonds on the surface of crystalline silicon.

Glow-discharge produced $a-Si$ contains considerable amounts of hydrogen (Carlson, 1980). Investigators have shown that the hydrogen content is in the range of 10-50 atomic % and that most of the hydrogen is bonded to silicon atoms. The best quality films are obtained with substrate temperatures in the range of 200°-400°C. The ESR intensity is below the detectable limit ($\lesssim 10^{16} cm^{-3}$). Films deposited at lower substrate temperatures exhibit higher defect densities. As the substrate temperature increases above $\sim 350°C$, the defect density starts to increase because of the evolution of hydrogen from the film and the concurrent generation of dangling bonds.

The spin density is most probably indicative of a lower limit to the defect density. There is a great deal of evidence for the existence of large concentrations of spinless defects in $a-Si$ films (Adler, 1980). The observed spin density is almost always several orders of magnitude lower than the density of localized states in the gap. When atomic hydrogen is introduced into pure silicon films, approximately 100 times as much hydrogen enters than the unpaired-spin density suggests.

We utilize the estimated ESR signals as estimates of the relative defect densities of the three types of *a—Si* studied here. The defect density has a profound effect upon the relaxation of photoexcited carriers. The relaxation times can vary from 4ps to 200ps depending upon the defect density.

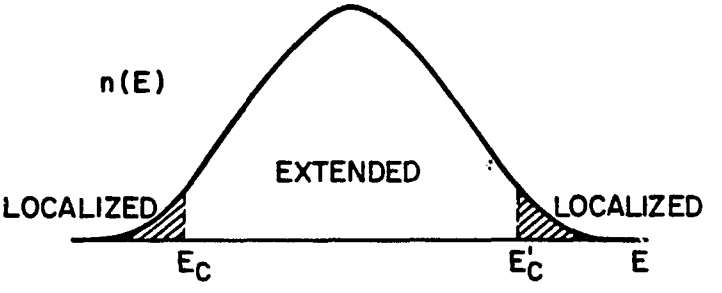

THE SIMPLEST MODEL FOR THE DENSITY OF STATES OF A SINGLE ISOLATED ENERGY BAND IN A DISORDERED MATERIAL. THERE IS A BAND OF EXTENDED STATES INSIDE THE ENERGIES E_C AND E'_C, WITH TAILS OF LOCALIZED STATES OUTSIDE (SHADED AREAS).

(E. N. ECONOMOU, M. H. BRODSKY, K. F. FREED, AND E. S. KIRKPATRICK: ELECTRONIC STRUCTURE OF DISORDERED MATERIALS. IN AMORPHOUS AND LIQUID SEMICONDUCTORS, ED. BY J. TAUC (PLENUM PRESS, LONDON, 1974).)

Fig. (2.2-1)

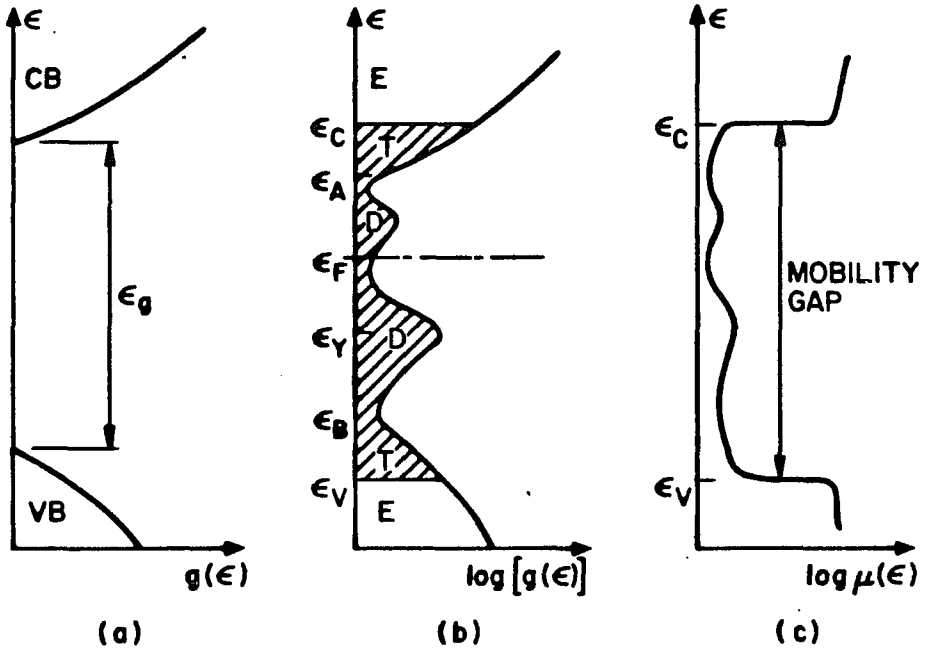

(a) DENSITY OF STATES FUNCTION $g(\epsilon)$ IN A CRYSTALLINE SEMICONDUCTOR; CB AND VB DENOTE THE CONDUCTION AND VALENCE BANDS RESPECTIVELY.

(b) DENSITY OF STATES IN AN AMORPHOUS SEMICONDUCTOR; E, EXTENDED STATES; T, LOCALIZED TAIL STATES; D, LOCALIZED DEFECT STATES.

(c) THE MOBILITY AS A FUNCTION OF ENERGY FOR THE AMORPHOUS SAMPLE SHOWN IN (b).

(P. G. LE COMBER: SCI. PROG. (OXF.) 66, 105(1979).)

Fig. (2.2-2)

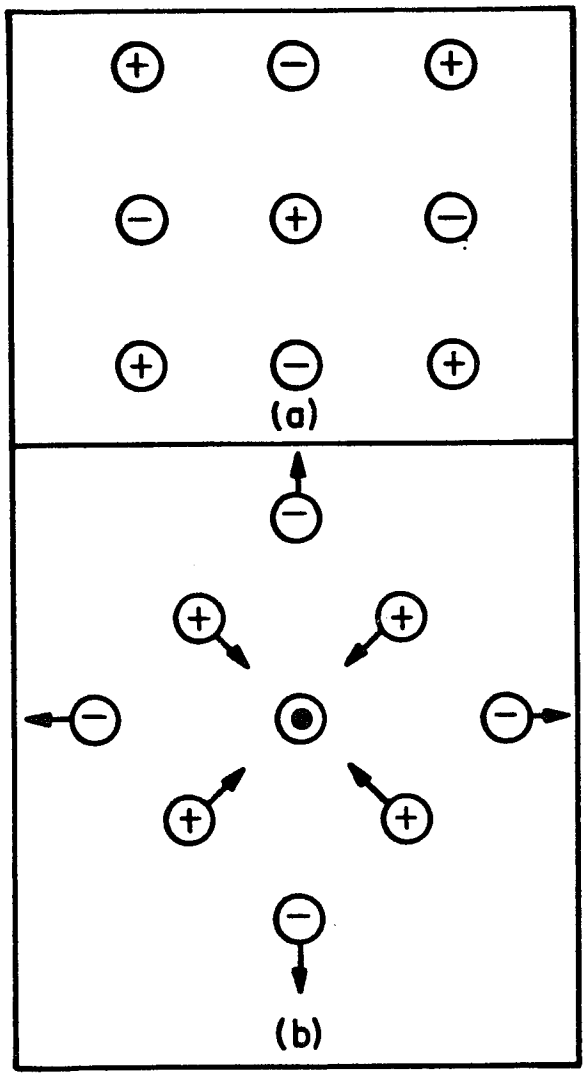

Fig. (2.2-3): Subfigure (a) depicts a portion of a lattice of ionic charges in which no excess charge carriers are present, while (b) illustrates the readjustment of the positions of the ions in response to an excess electron being placed on the central positive ion.
From: Emin (1976)

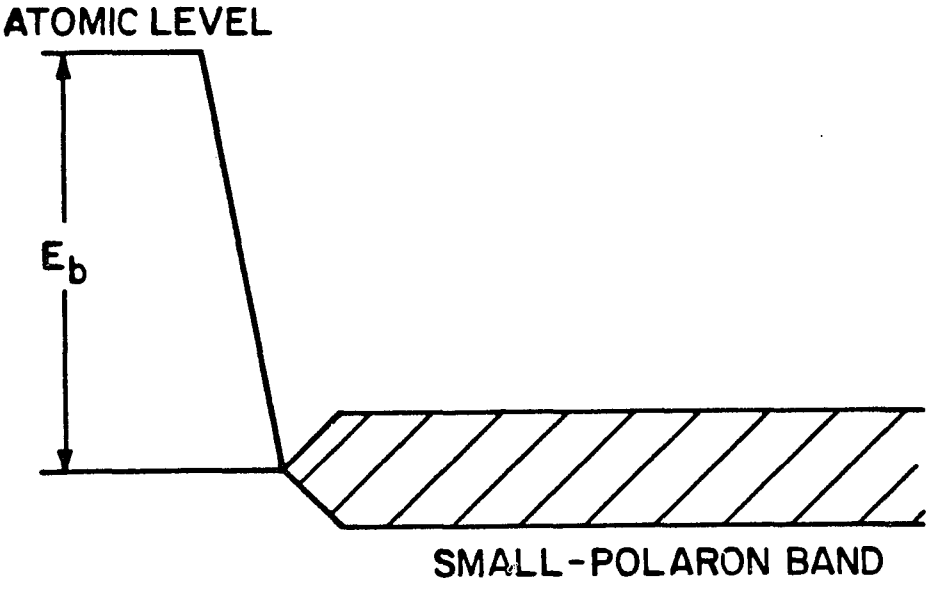

Fig. (2.2-4): As a result of allowing the atoms surrounding a charge carrier at a site in a crystal to adjust fully to its presence, the energy of the system is reduced (from its value in the tight-binding (zero-overlap) limit) by an amount E_b, the small-polaron binding energy. If one then takes cognizance of the fact that the degeneracy associated with the geometric equivalence of a regular lattice is lifted when finite electronic overlap exists, a typically very narrow small-polaron band is formed.
From: Emin (1976)

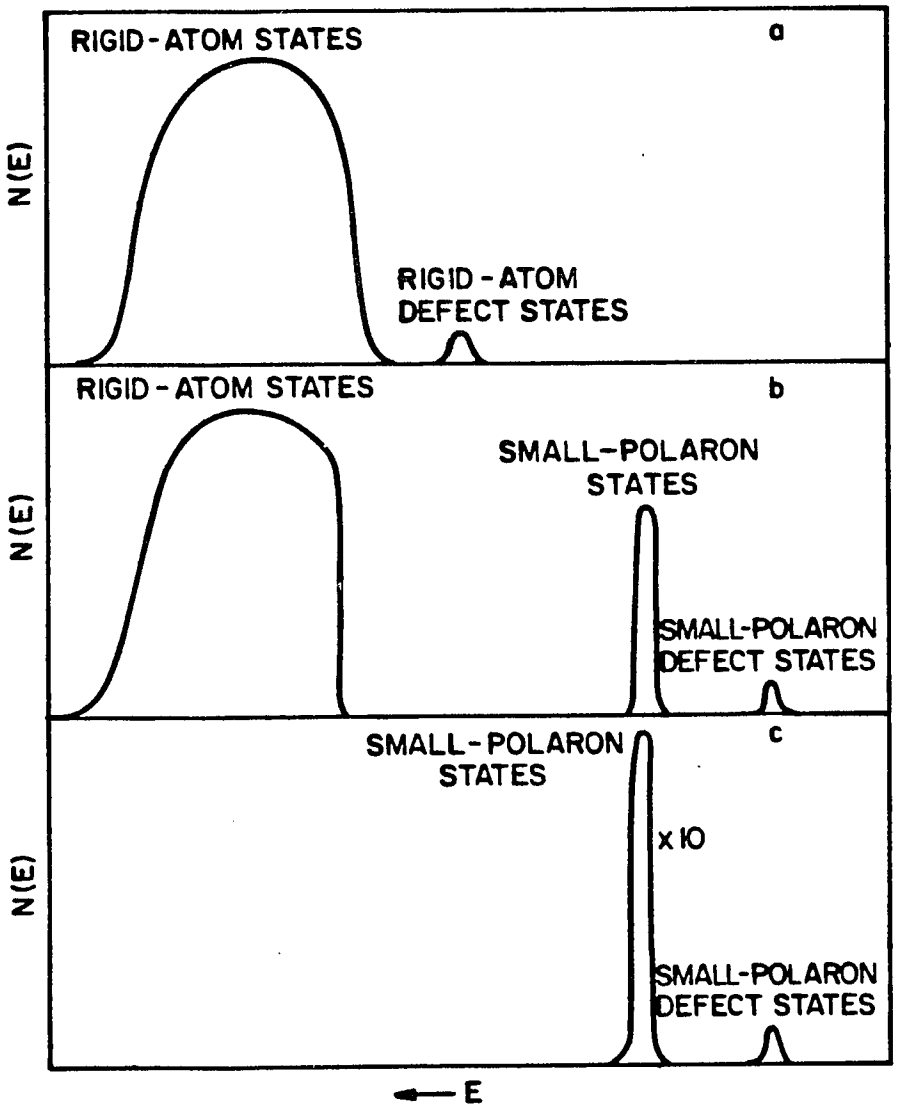

Fig. (2.2-5): In (a), a hypothetical rigid-atom density of states for a conduction band and set of defect levels in a noncrystalline solid is illustrated. With a finite electron-lattice interaction the deep-lying band-tail and defect states may be energetically unstable with respect to small-polaron formation. (b) illustrates the case when only some low-lying states have lower-lying small-polaron counterparts. In (c) the case when all the rigid-atom states are unstable with respect to small-polaron formation is depicted. From: Emin (1976)

III. EXPERIMENTAL TECHNIQUES AND APPARATUS

3.1 Photodetector Geometry

This section will concentrate on the make-up of the photodetector. First and foremost is a brief description of the various forms of a-Si that serve as the active area of the photodetector. Also discussed is the "general photoconductor geometry" and its speed limitations. In this thesis a photoconductor geometry that utilizes a microstrip transmission line is utilized to measure picosecond transients.

3.1.1 Preparation of a-Si Samples

The hydrogenated a-Si:H (GD) sample used in the study was grown by the standard technique of rf plasma-assisted decomposition of silane (SiH_4) in a capacitively coupled system (Knights, 1976). The substrates, consisting of 0.25mm thick polished fused silica, were positioned during growth on the grounded electrode (anodic) and held at a temperature of 250°C±5°C during deposition. The plate separation was 15mm. These undoped films were produced from 100% silane of semiconductor purity (minimum resistivity 100Ω-cm n-type). The films had a thickness of 0.9μm, as measured by a Sloan Dektak Surface Profile Measuring System. The films were deposited at a pressure of 0.36 torr and an rf power of 7 watts and frequency of 13.56 MHz to yield a power density of 40mW/cm^2. The silane flow rate was 50 standard cm^3/min (sccm). The deposition rate was 2.8μm/hr. These films were prepared by Dr. J. P. Harbison (Bell Laboratories).

The evaporated films of a-Si (EV) were prepared in the following manner. A 0.5μm film of a-Si was evaporated in ultra-high vacuum (UHV) on a 0.25mm fused silica substrate. The films were deposited by e-gun evaporation in a prebaked 18-in. stainless steel UHV chamber using a combination of ion, sublimation, and closed-cycle He cryopumping (Bean, 1980b; Bean, 1981). The chamber base pressure was $\sim 5\times10^{-11}$ Torr and depositions took place in a 95% hydrogen ambient of $(1-9)\times10^{-9}$ Torr.

Polycrystalline source silicon of 0.1 ppb (Boron) purity (Hemlock Semiconductor, Hemlock, Michigan) was evaporated from a 14-kW e-gun, modified for UHV. The deposition rate was approximately 5Å/s with a 23-in source-to-substrate separation. The fused silica substrates were out-gassed briefly at 600°C and then cooled to temperatures of 25-300°C for deposition. During selected depositions, high-purity oxygen was intentionally leaked into the chamber to a pressure of approximately 5×10^{-8} Torr. These films were prepared by Dr. J. C. Bean (Bell Laboratories).

The chemical-vapor deposited (CVD) a-Si sample is briefly described as follows. The a-Si film was prepared by the thermal decomposition of silane (Hirose et. al., 1977) onto fused silica substrates 0.2mm thick. The deposition apparatus (Sol, et. al, 1979) is a standard CVD system designed originally for epitaxial growth of crystalline silicon. Pure silane (2.3 l/min) is admitted with either argon or hydrogen into a vertical open flow reactor heated by induction at high frequency (400 kHz). At a 600°C substrate temperature undoped a-Si is deposited at a rate of 1μm/hr. We used film thicknesses of the order of 0.5μm. These films were prepared by Dr. D. Kaplan (Laboratoire Central de Recherches, Thomson CSF, Orsay, France).

A second CVD sample was prepared at Bell Laboratories by Dr. A. C. Adams. The 0.5μm thick CVD sample was prepared by the pyrolysis of silane in a LPCVD (low-pressure chemical vapor-deposition) (Hitchman, et. al., 1979) reactor at 0.25 torr and 600°C.

3.1.2 Photodetector

To measure photoconductive transients that occur on a picosecond time scale implies a bandwidth for the photoconducting circuit of tens to hundreds of gigahertz. The capacitance of the generally used "sandwich" configuration was responsible for the reduced bandwidth. To reduce the circuit capacitance and thereby increase the speed of response a 50-Ω microstrip transmission line (Schneider, 1969; Gunston, 1972) geometry was used. The capacitance was significantly reduced by the fact that it was

"distributed" along the transmission line as opposed to being "lumped" at the surface of a parallel plate capacitor.

Thin films of a-Si were deposited on 0.25mm thick fused silica substrates (Section 3.1.1). 5000Å of aluminum was evaporated through a shadow mask onto the a-Si in the form of a microstrip (Fig. 3.1.2-1). The bi-metallic (Cu-Ni) shadow masks were purchased from Towne Labs. The masks were fabricated by the standard photolithography techniques whereby the metal was removed selectively by the etching of chemicals. A Varian PS-10E Switch-Operated Vacuum Evaporator was pumped down to a pressure of 5×10^{-6} Torr for the aluminum evaporation. To complete the transmission line a uniform aluminum ground plane was evaporated on the bottom surface of the fused silica substrate. The microstrip was interrupted by a 25-μm gap. This gap forms the active area of the photodetector. This geometry is similar to what is commonly referred to as a "gap" or "planar" configuration as opposed to the "sandwich" configuration.

The characteristic impedance of the microstrip transmission line is determined by the relative dielectric constant, ϵ_r, and the height, h, of the fused silica substrate and the width, w, of the aluminum microstrip. A nominal characteristic impedance of 50-Ω was obtained for the following parameters: $\epsilon_r = 3.78$, $w = .55mm$, $h = .25mm$.

Since the electrode capacitance was distributed along the transmission line, the principal circuit limitation was due to the gap capacitance. Extensive examination of the gap capacitance in a microstrip transmission line was undertaken by Maeda (1972) and Rahmat-Samii, Itoh, and Mittra (1974). In their analysis the gap capacitance has two contributions. There was the shunt capacitance C_a (microstrip to ground plane) that was associated with the fringing effect of the edge of the strip. The second and larger contribution, in our case, was the series capacitance C_b (between the two microstrips) which was associated with the coupling phenomena between the two center microstrips. The calculated gap capacitances are displayed in Figures (3.1.2-2) and

(3.1.2-3) for a 50-Ω microstrip transmission line as a function of ϵ_r, h, and s (gap width). ($Z_0 = 50\Omega$, $\epsilon_r = 3.78$, $w = 0.55$mm, $h = 0.25$mm, $s = 25\mu$m, $s/h = 0.1$). In comparing Figures (3.1.2-2) and (3.1.2-3) for the experimental parameters above one comes to several conclusions. First of all, the series capacitance C_b dominates and we will refer to this quantity as C_g, the gap capacitance. For the above value of s/h (0.1), C_b is nearly independent of the dielectric constant, ϵ_r, but C_b varies considerably as a function of the substrate thickness, h. This follows from the fact that the capacitance is highly geometry dependent and merely confirms the notion that high speed implies "small packaging." Since the value of C_b varies little with ϵ_r for $s/h = 0.1$, we estimate the gap capacitance for $h = 0.25$m to be $C_b = C_g = 0.02$pF.

Electrical contact was made to the photodetector with either Omni-Spectra OSM (18 GHz) or OSSM (40 GHz) coaxial-to-microstrip connectors after placement of the photodetector "chip" in a suitable mount (Smith et al., 1981b). On one side of the photodetector (Fig. (3.1.2-1)) was a charged transmission line which served to bias the photodetector (Smith et al., 1981a) and on the other side the transmitted signal was directly coupled into a Tektronix 7904 Oscilloscope with an S-4 Sampling Head (25ps rise time). The biasing circuit consisted of a battery and blocking resistor. The blocking resistor served the purpose of controlling the amount of current entering the photodetector (100KΩ, typical). The blocking resistor also served as a precautionary device. The maximum signal that the sampling head could handle was ± 5V. Voltages as high as 100V were utilized. We chose the magnitude of the blocking resistor such that most of the voltage drop would be across it in case a short developed in the photodetector. In this manner ± 5V would never be applied to the sampling head.

If we think of this microstrip transmission line structure as a charged capacitor then the ultimate speed of response of the circuit is given by the characteristic time for the discharge of the capacitor. The circuit time constant is given by

$$\tau_0 = 2Z_0C_g \qquad (3.1.2\text{-}1)$$

The factor of 2 is required because the capacitance is in series with the two sections of microstrip (Auston, 1981). For a Z_0 of 50-Ω and a C_g of 0.02pF we obtain a circuit time constant of $\tau_0 = 2ps$. This response does not include the relaxation of the photoconductor, the duration of the optical pulses, reflections from the microstrip to coaxial cable transition, the bandwidth of the connectors, the bandwidth of the sampling oscilloscope, etc. Figure (3.1.2-4) is the photoresponse for a photoconductor whose active area is CVD a-Si (Section 3.1.1) activated by 3.5ps duration optical pulses from a mode-locked dye laser (Section 3.2). This sampling oscilloscope trace indicates a risetime of 25ps and width of 40 ps (FWHM) for this photodetector. This represents a sampling oscilloscope limited response and represents an improvement of several orders of magnitude in speed of response over traditional photoconductivity configurations.

3.2 Dye Laser

A photodetector with an electrical response ($2Z_0C_g$) of approximately 2 ps., clearly requires an optical source of comparable duration to fully utilize the speed capability of the device. The optical source consisted of a cw Rhodamine 6G dye laser that was synchronously pumped by a mode-locked argon ion laser (Chan and Sari, 1974; Harris et al., 1975; Frigo et al., 1977). Using synchronous mode-locking we have obtained optical pulses with a duration of 3.5ps. This section contains brief discussions of the mode-locked argon ion laser and the measurement of the optical pulsewidth using a radiation damaged silicon-on-sapphire photodetector (Smith, et al., 1981a); and the cw mode-locked dye laser and the measurement of the optical pulse width by nonlinear frequency mixing (second harmonic generation, SHG) in potassium dihydrogen phosphate (KDP).

3.2.1 Mode-Locked Argon Ion Laser

The single transverse mode (TEM_{∞}), 514.5nm line of a Spectra-Physics Model 171-03 Ion Laser was mode-locked with a Spectra-Physics Model 342 Mode-Locker and Spectra-Physics Model 452 Mode-Locker Driver. In this manner, an acousto-optic modulator is placed inside the argon ion laser cavity in order to "lock" the longitudinal modes (Hargrove, et al., 1964).

The output of the laser is a Gaussian-type gain curve (Doppler broadened) modulated by the longitudinal modes of the cavity. The longitudinal mode spacing is c/2L, where L is the length of the cavity and c is the speed of light. The cw output, as a function of time, will depend upon the amplitudes, frequencies, and relative phases of the oscillating modes. In general, the coupling between modes is not sufficiently strong to produce a definite phase relationship between the modes. The modes are thus uncorrelated in phase resulting in random fluctuations that cause the output to vary in time even though the average power may remain relatively constant. If these longitudinal modes are forced to maintain a fixed phase relationship, the output will be

a well-defined function of time and the laser is said to be mode-locked or phase-locked. The acousto-optic modulator provides strong coupling between phases of the longitudinal modes by modulating the cavity losses at a frequency equal to the longitudinal mode spacing. The output is the Fourier transform of this phase related frequency spectrum in the time domain and results in a narrow train of pulses separated in time by 2L/c. This minimum pulsewidth will be on the order of the inverse linewidth.

The minimum pulsewidth is obtained by tuning the RF drive frequency of the acousto-optic modulator and adjusting the length of the laser cavity. The pulsewidth was measured with a photodetector (Section 3.1.4) whose active area consisted of a radiation damaged silicon-on-sapphire (SOS) thin film (Smith et al., 1981a). A conventional van de Graaf accelerator was used to implant 3×10^{14} ions/cm^2 of 0.4 MeV O^+ ions into the SOS film. Our purpose in using ion implantation is to use the resulting damage as a means of introducing a predetermined defect density into the crystalline material in order to control the carrier lifetime and mobility. In this manner we obtain a very sensitive and extremely fast photodetector. The sampling oscilloscope trace of the photodetector response to argon laser pulses (Fig. 3.2.1-1) indicates a pulsewidth of 115ps (FWHM).

The acousto-optic modulator is driven by an RF signal that has an average power of 560mW and a frequency of 40.9575 MHz. For a current setting of 30 amps on the power supply, the laser output has an average power of 700mW and repetition rate of 81.951 MHz or approximately 82 MHz, resulting in a peak power of 74W.

3.2.2 Synchronously Mode-Locked CW Rh6G Dye Laser

The longitudinal modes of the argon ion laser were mode-locked by introducing intracavity loss modulation at a frequency equal to the longitudinal mode spacing (c/2L). In a similar manner, the gain of the dye was modulated at the synchronized periods of the intense mode-locked argon pump pulses and the cavity round-trip transit

time (2L/c).

The dye laser configuration (Fig. 3.2.2-1) was a folded, three-mirror astigmatically compensated (Kogelnik et al., 1972) cavity, a free-flowing Brewster angle jetstream of approximately 3×10^{-3} M/l Rh6G in ethylene glycol, and a birefringent filter at Brewster's angle for tuning and bandwidth control. Figure (3.2.2-1) indicates a mode-locker driver which was the source of the RF signal to drive the acousto-optic modulator. The mode-locked argon pulses were directed into the cavity by flat ($R = \infty$) mirrors and was focussed into the jetstream by the 10-cm radius of curvature folding mirror. A relatively high loss output coupler ($T = 53\%$ @ $575nm$) was used to quench the gain of any secondary oscillations in the cavity. Secondary oscillations have arisen from the fact that a dye pulse originating in the jetstream can propagate in either of two direction. The difference in pathlength for the two optical paths was the 10-cm round-trip distance (333 ps) between the jetstream and the 5-cm of curvature end-mirror. For lower transmission output couplers, secondary optical pulses were observed in nonlinear optical autocorrelation (Section 3.2.3) measurements. The birefringent filter consists of two or three flat and parallel crystalline quartz plates placed inside the dye laser cavity at Brewster's angle. The plates form a birefringent filter (Bloom, 1974) which has low loss for linearly polarized light at a particular wavelength.

Short pulse formation, in this synchronous pumping scheme, has generally been discussed in the time domain to obtain an intuitive feeling for the nonlinear processes involved in the pulse narrowing. Pumping the dye laser with a train of short mode-locked pulses is an example of gain modulation. The short pump pulses, very rapidly, generate high gains in the dye. The spontaneous fluorescence emitted by the dye molecules will imitate the time integral of the argon pulse since the fluorescence lifetime is long compared to all times of interest (Frigo et al., 1977). The fluorescence lifetime of Rh6G is approximately 3 nsec (Malley and Mourou, 1974). If the intensity of the argon pulses were insufficient to produce stimulated emission, the gain would

relax in a fluorescence lifetime and a repetition rate equal to the pumping rate. Thus we have a dye pulse oscillating in the cavity. Since the gain is proportional to an integral of the pump pulse intensity, the dye laser gain rises more rapidly for a shorter pump pulse with a given pump energy (Heritage and Jain, 1978). This assumes that the pump pulse width is larger than the relaxation time within the excited singlet states and the pump power densities are insufficient for saturation of the gain. The thermalization of excited vibrational-rotational or vibronic states to the lowest vibronic state of the first excited singlet state occurs within picoseconds (Shank, 1975). Therefore, the shorter the pumping pulse the steeper the slope of the gain, leading to a sharp leading edge on the dye pulse.

Population inversion, in the dye, is achieved very rapidly by argon pump excitation. The arrival of the sharp leading edge of the dye pulse saturates the gain. The loss of inversion is due to the stimulated emission caused by the dye pulse passing through the jetstream, depleting the excited state population (Frigo, et al., 1977). The depletion of the gain by the dye pulse provides net loss in the trailing edge of the pulse. Thus, the steep slope of the gain due to short pump pulses and the saturation of the gain by the dye pulse results in a train of picosecond mode-locked dye pulses.

The output of the dye laser is characterized by the parameters of Fig. (3.2.2-2). The measurement of the optical pulsewidth is briefly described in the next section.

3.2.3 Dye Laser Pulsewidth - Nonlinear Optical Autocorrelation

The maximum pulse response of a sampling oscilloscope would have a risetime of 25ps and a duration of 40ps (FWHM). This sampling oscilloscope response is insufficient to measure the optical pulsewidth of the dye laser output.

A common technique for pulse measurement utilizes the optical pulse itself. The intensity profile of the optical pulse is correlated with itself by mixing two optical pulses in a nonlinear optical medium to yield sum frequency generation (second harmonic

generation in this case, SHG). The intrinsic speed of this electronic nonlinearity is on the order of 10^{-15} sec. This speed is utilized in the measurement of the pulsewidth.

Nonlinear optical techniques for pulse measurements do not provide a direct display of the pulse shape but give instead measurements of correlation functions (Ippen and Shank, 1977). The second-order autocorrelation function of the intensity $I(t)$ is given by

$$G^{(2)}(\tau) = \int_{-\infty}^{+\infty} I^{(\omega)}(t) I^{(\omega)}(t+\tau) dt \qquad (3.2.3\text{-}1)$$

where τ is the optical delay between the two pulses. This is the function we obtain by SHG in KDP (KH_2PO_4) since the SHG intensity $I^{(2\omega)}(\tau)$ is proportional to the product of the intensities of the two fundamental pulses

$$I^{(2\omega)}(\tau) \propto G^{(2)}(\tau) \qquad (3.2.3\text{-}2)$$

If $I^{(\omega)}(t)$ is a single isolated pulse, $G^{(2)}(\tau)$ vanishes for large relative delay τ and its half-width provides a measure of the duration of $I^{(\omega)}(t)$. Precise determination of a pulsewidth requires further knowledge about the shape of $I^{(\omega)}(t)$. $G^{(2)}(\tau)$ is always symmetric regardless of any asymmetry in $I^{(\omega)}(t)$ as can be seen from the nature of Eqn. (3.2.3-1).

We utilized noncollinear background-free SHG (Maier et al., 1966; Ippen and Shank, 1975) in a 0.3mm thick crystal of KDP to measure the $G^{(2)}(\tau)$ of the dye laser pulses (Fig. 3.2.3-1). The output of the dye laser was divided and directed into the two arms of a modified Michelson-interferrometer. The relative time delay between the two beams was achieved by leaving one arm of the interferrometer fixed and varying the other by a Model MT160 Klinger Scientific Translation Stage with incorporated stepping motor. The translation stage possessed 200mm of travel and a Microcontrol Planetary Gear Reduction Unit for a 2-micron step size. The stepping motor controller consisted of a Model SP151 Superior Electric Company Preset Indexer and a unit, built by P. R. Smith (Bell Laboratories), that provided the Preset Indexer with a directional signal and a cycling function that permitted the user to select the number of steps and

roundtrips.

The two beams, parallel but noncollinear were focussed into the KDP crystal. These fundamental beams were blocked, by appropriate beam stops, upon passage through the KDP crystal. Second harmonic generation proportional only to the product of the two beam intensities, is detected at an angle bisecting the angle between the two focussed fundamental beams. The KDP crystal was oriented for phase matching at this angle that bisected the two beams. Thus second harmonic radiation was produced only when both pulses were present in the crystal, thereby eliminating a background signal (background-free SHG).

The detection system consisted of a RCA 4459 S-2 Photomultiplier Tube whose output was filtered by a PAR Model 124 Lock-In Amplifier. One arm of the interferrometer was chopped at 2 kHz by a PAR 125A Chopper which provided the reference signal for the lock-in amplifier. The output of the lock-in amplifier contained the SHG autocorrelation signal as a function of the relative delay between the two arms of the interferrometer. This signal was stored in a Nicolet 1074 Multi-Channel Analyzer that was indexed by a signal derived from the stepping motor controller. This was digitized and averaged to increase the signal-to-noise ratio.

The temporal resolution was not obtained from the bandwidth of the electronics mentioned above, but resulted from the fact that it was a coincidence measurement - the signal depended upon the presence of both optical pulses. The temporal resolution depended upon the ability to accurately control the optical path difference between the two arms of the interferrometer (2-micron step size) and the speed of the electronic nonlinearity responsible for SHG. These two criteria yield a maximum temporal resolution of $10^{-14}s$—$10^{-15}s$. This coincidence measurement technique was utilized to measure the electronic correlation function (Section 3.3.2) of a-Si. In the electronic correlation the time constant for SHG is replaced by the circuit time constant, the material relaxation time, and the time associated with the duration of the optical pulses.

The optical autocorrelation function ($G^{(2)}(\tau)$) of the dye laser is shown in Fig. (3.2.3-2). As mentioned earlier, to obtain the precise pulse duration from the FWHM of $G^{(2)}(\tau)$, some form for the shape of $I^{(\omega)}(t)$ must be assumed. A pulse shape of the form

$$I^{(\omega)}(t) \sim sech^2\left\{\frac{1.76t}{\Delta t}\right\} \qquad (3.2.3\text{-}2)$$

gives a ratio of $\Delta\tau/\Delta t = 1.55$, where Δt and $\Delta\tau$ are the FWHM of $I^{(\omega)}(t)$ and $G^{(2)}(\tau)$ respectively (Ippen and Shank, 1977). Thus an optical pulsewidth of 3.5ps is estimated.

The output coupler was placed on a translation stage in order to vary the length of the dye laser cavity. This length adjustment controls the timing of the dye pulse with respect to the argon pump pulse. The shortest optical pulses are obtained by first adjusting the cavity length to yield the maximum SHG and then reducing the length of the cavity by fractions of a millimeter (Ausschnitt et al., 1979). The background-free measurement of the autocorrelation function gave an accurate measure of the energy in the wings of the pulses (Ippen and Shank, 1975). Thus the cavity length was chosen with two criterion in mind: the minimum pulsewidth that would yield a zero background level.

3.3 Picosecond Photoconductivity

The initiation of photocurrents in semiconductors by optical pulses is essentially an instantaneous process. This property has previously been utilized for the picosecond optoelectronic switching and gating of *dc* and microwave signals in crystalline silicon (Auston, 1975; Johnson and Auston, 1975). Although relatively easy to obtain fast risetimes in crystalline semiconductors, it is difficult to terminate the photocurrent rapidly, due to the generally long carrier relaxation times. In the case of crystalline silicon two optical pulses were required to obtain the picosecond transients (Auston, 1975; Johnson and Auston, 1975): the first optical pulse initiated a rapid initial photoresponse and a second "short-circuiting" optical pulse was required to rapidly terminate the photocurrent. In the case of amorphous (Auston, et al., 1980a, b, c, d; Johnson et al., 1980a, b, 1981a, b, c) and radiation-damaged (Smith et al., 1981a) semiconductors, both of which contain very high densities of localized states, the rapid termination of the photocurrent is due to carrier relaxation so that a second "short-circuiting" optical pulse is not required. The localized states (due to structural defects and the lack of long-range order) serve as effective "traps" for the photoexcited carriers and results in very short carrier relaxation times.

In the traditional approach to transient photoconductivity, electrodes (Ohmic) are placed on a sample in the "sandwich" geometry and biased through a load resistor (Fig. 3.3-1). Carriers are excited with a "chopped" *cw* or pulsed laser and the response observed on an oscilloscope. This approach has limitations on the speed of response which include the duration of the optical pulses, circuit *RC* time constant, and oscilloscope rise time. Microsecond to nanosecond time resolution can be obtained with this approach. This has been a very effective approach for obtaining mobilities and relaxation times of photoexcited carriers in crystalline semiconductors. When the relaxation time of the photoexcited carriers is faster than the time resolution of your measurement system, the photocurrent that is measured will be proportional to the

product of the mobility (μ) and the relaxation time (τ). Consequently, most transient photoconductivity measurements in amorphous semiconductors measure a mobility-relaxation time product, $\mu\tau$, and fail to individually resolve μ and τ.

With picosecond time-resolved photoconductivity we can make direct measurements of the mobility and relaxation time. The following is a brief description of the high speed measurement capability that enables us to observe the early time history of electronic transport in amorphous semiconductors.

3.3.1 Sampling Oscilloscope Measurement

Sampling oscilloscope measurements are made in the high speed single gap photodetectors described in Section (3.1.2). The best response of the sampling oscilloscope consisted of an electrical transient with a 25 ps risetime and 40 ps FWHM. The constraints on the response time of the sampling oscilloscope necessitates separating the materials to be studied into two classes. In the first class of materials the carrier relaxation time is sufficiently long to be resolved on the sampling oscilloscope, and the initial mobility of the carriers can be obtained from the time resolved peak of the photocurrent (i.e. GD). In the second class of materials the relaxation of the photoexcited carriers is on the order of or faster than the response of the sampling oscilloscope (i.e., CVD and EV). In this case the initial mobility cannot be directly taken from the unresolved photocurrent peak. However, the mobility-carrier-relaxation-time product ($\mu\tau$) can be obtained by integrating the observed photocurrent pulse. One then performs a high speed electronic correlation measurement (Section 3.3.2) to obtain the relaxation time, τ. In this two-step process we can separate out the initial mobility and the relaxation time.

To obtain to photoresponse, the output of the dye laser (Section 3.2) is split and focussed onto the "active regions" of two photodetectors (Fig. 3.3.1-1). The active area of the first photodetector consists of the material of interest. The second photodetector was the radiation damaged silicon-on-sapphire photodetector described in Section

(3.2.1). The output of this second photodetector is used as an external "trigger" for the sampling oscilloscope. The use of the sharp synchronous leading edge of this detector as a trigger source considerably reduced the unavoidable jitter in the sampling circuitry. With these two sources the photoresponse of the amorphous semiconductor is observed on the sampling oscilloscope. Also available in the Tektronix 7511 Sampling Unit is a Vertical Signal Output jack that contains a facsimile signal (the same output signal that drives the vertical amplifier). This signal is taken after the sampling process and is a proportional representation of the display signal rather than the input signal itself. Since the signal at the Vertical Signal Output jack is an equivalent time signal, it is available for signal processing in the multi-channel analyzer (MCA). The signal is digitized and averaged to increase the signal-to-noise ratio.

In those materials which have carrier relaxation times sufficiently long to resolve to photoresponse, the peak photocurrent is given by the following expression (Appendix I):

$$i_p = \eta \frac{e}{\hbar\omega} (1-R)\,(1-e^{-\alpha d}) \frac{V_b}{\ell^2} \mu\, \epsilon_p, \qquad (3.3.1\text{-}1)$$

where η is the quantum efficiency for the generation of electron-hole pairs, $\hbar\omega/e$ is the photon energy in volts, R is the reflectivity, α is the absorption constant, d is the film thickness, V_b is the bias voltage, ℓ is the gap spacing, μ is the mobility, and ϵ_p is the optical pulse energy coupled into the active region of the photoconductor. This measurement yields two parameters that describes electronic transport in amorphous semiconductors. The peak amplitude of the time-resolved photocurrent is proportional to the sum of the initial mobilities of photoexcited electrons and holes and the slope of the initial relaxation of the displayed photocurrent yields an effective time constant for relaxation of the carriers into localized states.

In those materials with carrier relaxation times faster than the time resolution of the sampling oscilloscope we integrate the photocurrent pulse to obtain the charge, Q, in

the pulse. The MCA measures the area under the photocurrent pulse, which is equivalent to measuring the total charge. Integrating the expression for the time dependent photocurrent yields (Appendix I):

$$Q = \eta \frac{e}{\hbar\omega} (1-R) (1-e^{-\alpha d}) \frac{V_b}{\ell^2} \mu\tau \epsilon_p, \qquad (3.3.1\text{-}2)$$

where τ is an effective time constant for the relaxation of carriers into localized states. For this class of very fast materials the sampling oscilloscope can at best yield a $\mu\tau$ product. To separate this product a high speed electronic correlation measurement (Section 3.3.2) is performed to determine the carrier relaxation time τ.

3.3.2 Electronic Correlation

It was mentioned in Section (3.3.1) that in materials in which the relaxation of photoexcited carriers is faster than the response of the sampling oscilloscope, improved temporal resolution is needed to measure the carrier relaxation time, τ. The improved temporal resolution ($\lesssim$ 10 ps) and the measurement of τ is obtained by the electronic correlation of two high speed photoconductors (Auston et al., 1980b). This correlation method is very similar to the nonlinear optical autocorrelation used to measure the optical pulse widths (Section 3.2.3). In the optical measurement, the temporal resolution is limited by the speed of the electronic nonlinearity responsible for second harmonic generation. The temporal resolution of the electronic correlation is limited by the carrier relaxation time, τ, the finite capacitance of the photoconducting circuit, and the duration of the optical pulses used to activate it. With an approximate deconvolution of the electronic autocorrelation function (identical photoconductors) or cross-correlation function (different photoconductors), we can obtain τ and use it in conjunction with the measured total charge, Q, from a sampling oscilloscope measurement (Section 3.3.1), to obtain the mobility, μ. The similarity between the optical and electronic correlations measurements is further emphasized by the fact that the detection and signal processing equipment are identical. The difference is that the

charge, Q, at the output of the photomultiplier tube, replaces the charge, Q, at the output of the photoconductor.

The standard technique for measuring the duration of picosecond optical pulses is to make a nonlinear optical autocorrelation of two identical pulses by delaying one with respect to the other and then mixing them in a second harmonic generating crystal. The effect is to convolve the temporal profile of the optical pulse with itself. The analogous electrical measurement is the electronic correlation of the responses of two photoconductors.

In this scheme (Fig. (3.3.2-1)) one of the photoconductors has a *dc* bias, and the output signal from it is used to bias the second photoconductor. The quantity that is measured is the total charge produced at the output of the second photoconductor as a function of the relative delay between the two activating optical pulses. This is a coincidence measurement which correlates the arrival of the signal from the first photoconductor with the response of the second photoconductor which acts as a sampling gate. By measuring the charge as a function of optical delay, $Q(\tau)$, a second order correlation function, $G^{(2)}(\tau)$, is obtained which contains the desired information about the response of each photoconductor. The charge is proportional to the convolution of the two photoconductances, $g_1(t)$ and $g_2(t+\tau)$ (Appendix II),

$$G^{(2)}(\tau)\alpha Q(\tau)\alpha\, V_b\, Z_o \int_{-\infty}^{+\infty} g_1(t)g_2(t+\tau)dt, \qquad (3.3.2\text{-}1)$$

where V_b is the bias voltage and Z_o is the characteristic impedance of the transmission line. The time resolution of the measurement is determined entirely by the response of the two photoconductors and the interconnecting circuit and does not require any high speed external circuitry. The detection equipment is identical to that used in the optical autocorrelation measurement (Section 3.2.3). The optical beam which illuminates the bias photoconductor is chopped at a 2 *kHz* rate and the total integrated charge is measured in the lock-in-amplifier. This procedure also has the advantage that it does

not contain a contribution from the signal which is capacitively-coupled across the second gap. This is due to the fact that the lock-in-amplifier integrates both the equal negative and positive contributions of the differentiated time-varying component of the signal. As the optical delay between the two beams is varied with a translation stage, the signal is recorded and averaged in the multi-channel analyzer synchronized to the stepping motor driving the translation stage.

During the course of this thesis several correlation "geometries" we studied. Two of the geometries were utilized to obtain the data for this thesis.

Figure (3.3.2-2) is the transmission line electrode pattern of a geometry we call a "tandem gap correlator." This geometry consists of two photoconductors in the same transmission line between which a matched attenuator has been inserted to suppress reflections and provide the necessary isolation to prevent the *dc* bias on the first photoconductor from being transferred to the second photoconductor. We have used this geometry in a modular form whereby both photoconductors are on separate substrates and the interconnections are made with 3-mm microstrip-to-coax connectors. Typical rise times for this geometry are 17 ps which is equivalent to a bandwidth of approximately 18 *GHz*, which happens to be the bandwidth of the 3-mm connectors between the photoconductors. Faster risetimes are obtained in those situations in which the two photoconductors are on the same substrate and the transmission line isn't interrupted. This is due to the fact that the transmission line has a larger bandwidth than the 3-mm connectors. However, this modular scheme has the advantage of being more flexible in that samples can be readily interchanged and cross-correlations are possible between unlike samples. The cross-correlation technique is an important tool that enables one to accurately characterize the response of a new material by correlating it against a known material with a fast response. This can be done in two ways. The material of interest can be used as a first photoconductor with a *dc* bias applied to it, and the signal it produces can then be measured by the second

high-speed photoconductor, which acts as a linear sampling gate. Alternatively, the high-speed photoconductor can be used with a *dc* bias to act as an electrical impulse generator (Fig. 3.3.2-2) which then probes the relaxation of the photogenerated carriers in the material of interest. This latter approach generally gives better signal-to-noise ratios.

Figure (3.3.2-3) is the transmission line electrode pattern of a geometry we call the "symmetric gap autocorrelator." In this scheme the *dc* biased electrode injects a charge into the main transmission line when the first optical pulse strikes the gap. This signal is split equally into two components traveling to the left and right on the main transmission line. The main transmission line, which is terminated at both ends, serves as a rapid, low impedance, lead for the two gaps, permitting the charge to propagate away quickly. This main transmission line also serves to isolate the two photoconductors, thus eliminating the need of an attenuator, as in the "tandem gap correlator." Before the charge dissipates along the terminated main transmission line, it is sampled by the second optical pulse activating the second photoconductor. Thus, when the second optical pulse strikes the sampling gap, a small sample of charge is transferred from the signal on the main transmission line to the sampling line. This geometry has a response time of $\lesssim 10ps$. This "pulse injection" scheme has the advantage that reflections are minimized by the terminated ends of the main transmission line. In addition any dispersion of this short electrical pulse is eliminated by virtue of the fact that the signal is sampled immediately after pulse injection.

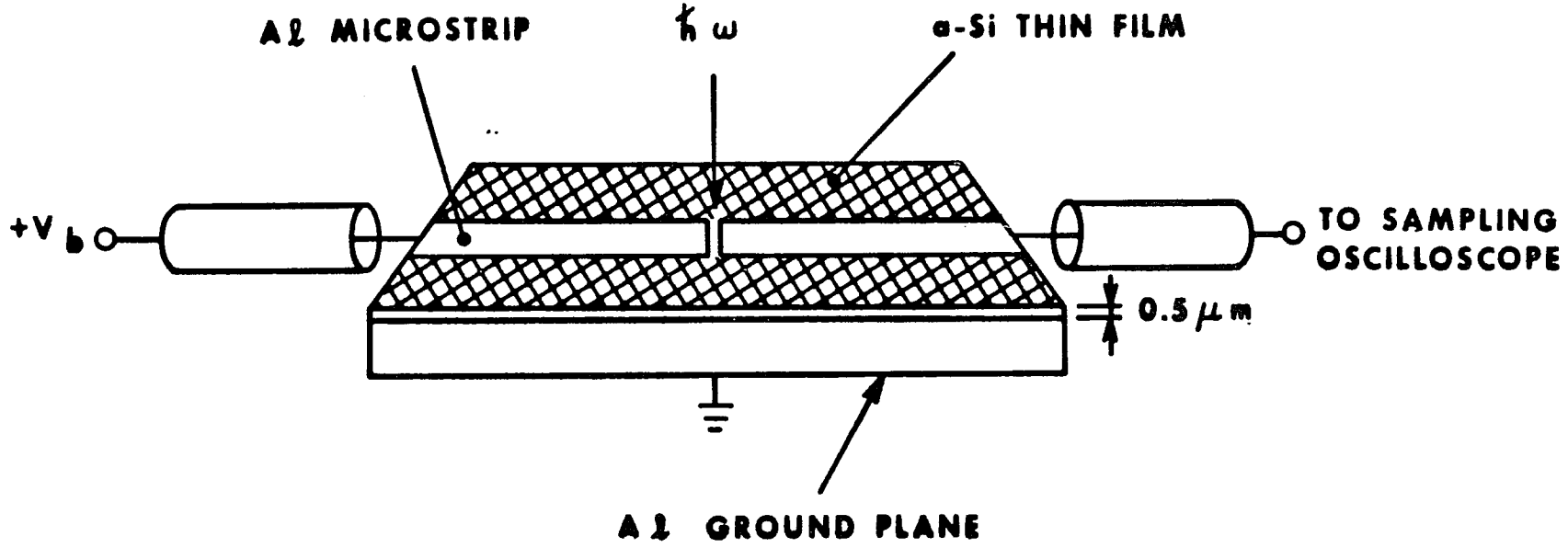

Fig. (3.1.2-1a): Schematic drawing of photodetector geometry. The end-on electrodes form a 50-Ohm microstrip transmission line. A small gap in the centre is used as the active area of the photodetector.

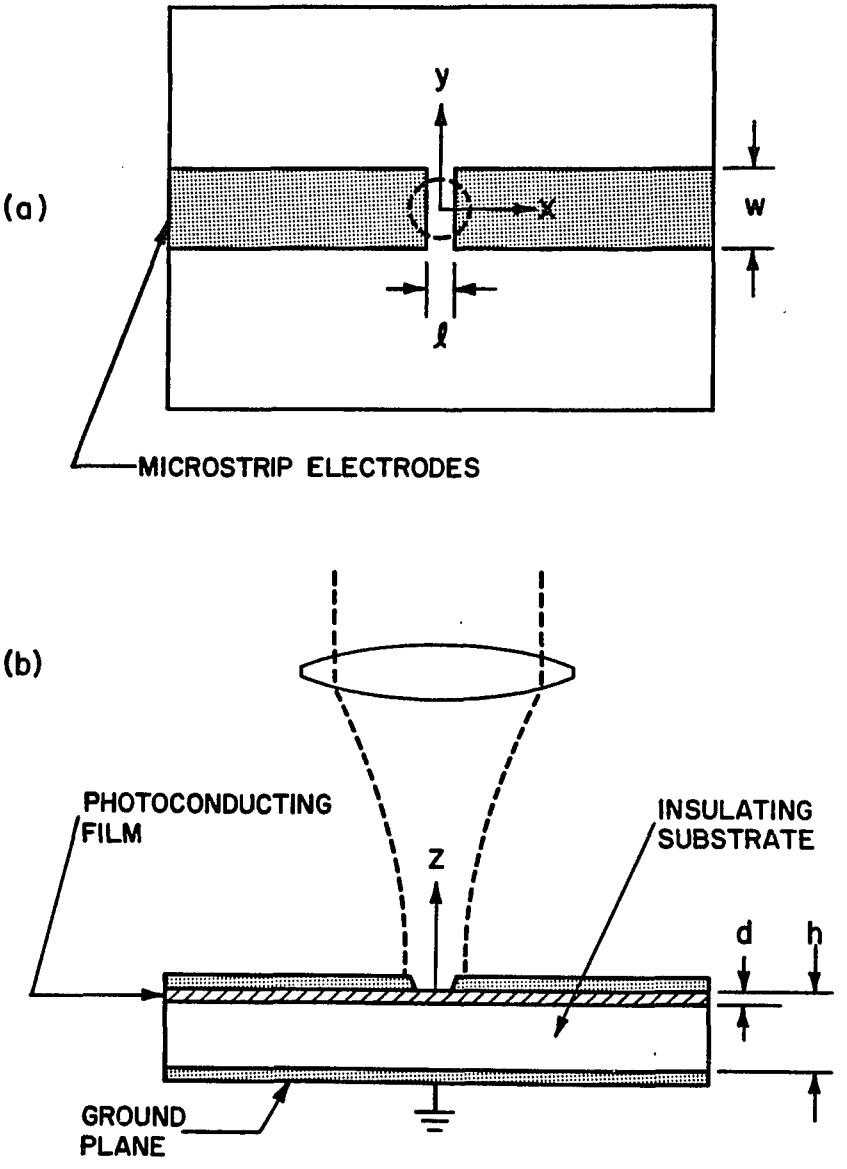

Fig. (3.1.2-1b): Schematic diagram of a thin-film photoconductor as an integral component of a high-speed microstrip transmission line. The active region is the gap in the top electrode at which the light is focussed.

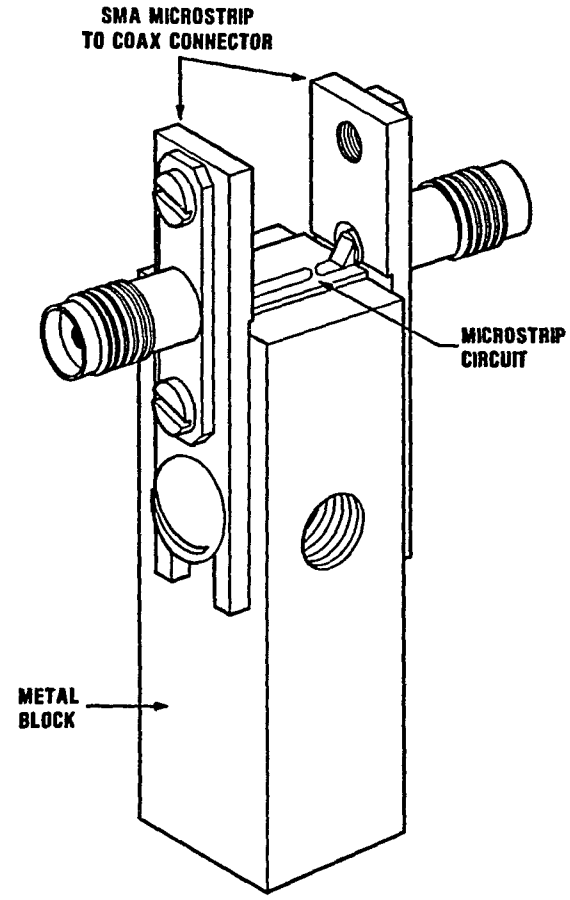

Fig. (3.1.2-1c): Block Type Mount Indicating Photodetector "Chip" and OSM Coaxial-To-Microstrip Connectors

GAP CAPACITANCES FOR 50-Ω
MICROSTRIP TRANSMISSION LINE
AS A FUNCTION OF s/h (h=0.50 mm)

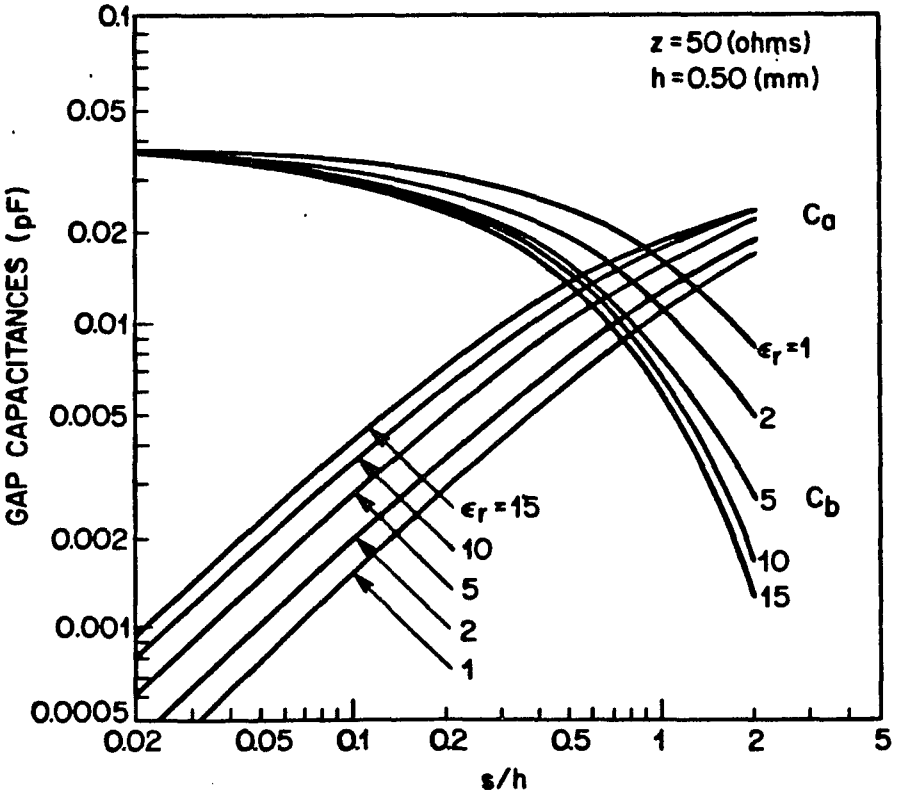

FROM: M. MAEDA: IEEE TRANS. MICROWAVE THEORY TECH. MTT-20, 390 (1972)

Fig. (3.1.2-2)

GAP CAPACITANCE FOR 50-Ω
MICROSTRIP TRANSMISSION LINE
AS A FUNCTION OF s/h (ϵ_r =10)

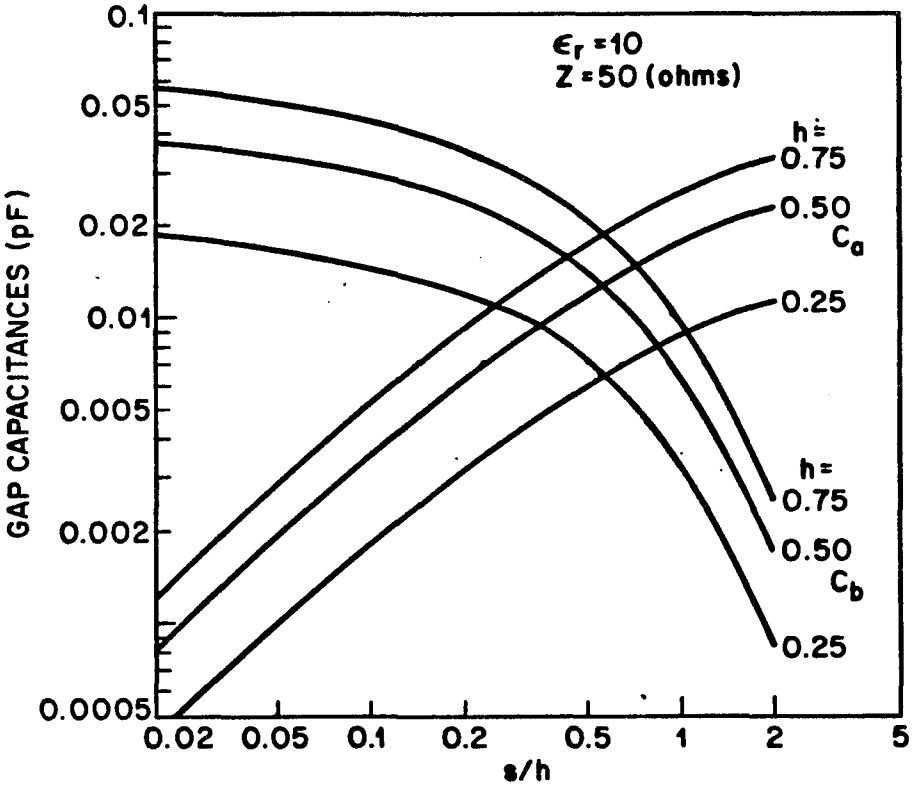

FROM: M.MAEDA: IEEE TRANS. MICROWAVE THEORY TECH. MTT-20, 390 (1972)

Fig. (3.1.2-3)

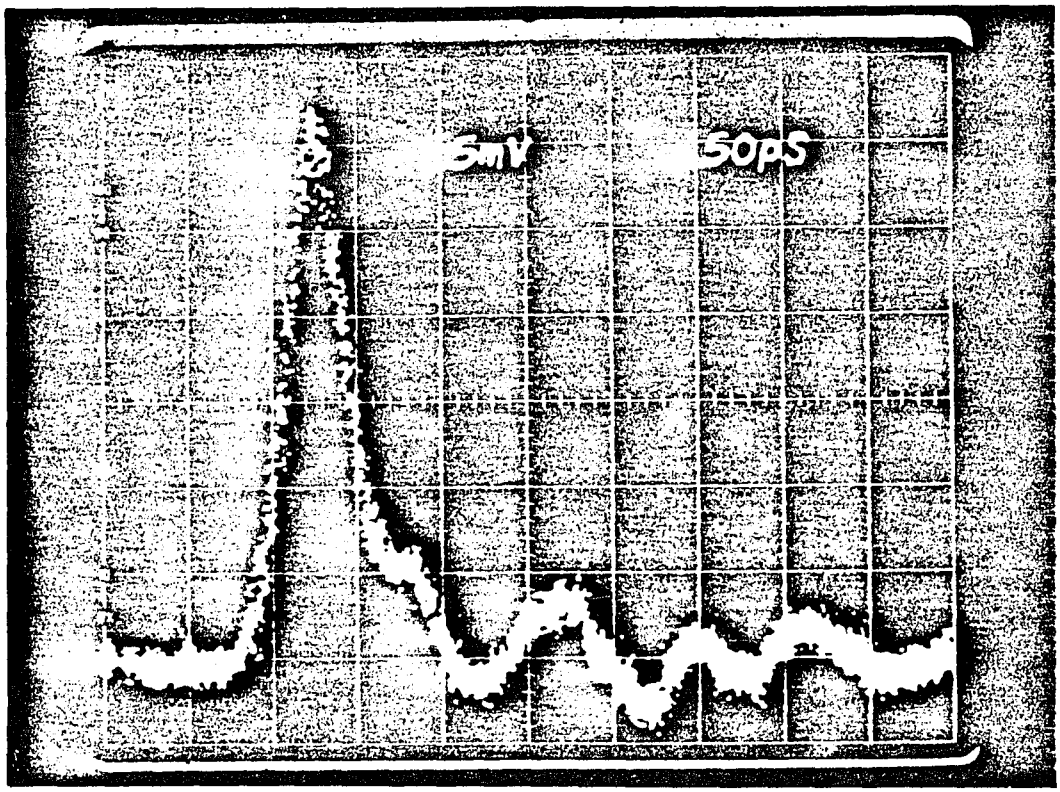

Fig. (3.1.2-4): Sampling Oscilloscope Trace of a Chemical Vapor-Deposited (CVD) a-Si Photodetector Activated by 3.5-ps Optical Pulses From a Mode-Locked Dye Laser.

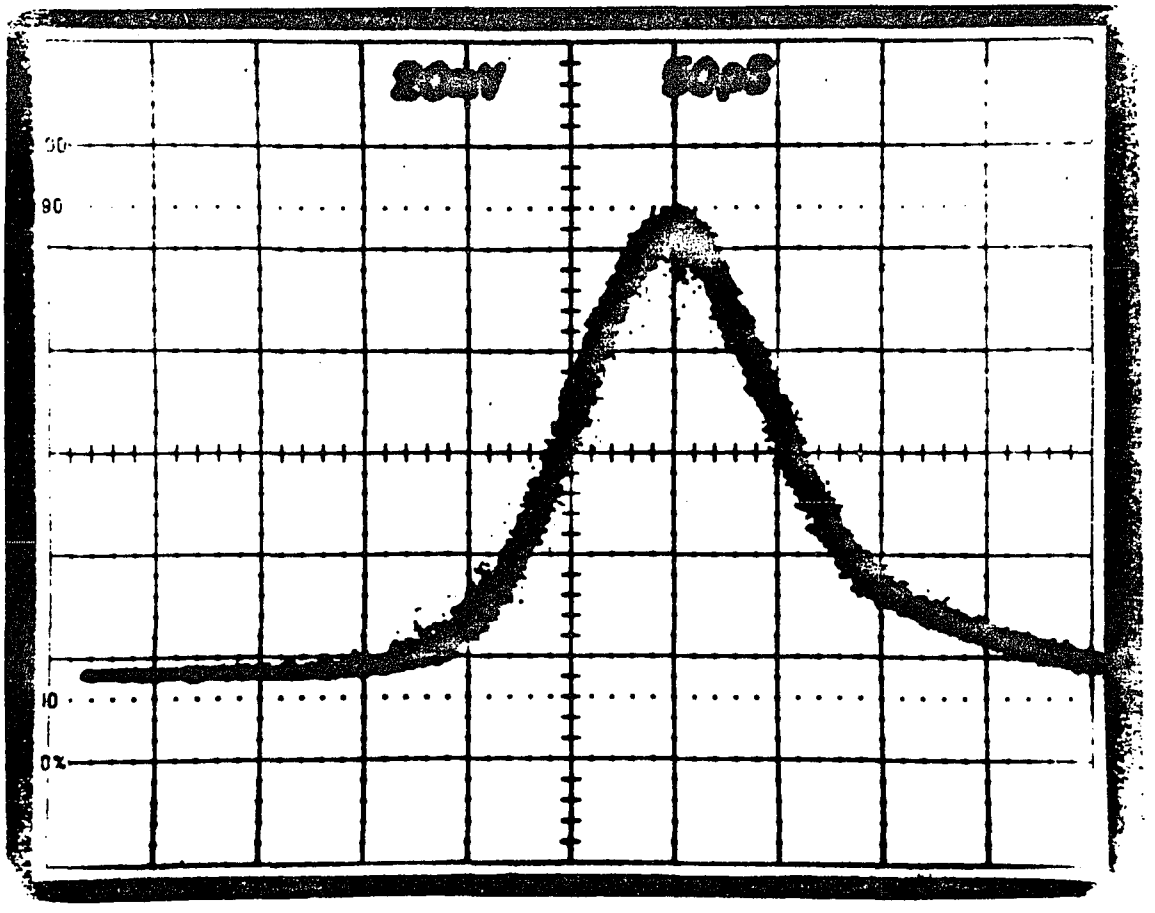

Fig. (3.2.1-1): Mode-Locked Argon Laser Pulsewidth as Determined by the Sampling Oscilloscope Response of a Radiation Damaged Silicon-On-Sapphire (SOS) Photodetector (t_p = 115-ps (FWHM))

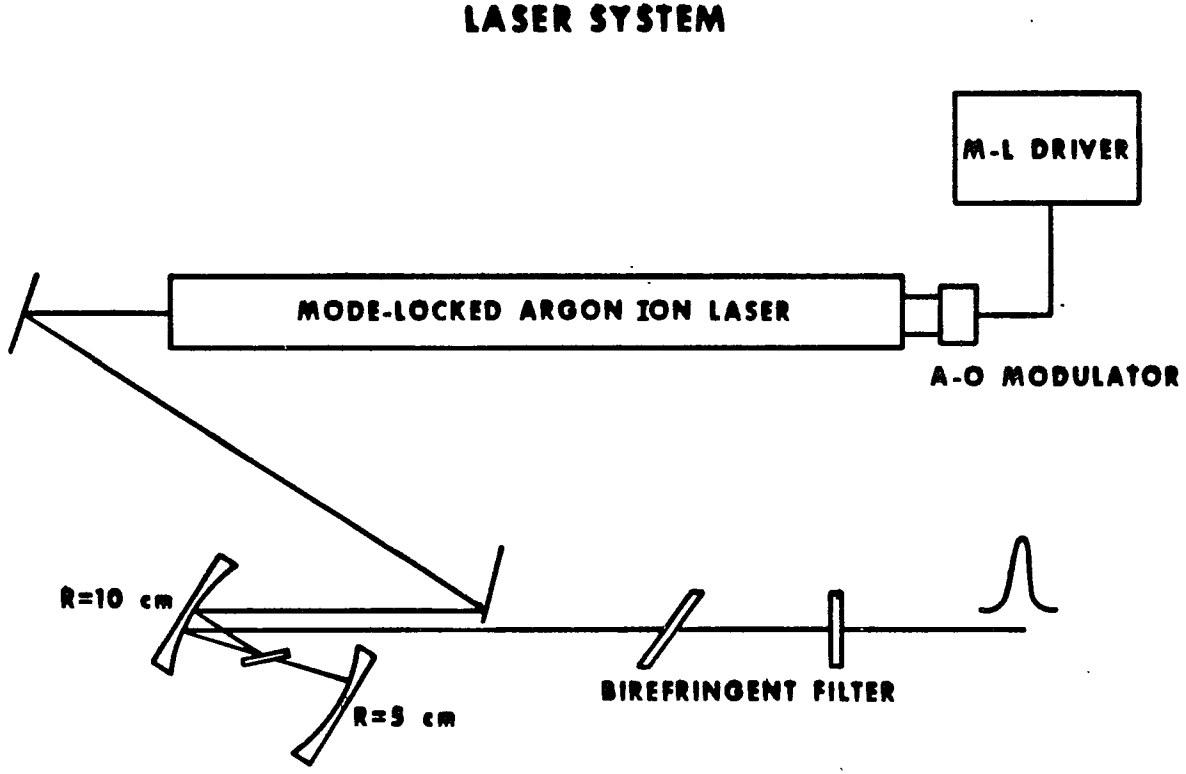

Fig. (3.2.2-1): Synchronously Mode-Locked CW Rh6G Dye Laser

LASER PARAMETERS

MODE-LOCKED ARGON ION LASER

WAVELENGTH	λ = 514.5 nm
AVERAGE POWER	P_{AV} = 700 mW
PULSE DURATION	τ_p = 115 ps
REPETITION RATE	f_r = 81.9 MHz
PEAK POWER	P_p = 74 W

SYNCHRONOUSLY MODE-LOCKED DYE LASER

WAVELENGTH	λ = 575 nm = 2.15 eV
AVERAGE POWER	P_{AV} = 100 mW
PULSE DURATION	τ_p = 3.5 ps
REPETITION RATE	f_r = 81.9 MHz
PEAK POWER	P_p = 350 W
PULSE ENERGY	$\epsilon_p = 1.2 \times 10^{-9}$ J = 3.5×10^9 PHOTONS

Fig. (3.2.2-2)

NONLINEAR OPTICAL AUTOCORRELATION

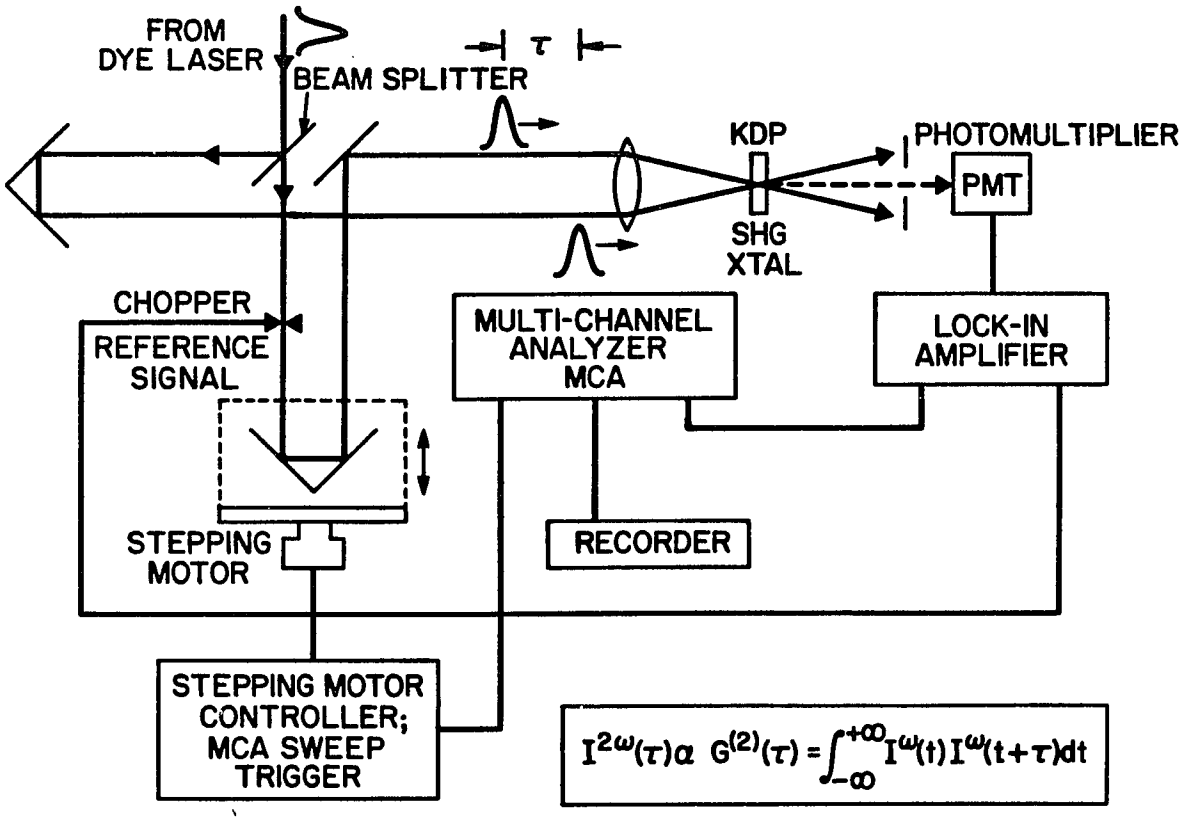

Fig. (3.2.3-1)

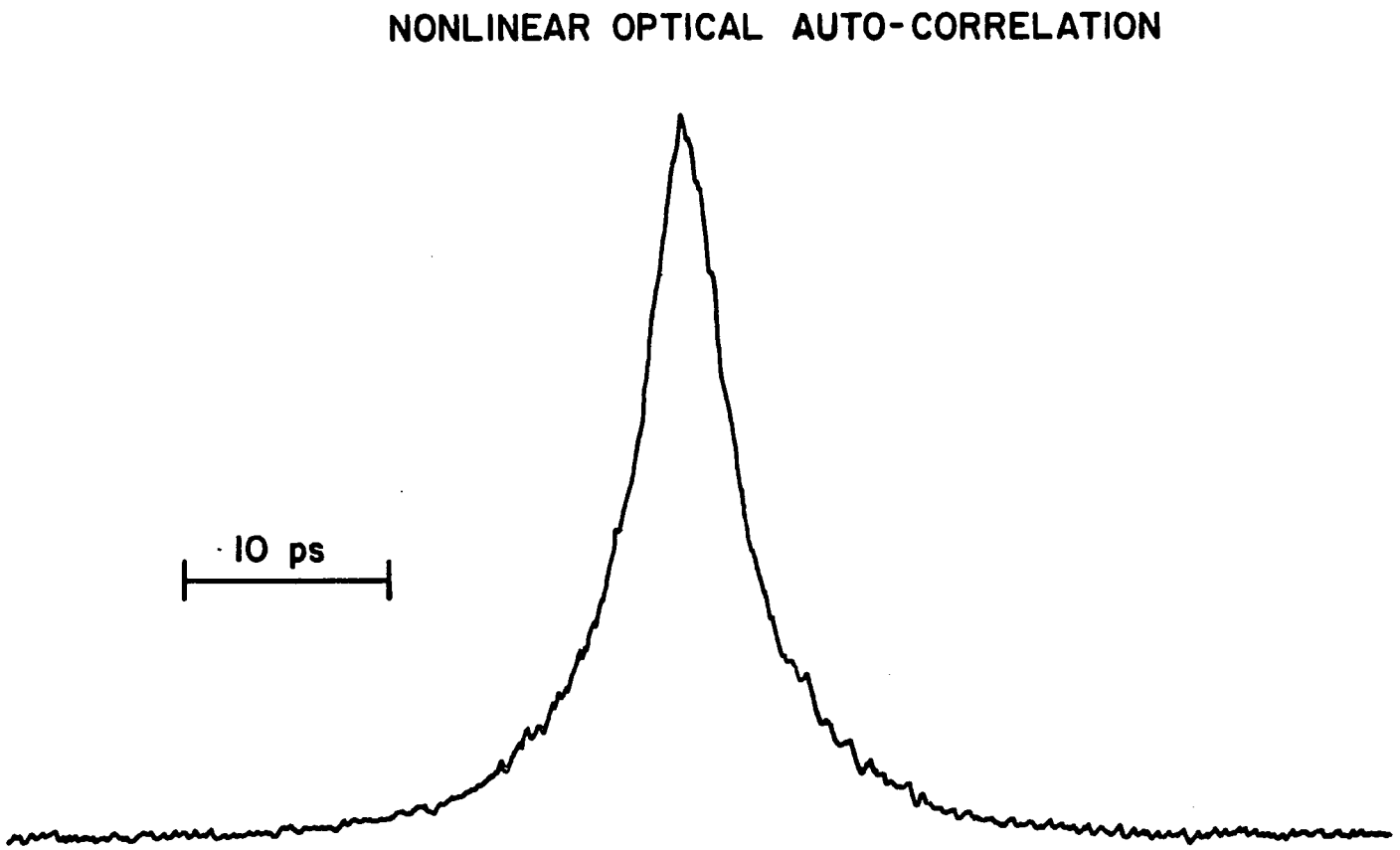

Fig. (3.2.3-2): Dye Laser Pulsewidth Using Nonlinear Optical Autocorrelation

PHOTOCONDUCTIVITY (THE TRADITIONAL APPROACH)

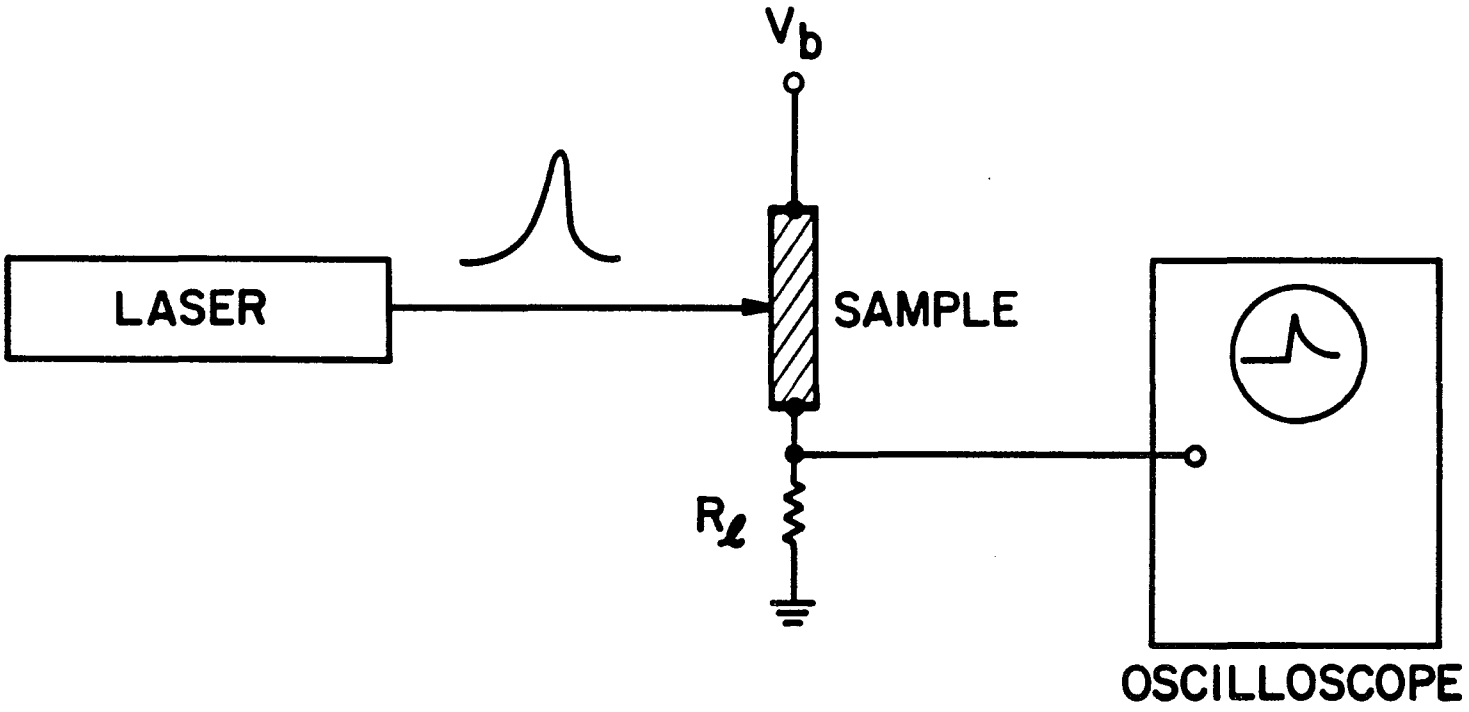

Fig. (3.3-1)

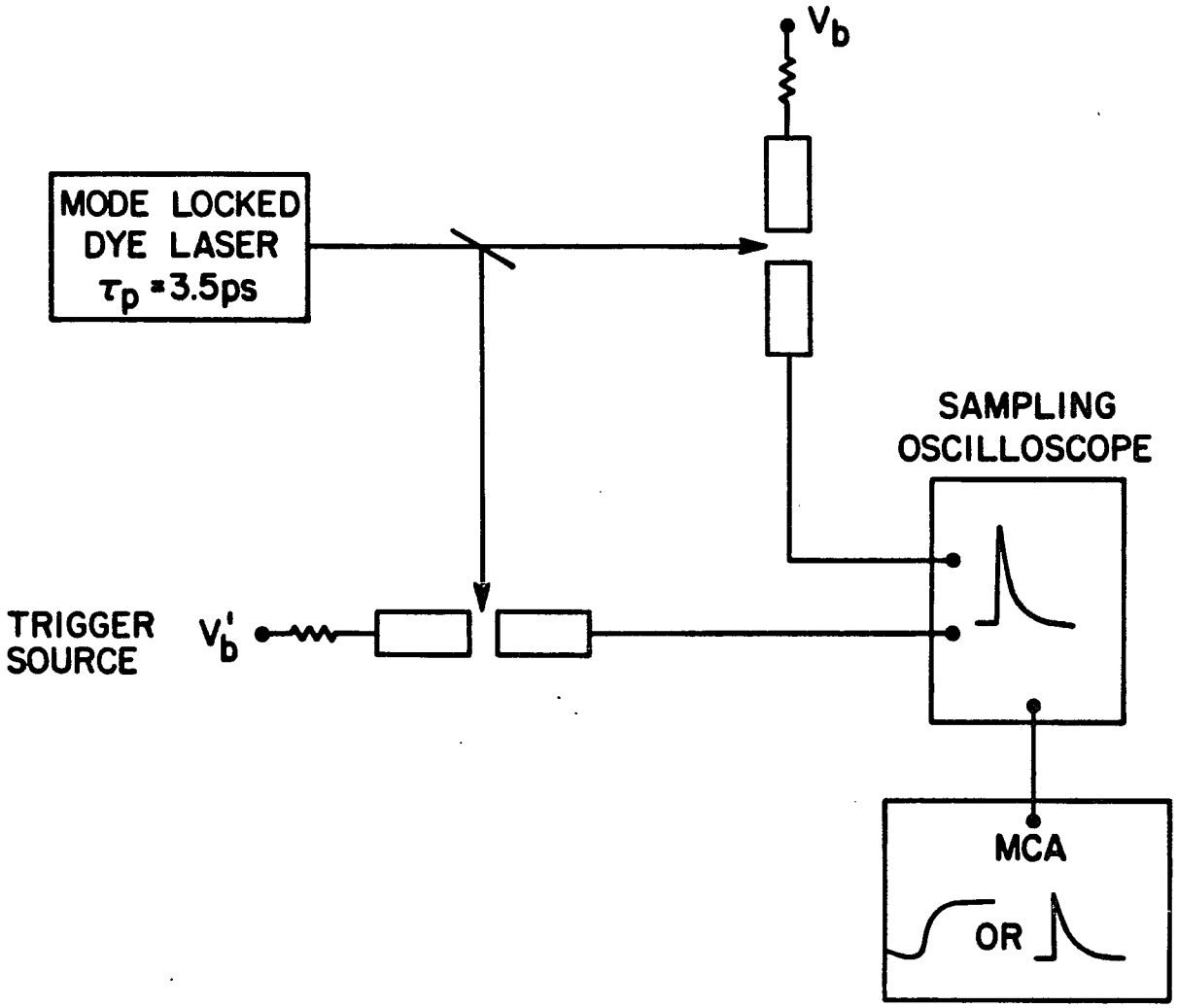

Fig. (3.3.1-1): Sampling Oscilloscope Measurement of Picosecond Photocurrent Transients

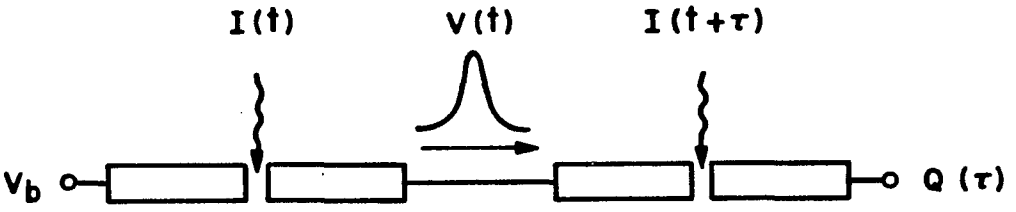

$$G^{(2)}(\tau) \propto Q(\tau) \propto V_b Z_o \int_{-\infty}^{+\infty} g_1(t)\, g_2(t+\tau)\, dt$$

Fig. (3.3.2-1): Electronic Correlation of the Response of Two Photoconductors

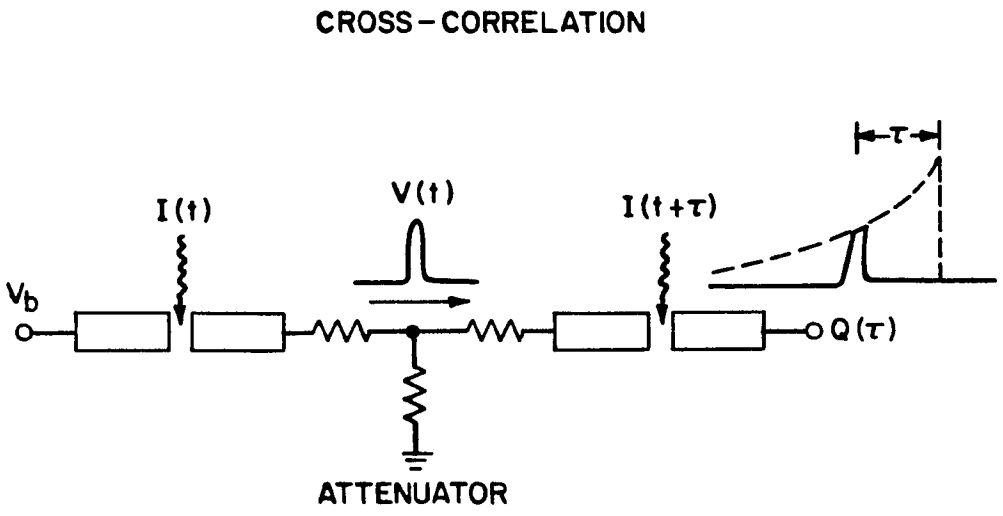

Fig. (3.3.2-2): Electronic Cross-Correlation of the Response of Two Dissimiliar Photoconductors

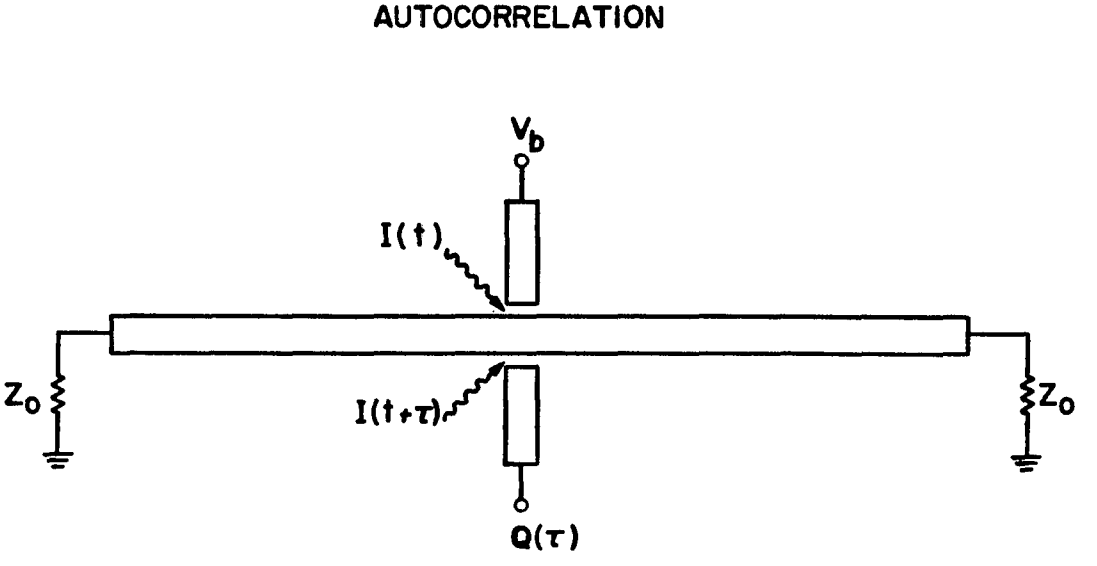

Fig. (3.3.2-3): "Symmetric Gap" Electronic Autocorrelation Scheme

IV. EXPERIMENTAL RESULTS

This chapter describes the experimental results of electronic transport, utilizing picosecond photocurrent transients, in amorphous silicon. Three different film-growth techniques were utilized to intentionally produce large differences in the electrical and optical properties of amorphous silicon. The three types studied were ultra-high vacuum evaporated a-Si (EV), chemical vapor deposited a-Si (CVD), and rf glow-discharge deposited a-Si: H (GD).

4.1 Summary of Results

Tables (4-1) and (4-2) summarize the room temperature results for the three types of a-Si studied. The specific data for each type of a-Si will be discussed in the ensuing sections. The different types of a-Si can be classified by the defect densities incorporated in the different methods of preparation. A lower limit to this density is the number of dangling bonds that yield a strong electron spin resonance (ESR) signal due to unpaired spins. Table (4-1) lists the different types of a-Si according to the spin densities noted in the literature (Davis, 1979; Hirose et al., 1977; Solomon, 1979). The differences between the materials is even further emphasized by the large variations in the measured dark resistivity, ρ_d, mobility-relaxation time product, $\mu\tau$, relaxation time, τ, photosensitivity, g, photoconductive gain, G, and mean drift distance, $<x>$.

Numerical values for the mobility and the mobility-relaxation time product were obtained from the photoconductivity expressions (Section 3.3.1 and Appendix I):

$$i_p = \eta \frac{e}{\hbar\omega}(1-R)(1-e^{-\alpha d})\frac{V_b}{\ell^2}\mu\,\epsilon_p \qquad (4.1\text{-}1)$$

and

$$Q = \eta \frac{e}{\hbar\omega}(1-R)(1-e^{-\alpha d})\frac{V_b}{\ell^2}\mu\,\tau\,\epsilon_p\,. \qquad (4.1\text{-}2)$$

The above expressions assume a uniform electric field in the gap uniquely determined

by the stored charge on the electrodes ($Q = C_g V_b$). In addition it is assumed that this field is unperturbed by the free carriers created in the gap by the absorption of the optical pulses. For volume-excited photocurrents, with minor exceptions, positive and negative charges are equally distributed, the material is electrically neutral and space-charge effects do not enter in (Rose, 1951). The term volume-excited photocurrents is used to define those photocurrents that result when an insulating sample is uniformly illuminated between electrodes. This is to distinguish the currents from those resulting when only one end of the insulating sample is illuminated. Thus the neutralizing effect of the equal and opposite charges of electrons and holes satisfies the condition of an unperturbed electric field if the illumination is uniform and no space-charge accumulation occurs at the electrodes (i.e. ohmic contacts). In addition it was assumed that the carrier velocities varied linearly with electric field, with the mobility being a constant of proportionality.

As mentioned above, an important aspect of a linear photoconductor is the nature of the metal-to-semiconductor contact. When a metal is brought into contact with a semiconductor, there is usually a redistribution of charges which results in the formation of a depletion layer in the semiconductor (Rhoderick, 1978). This deformation of the band edge at the interface is called a Schottky barrier. A voltage applied across the metal and semiconductor will be largely concentrated at the barrier and not across the volume of the semiconductor, because of the high barrier resistance (Bube, 1978). If a Schottky barrier is formed whose width is such that the contact resistance is considerably greater than the bulk resistance of the semiconductor, then most of the bias voltage will be dropped across the electrodes rather than the amorphous semiconductor. In other words, the applied electric field will tend to be concentrated near the electrodes rather than being uniformly distributed across the gap so that the photogenerated carriers which are produced in the relatively low field region of the gap will not make a significant contribution to the photocurrent.

The built-in field associated with a Schottky barrier can also produce a photocurrent in the absence of a bias field whose amplitude and temporal characteristics are determined by the metal-to-semiconductor interface rather than the bulk properties of the semiconductor (Rhoderick, 1978). An additional complication which can arise at moderate optical excitation levels is the accumulation of charge at the electrodes due to the blocking effect of the potential barriers at the metal-to-semiconductor interface. The resulting space-charge field acts in opposition to the bias field and if sufficiently strong will retard the flow of current in the gap between the electrodes. In this case the observed current waveform can have a decay rate which is determined by dielectric relaxation rather than the true carrier relaxation time of the semiconductor.

To avoid these problems, one attempts to make ohmic contacts. For our purposes we can define an ohmic contact as one in which the response of the photoconductor is determined by the bulk properties of the semiconductor rather than the contacts. More specifically, the contact resistance should be negligible compared to the resistance across the gap of the semiconductor. A frequently used approach is to heavily dope the region of the semiconductor in contact with the metal (Rhoderick, 1978). The effect is to make the width of the potential barrier very thin ($< 100\text{Å}$) enabling efficient tunneling currents to flow through the barrier.

Medium and small bandgap amorphous semiconductors ($\epsilon_C - \epsilon_F < 0.8eV$) (this includes a-Si) contacted by metals show hardly any rectification or polarity asymmetry (Fritzsche, 1971, 1974). The contact resistance is usually a small fraction of the total resistance. They do not show the characteristic Schottky barrier layers typical of contacts with crystalline semiconductors. The space-charge regions are only a few hundred Angstrom units wide when they contain a large density of gap states near the Fermi level. The above considerations hold for a density of states at the Fermi level on the order of $g(\epsilon_F) \gtrsim 10^{18}\, cm^{-3}eV^{-1}$. Thus one can readily make ohmic contacts to most varieties of a-Si by the evaporation of aluminum or gold electrodes. This is not

necessarily true of the lower defect density hydrogenated a-Si (GD) which can have Schottky barriers with widths as large as 0.2μm (Wronski, et al., 1976). Nevertheless, due to the extremely high resistivity of a-Si:H (GD) ohmic behavior can be observed in this material if the gap lengths are not too small and low light levels are used.

In cases where it is difficult to make good contacts, it is nevertheless often possible to modify the experiment to neutralize the influence of bad contacts (Auston, 1981). For example, if the electric field due to a dc bias is not uniform, a pulsed bias can be used. If a bias pulse of short duration is applied such that the measurement interval is less than the dielectric relaxation time ($\tau_{REL} = C_g/G$, where G is the conductance and C_g is the capacitance of the gap), then the field will be essentially uniform. The initial photoexcited packet of charge is neutral by virtue of the equal numbers of holes and electrons. The electric field will tend to separate the electrons and holes and in doing so set up a polarization field, whose direction is opposite that of the applied field. The net result is the reduction of the applied field by the action of the polarization field which manifests itself by reducing the photocurrent signal. The characteristic time constant for the decay of the current signal, due to this space-charge induced polarization field, is the dielectric relaxation time. By comparing signals with pulsed and dc bias, one can estimate the extent of the nonuniformity of the dc bias field. The problem of space-charge accumulation at partially blocking electrodes can also be minimized by using low intensity illumination so that the total charge in the photocurrent signal is much less than the stored charge on the gap capacitance due to the bias. This condition is equivalent to requiring the photocurrent to decay in a time much less than the dielectric relaxation time ($\tau \ll \tau_{REL}$). Picosecond time-resolved photoconductivity meets the above criteria and allows the reliable extraction of electronic transport parameters from the photocurrent transients of a-Si.

Figure (4.1-1) summarizes the electronic correlation measurements (Section 3.3.2) of the relaxation of the photocurrent in the three types of a-Si. The correlation

function (Appendix II)

$$G^{(2)}(\tau)\alpha Q(\tau)\alpha\ V_b Z_o \int_{-\infty}^{+\infty} g_1(t)g_2(t+\tau)dt \qquad (4.1\text{-}3)$$

is proportional to the total charge, $Q(\tau)$, produced at the output of the second (sampling) photoconductor, as a function of the relative delay, τ, between the two optical pulses used to activate the two photoconductors. $G^{(2)}(\tau)$ is normalized to unity at zero delay (τ=0), for ease of comparison. Immediately evident is the rapid relaxation of the photocurrent with increasing defect density. The relaxation times, as indicated in Table (4-1), for samples EV, CVD, and GD (room temperature) were 4ps, 16ps, and 200ps respectively. The low temperature (144°K) relaxation time in GD was 25 ps.

4.2 Ultra-High Vacuum Evaporated a-Si (EV)

The evaporated sample contained the highest density of defects, of the samples studied and accordingly had the smallest photosensitivity and photoconductive gain (Table 4-2) due to the rapid relaxation of the photoexcited carriers into the high density of localized states. This sample resulted in a sampling oscilloscope limited response and thus we could not resolve the carrier relaxation time. Thus we integrate the photocurrent response to obtain the charge, Q, and measure the relaxation time, τ, in a separate electronic correlation measurement. For an incident pulse energy, ϵ_p, of 0.26 nJ and an electric field of $2.4\times10^4\ V/cm$, the integrated photocurrent pulse yields a charge, Q, of 2.6×10^{-15} Coulomb. (Gap resistance: Dark, $R_d = 3\times10^6\Omega$; Illuminated, $R_\ell = 2\times10^6\Omega$).

The "symmetric gap" autocorrelation scheme described in Section (3.3.2) was utilized to measure the carrier relaxation time of EV. The experiment is performed twice and results in two autocorrelation responses (Fig. 4.2-1). The central trace is the nonlinear optical second-harmonic autocorrelation (Section 3.2.3) and its peak represents zero optical delay (τ=0). The second-harmonic autocorrelation has a duration of 5.5ps FWHM which results in a pulse width of 3.5ps upon deconvolution. The response on the right-hand side ($\tau > 0$) corresponds to the normal biasing scheme (upper left-hand corner of Fig. (4.2-1) and see Fig. 3.3.2-2) in which the dc biased "impulse generating" gap is activated by an optical with a fixed optical path length and the charge collecting "sampling" gap is activated by an optical pulse with a variable optical path length. The positive delay of the peak is electronic in nature and is due to the finite circuit response arising from the capacitance of the two gaps and the propagation delay across the main transmission line. It takes approximately 1.5ps for the charge to propagate across the main transmission line. The response on the left-hand side ($\tau < 0$) corresponds to a situation in which the bias and charge collecting electrodes are interchanged, leaving the optics unaltered (upper right-hand corner of

Fig. (4.2-1)). This merely corresponds to interchanging two cables. In this case the "sampling" gap is activated by an optical pulse with a fixed path length. Due to the electronic delay mentioned above the "impulse" must be initiated earlier ($\tau < 0$) in order to be "sampled" by the charge collecting electrode. Thus, this interchange of cables is equivalent to a time reversal, and enables an accurate determination of the zero time delay (i.e. the simultaneous arrival of the two optical pulses). The electronic autocorrelation function reaches a maximum at a delay of 3.5ps, and has a duration of 11ps FWHM. The wings are exponential and slightly asymmetric, having logarithmic slopes of 5.0 and 6.6ps/neper compared to the second-harmonic autocorrelation function, which has a slope of 4.7ps/neper. The width, however, is broader by a factor of two due to both the finite relaxation time of the photogenerated carriers, the circuit response, and the propagation delay between the gaps. A detailed analysis of this particular circuit shows that the asymmetry and delay in the autocorrelation function are determined solely by the circuit response function and is not affected by the finite optical pulse width and carrier relaxation time (Auston, 1981; Appendix II). With this knowledge the autocorrelation function can be approximately deconvolved for the carrier relaxation time. We estimate the carrier relaxation time, τ, to be $4 \pm 1ps$ and the circuit time constant to be $4 \pm 2ps$. This circuit time constant (two gaps) is consistent with an estimated gap capacitance of 0.02pF (Section 3.1.2). The duration of the electrical pulse on the main transmission line is estimated to be 8ps (FWHM). Thus the time resolution of this scheme is $\lesssim$ 10ps.

Insertion of the measured charge, Q, into Eqn. (4.1-2) yields $\eta\mu\tau = 4.2\times10^{-12}\ cm^2/V$. Dividing this quantity by τ (= 4ps) yields $\eta\mu = 1.1\ cm^2/Vs$. (Figure 4.2-2 is a single trace of the EV autocorrelation).

4.3 Chemical Vapor Deposited a-Si (CVD)

The CVD sample has an intermediate density of defects, and a photosensitivity and photoconductive gain that is somewhat higher than EV. This sample also resulted in a sampling oscilloscope limited response and thus we could not resolve the carrier relaxation time. An example of the sampling oscilloscope response of this material was given in Fig. (3.1.2-4).

As in the case of EV, we integrate the photocurrent response to obtain Q and measure τ in a separate electronic correlation measurement. For an incident pulse energy of 0.24 nJ and an electric field of $2.8\times10^4\ V/cm$, the integrated photocurrent pulse yields a charge, Q, of 1.5×10^{-14} Coulomb. (Gap resistance: Dark, $R_d = 9\times10^9\Omega$; Illuminated, $R_\ell = 5\times10^5\Omega$).

As in the case of EV, the "symmetric gap" autocorrelation scheme was utilized to measure the carrier relaxation time of CVD. The electronic autocorrelation function of CVD is given in Fig. (4.3-1). In this material the carrier relaxation time is somewhat slower than the circuit response and the "time reversal" procedure used in the case of EV is unnecessary to separate out the circuit response. The slower decay of the CVD sample permits us to obtain a measure of τ directly from the initial exponential decay of the autocorrelation function, without the need for deconvolving the circuit and material responses. We thus obtain a value of $\tau = 16ps$. As an indication of the reproducibility of this technique, it is interesting to note that identical autocorrelation traces were measured from the CVD sample of D. Kaplan (France) and the LPCVD sample of A. C. Adams (Bell Labs).

Insertion of the measured charge, Q, into Eqn (4.1-2) yields $\eta\mu\tau = 2.3\times10^{-11}\ cm^2/V$. Dividing this quantity by τ (= 16ps) yields $\eta\mu = 1.4cm^2/Vs$.

Figure (4.3-2) is the electronic cross-correlation of EV and CVD. This trace is the result of using the fast response of EV as a very fast impulse generator to probe the

slower response of CVD. In this situation the slower response dominates and results in a very fast, jitter-free, sampling (oscilloscope) with a risetime of 17ps.

4.4 RF Glow-Discharge Deposited a-Si: H (GD)

The plasma-deposited sample has the lowest density of defects and the highest photosensitivity and photoconductive gain and is technologically the most interesting of the samples (a low density of defects is necessary for device applications; see Introduction). The lower defect density of GD results in a longer carrier relaxation time that can be resolved on the sampling oscilloscope. The slope of the initial non-exponential decay yields a carrier relaxation time of approximately 200ps (Fig. 4.4-1). For an incident pulse energy of 0.26nJ ($P_{avg} = 21mW$, 1.4×10^{14} photons/cm^2, 7×10^{18} photons/cm^3, 1.2×10^{22} photons/cm$^2 s$) and an electric field of $1.8\times10^4\ V/cm$, the peak value of the photocurrent, i_p, is 0.4mA. Insertion of this quantity into Eqn (4.1-1) yields $\eta\mu = 0.8cm^2/Vs$. (Gap resistance: Dark, $R_d = 2\times10^{11}\,\Omega$; Illuminated, $R_\ell = 2\times10^5\,\Omega$).

As discussed in Section (4.1), of the materials studied, GD is the one material in which the effects of the electrodes must be considered, due to the lower density of defects. As already mentioned, the combined effects of the high resistivity and a carrier relaxation time, τ, approximately an order of magnitude smaller than the dielectric relaxation time, τ_{rel}, (Table 4-2) should eliminate any electrode effects upon the data. Several tests were made to test this assertion.

A very strong indication that the effects of the contacts are minimal is the pulsed-bias cross-correlation (Section 3.3.2) of GD (Fig. 4.4-2). This non-exponential decay of GD is a cross-correlation between itself and a fast ($\tau = 22ps$) high-mobility ($40cm^2/Vs$), radiation damaged silicon-on-sapphire sample discussed in Section (3.2.1). In this case an electrical pulse is applied to GD in a time, two orders of magnitude shorter than the dielectric relaxation time. The result is a photocurrent decay that is very similar to the dc biased sampling oscilloscope measurement (Fig. (4.4-1)) in the early stages of the transient photocurrent. By comparing the tails in the two measurements one can see what may be evidence of the early stages of dielectric relaxation in

the tail of the dc biased measurement. Dielectric relaxation would tend to reduce the applied field, thereby reducing the amplitude of the photocurrent. The pulsed bias case results in a long slowly decaying tail. The dc biased case reveals a more rapidly decaying tail, which is down to ~1% of the initial peak amplitude before the arrival of the next optical pulse (~ 12 ns). The improved time resolution and further sharpening of the peak in the cross-correlation measurement tends to indicate that the response isn't completely resolved in the sampling oscilloscope measurement. This would result in an underestimated mobility and tend to push it up further toward a value of 1 cm^2/Vs.

If space-charge was a problem in these measurements, one would expect to see a nonlinear dependence of the amplitude of the photocurrent with respect to light intensity. Both the peak photocurrent (Fig. 4.4-3) and the photocurrent integrated in a 160 Keithley Digital Multimeter (Fig. 4.4-4) show a linear dependence upon photon flux.

The GD sample was placed in a liquid nitrogen dewar that was fitted with high speed stainless steel coaxial cable and feedthroughs, which permitted both sampling oscilloscope and cross-correlation measurements. The field dependence was tested at two lower average powers. The lower power was due to, in part, loss in the optical window of the dewar and the need to use a longer focal length lens (from 3-cm to 8-cm focal length) to get the light in. The field dependence was performed at average powers of 2mW (1.1×10^{21} photons/cm^2s, Fig. 4.4-5) and 7mW (4×10^{21} photons/cm^2s, Fig. 4.4-6), well within the linear range of the photocurrent-photon flux curves. For bias voltages above 20V (7.7×10^3 V/cm) the field dependence of the peak photocurrent is roughly linear. (The previously mentioned mobility measurement was performed at $V_b = 47V$ or 1.8×10^4 V/cm). The deviation at low bias voltage is probably due to the fact that the number of photoexcited carriers is approaching the number of carriers supplied by the electrodes ($q = C_g V_b$). If this happens then the field is no longer determined solely by the charge in the electrodes, but is perturbed by the photocreated charges.

The intensity dependence of the photocurrent was measured at $T = 155K$ ($1/T = 6.5\times10^{-3}\ K^{-1}$). Figure (4.4-7) is the integrated photocurrent measured as a function of photon flux. The photocurrent is a linear function of photon flux up to a value of approximately 2×10^{21} photons/cm^2s ($P_{avg} = 4mW$), after which the photocurrent varies with photon flux raised to the power of 1.86. The super-linear intensity dependence is believed to be due to optical heating. The low temperature measurements were done on the linear portion of this curve. (See Appendix III for an estimate of the laser-induced temperature rise in a-Si.)

The temperature dependence of the peak photocurrent, i_p, and therefore the initial mobility was measured in the cross-correlation scheme. As in the room-temperature cross-correlation measurement of GD (Fig. (4.4-2)) the radiation-damaged silicon-on-sapphire photodetector ($\tau = 22ps$) was used as an impulse generator to probe the temperature dependence of the response of GD. In the room temperature measurement an attenuator separated the two photoconductors. In this experiment the sample GD was silver pasted onto the copper cold-finger of the cryostat and fitted with 18 GHz coaxial-to-microstrip connectors. Approximately 20cm of stainless-steel UT-85 coaxial cable connected the photodetector to a high-speed coaxial feed-through. Outside the cryostat, the radiation damaged silicon-on-sapphire photodetector and attenuator were connected to the feed-through to complete the impulse-generator. The output of the GD photoconductor was connected to a similar length of coaxial cable and connected to the lock-in-amplifier through a similar feed-through. The resolution of this measurement is approximately 25ps. The time resolution is primarily limited by the response of the radiation damaged silicon-on-sapphire photodetector ($\tau = 22ps$). The extra length of coaxial cable between photoconductors may introduce skin effect losses (vary as the square root of the frequency) which can be considerable at very high frequencies. Such losses could degrade the circuit response time. By measuring the relative change of the peak amplitude of the cross-correlation function as a function of temperature, we

obtained the temperature dependence of the initial mobility normalized to it's value at 282K. To equate the temperature dependence of the photoconductivity with the mobility requires a temperature independent absorptance. Using a silicon photodetector we measured a transmission of 2.8% at 292K and 3.5% at 158K which results in an insignificant change in the absorptance.

Figure (4.4-8) is an Arrhenius plot of the normalized mobility. The temperature dependence of the initial mobility has the form:

$$\mu = 8 \exp(-0.058/kT) .$$

The preexponential factor, which is an infinite temperature extrapolation, has the value

$$\mu_o = 8 cm^2/Vs ,$$

and the slope yields a thermal activation energy of approximately 58meV.

In cooling the sample from 292K to 144K the relaxation time decreases (Fig. 4.1-1 and 4.4-9) from 200ps to 25ps (resolution limit of the cross-correlation measurement) and the initial mobility falls from $0.8 cm^2/Vs$ to $0.07 cm^2/Vs$. The initial decay at 144K is very fast but begins to level off and decay at a slower rate after a delay of 140ps. The mobility at this point is approximately $0.006 cm^2/Vs$.

SAMPLE	[cm^{-3}] ESR	[°C] T_d	[Ω-cm] ρ_d	[cm^2/V] $\eta\mu\tau$	[ps] τ	[cm^2/Vs] $\eta\mu$
EV	10^{19}-10^{20}	300	2800	4.2×10^{-12}	4	1.1
CVD	10^{18}-10^{19}	600	9.2×10^{6}	2.3×10^{-11}	16	1.4
GD	$<10^{16}$	250	10^{8}	–	200	0.8

T_d : DEPOSITION TEMPERATURE

ρ_d : DARK RESISTIVITY

Table (4-1): Initial Mobility (Room Temperature), Typical Spin Densities Noted in the Literature, as Determined by Electron-Spin Resonance (ESR), and Material Properties of Ultra-High Vacuum (UHV) Evaporated a-Si (EV), Chemical Vapor Deposited a-Si (CVD), and RF Glow-Discharge Deposited a-Si:H (GD)

SAMPLE	[V/cm] E	[mhos/J] g	ηG	[Å] $\eta\langle X\rangle$	[ns] τ_{REL}
EV	2.4×10^{4}	1.8×10^{3}	3.6×10^{-5}	10	32
CVD	2.8×10^{4}	7.9×10^{3}	2.5×10^{-4}	64	8
GD	1.8×10^{4}	2.5×10^{4}	1.1×10^{-3}	288	2

g : PHOTOSENSITIVITY ($i_p / V_b \epsilon_p$)

G : PHOTOCONDUCTIVE GAIN ($\mu \tau V_b / \ell^2$)

$\langle X \rangle$: MEAN DRIFT DISTANCE ($\mu \tau E$)

τ_{REL} : DIELECTRIC RELAXATION TIME

Table (4-2): Room Temperature Photoconductive Properties of Ultra-High Vacuum (UHV) Evaporated a-Si (EV), Chemical Vapor Deposited a-Si (CVD), and RF Glow-Discharge Deposited a-Si:H (GD)

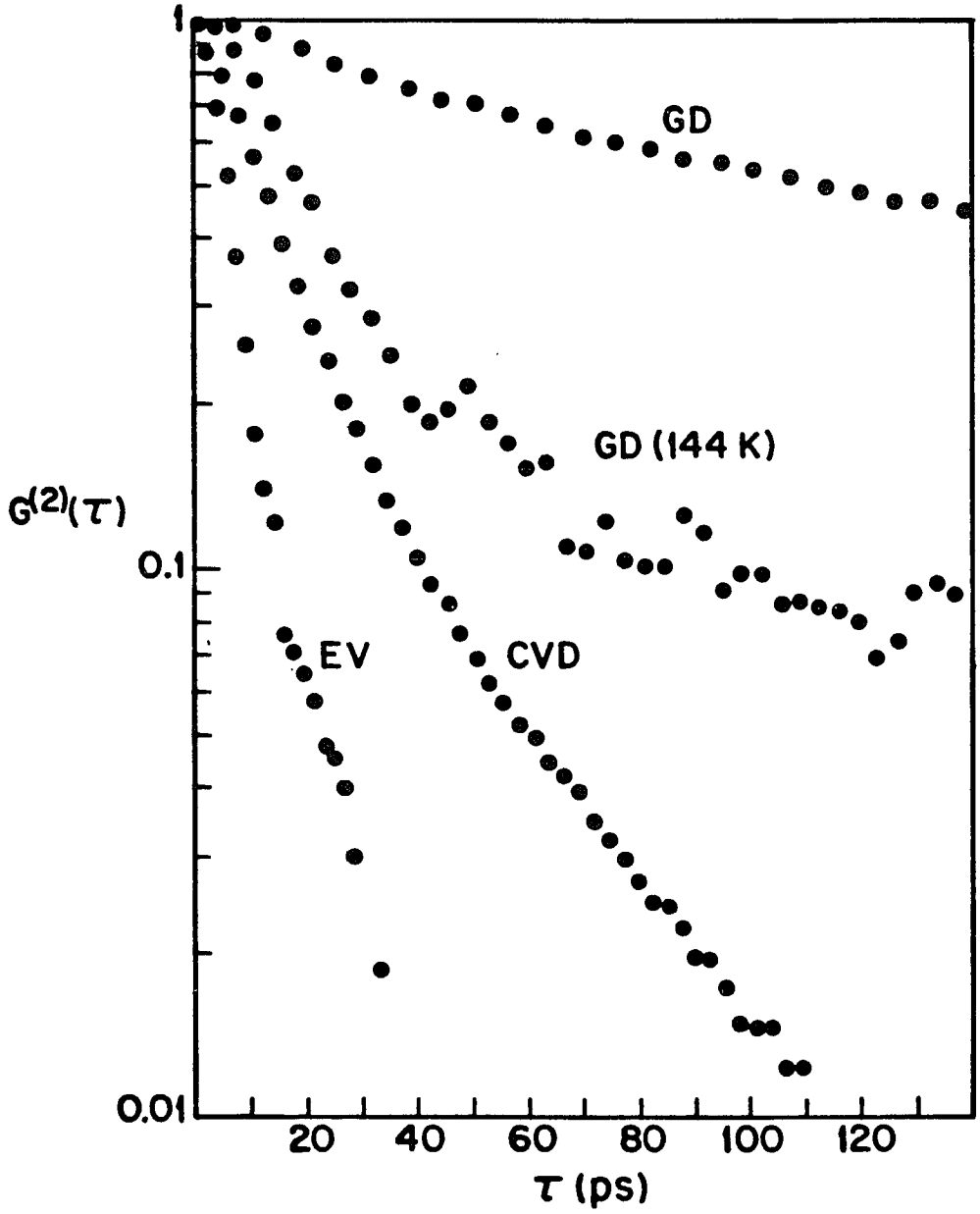

Fig. (4.1-1): Room Temperature Electronic Correlation Functions (Normalized to Unity for Ease of Comparison) of the Various Forms of a-Si as a Function of the Relative Delay Between the Responses of the Two Photoconductors and the Response of GD at T = 144K

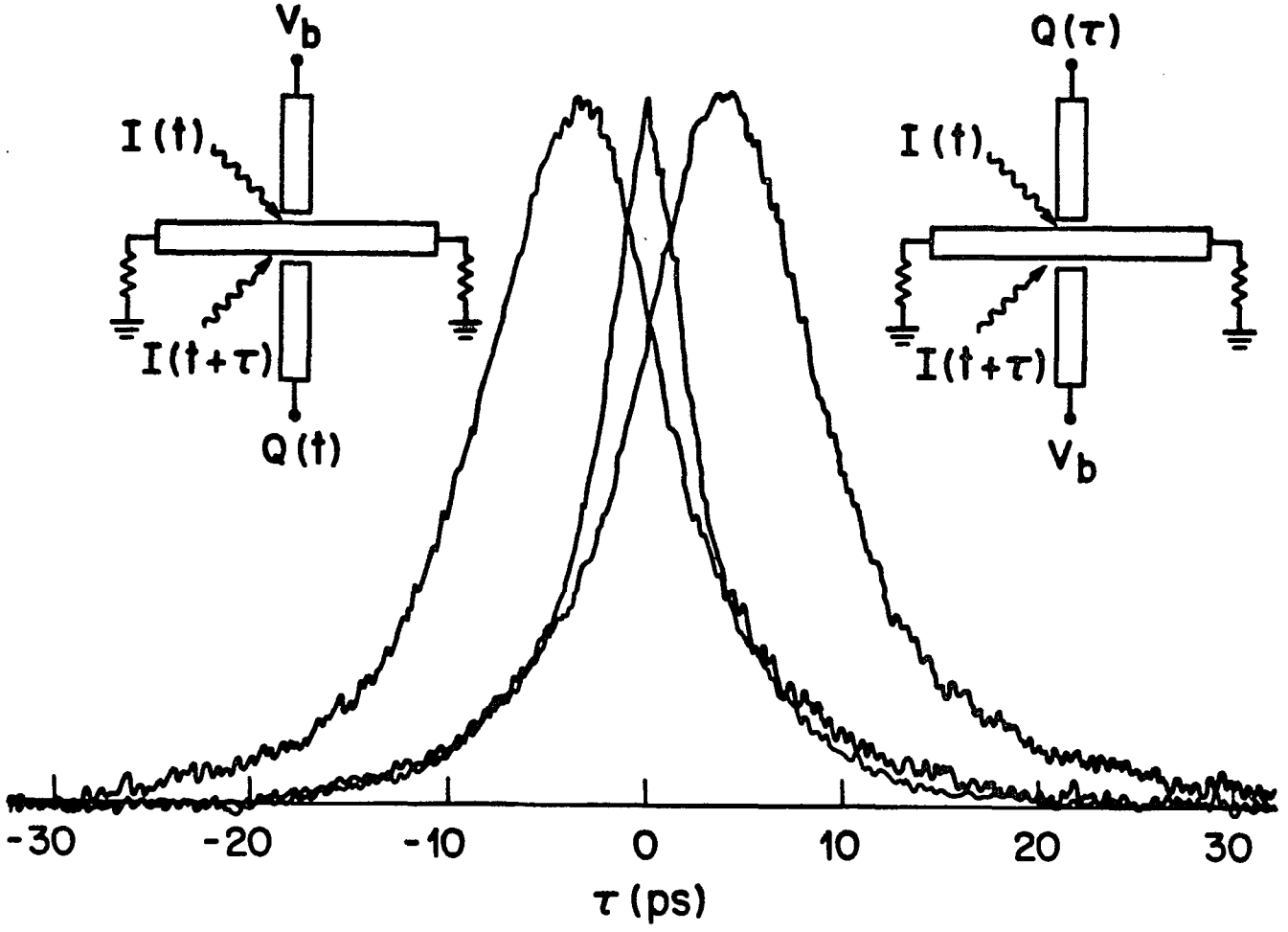

Fig. (4.2-1): Room Temperature Electronic Autocorrelation of Ultra-High Vacuum Evaporated a-Si (EV) and Nonlinear Optical Autocorrelation of the Dye Laser Pulses

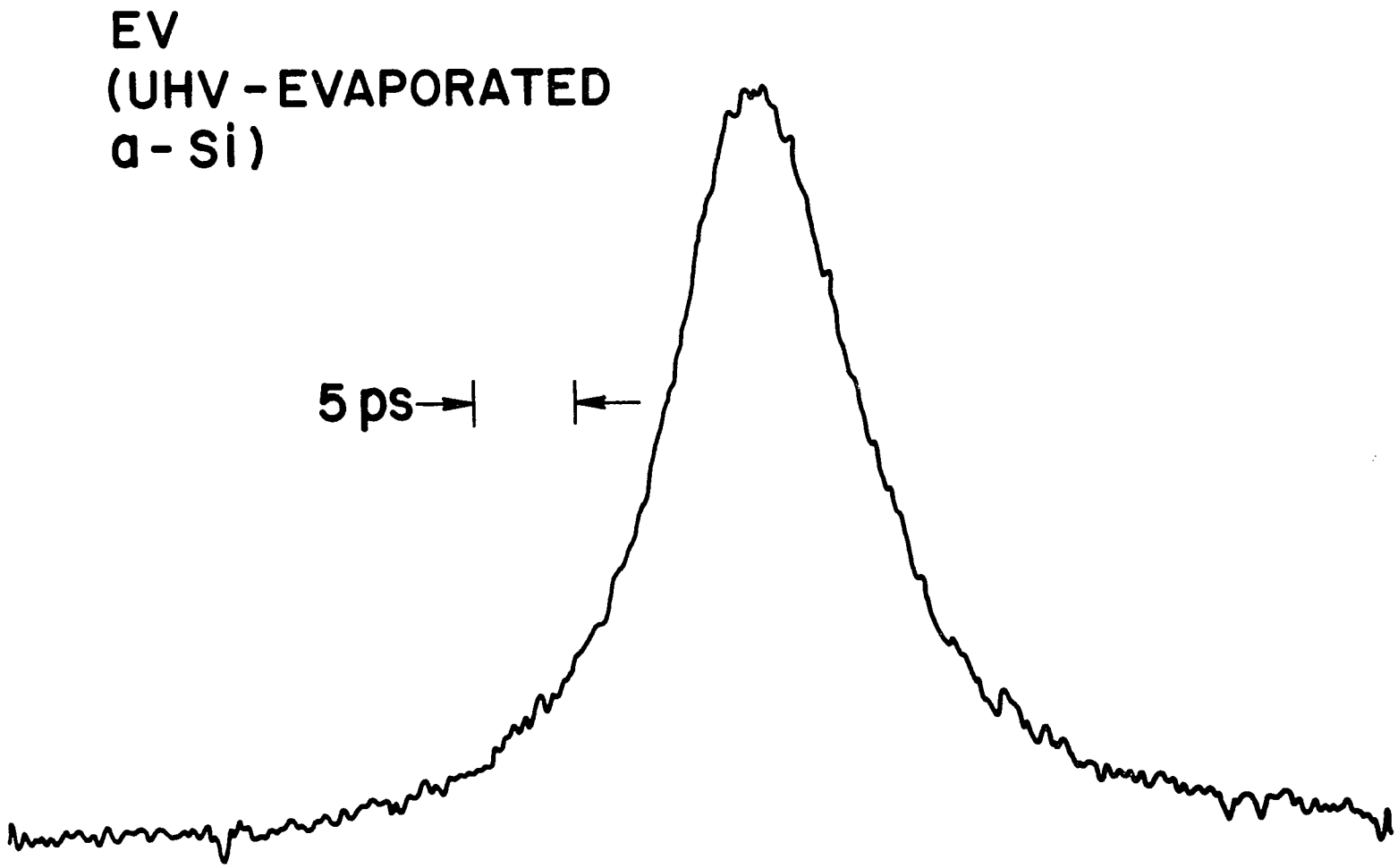

Fig. (4.2-2): Room Temperature Electronic Autocorrelation of Ultra-High Vacuum (UHV) Evaporated a-Si (EV)

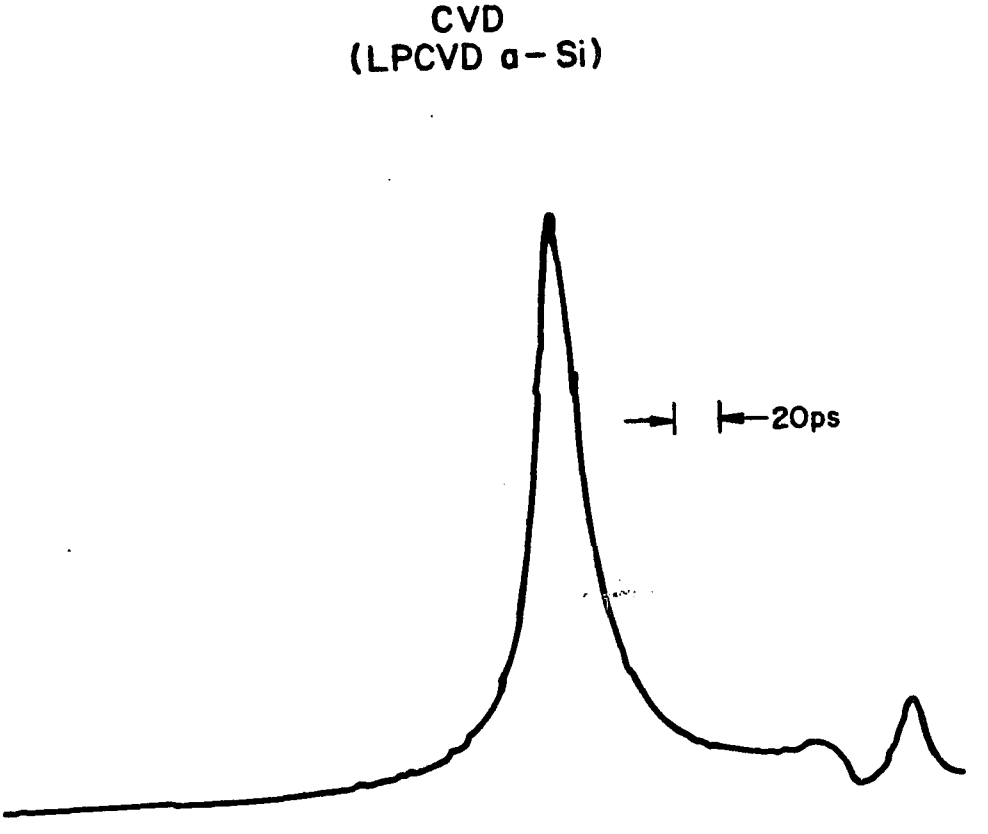

Fig. (4.3-1): Room Temperature Electronic Autocorrelation of Low-Pressure Chemical Vapor Deposited (LPCVD) a-Si (CVD)

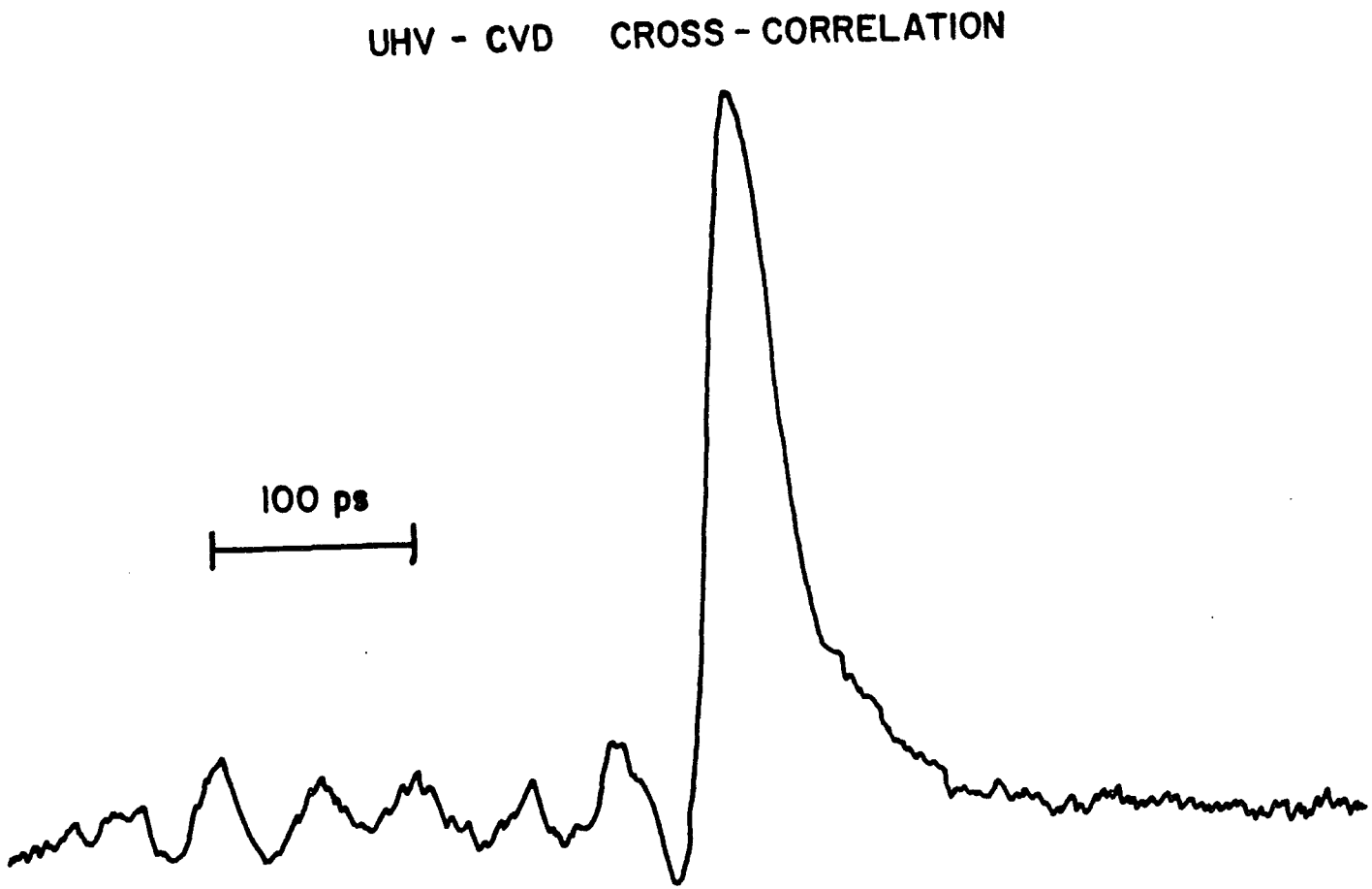

Fig. (4.3-2): Room Temperature Electronic Cross-Correlation of Ultra-High Vacuum (UHV) Evaporated a-Si (EV) and Chemical Vapor Deposited a-Si (CVD)

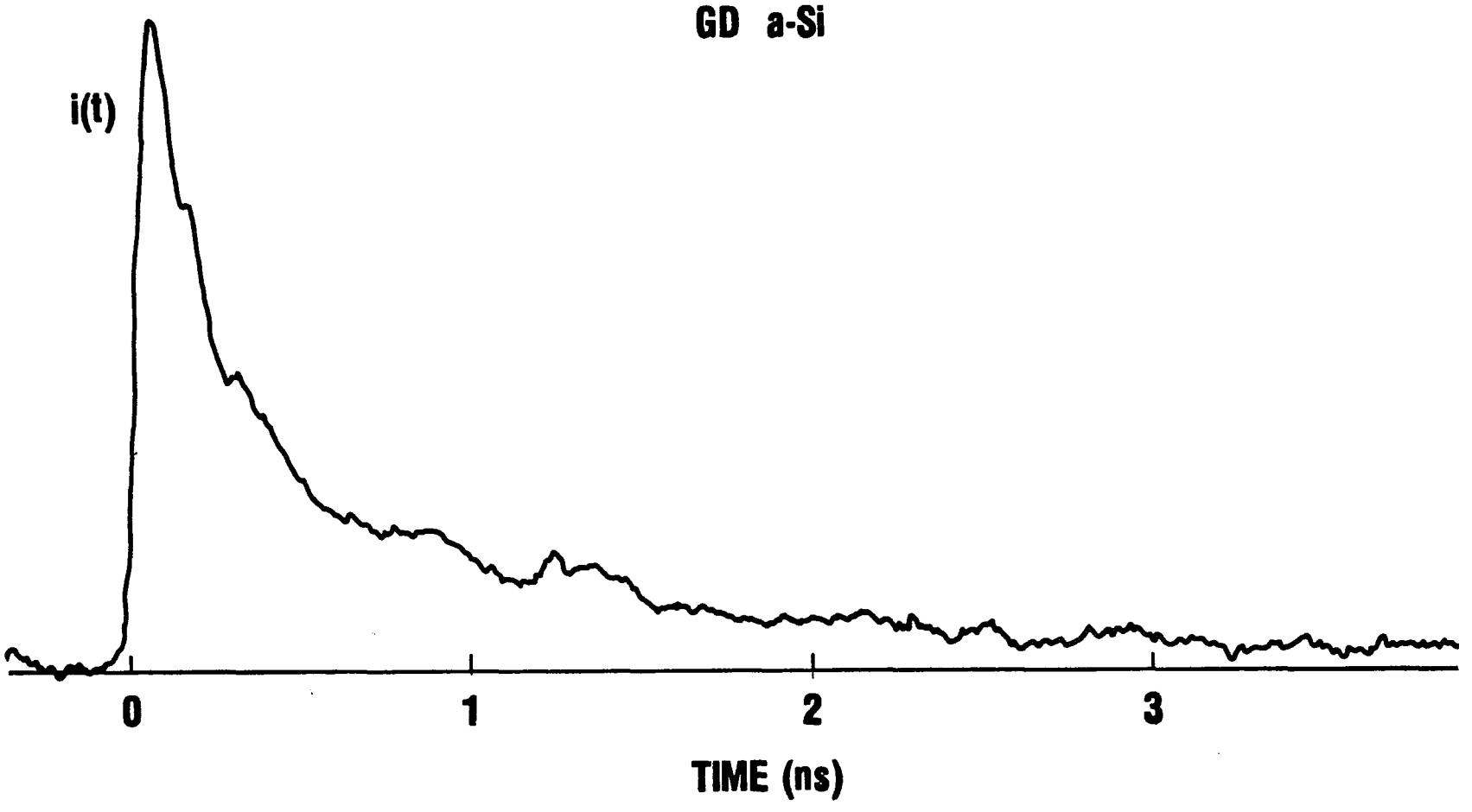

Fig. (4.4-1): Room Temperature DC Biased Sampling Oscilloscope Response of RF Glow-Discharge Deposited a-Si:H (GD)

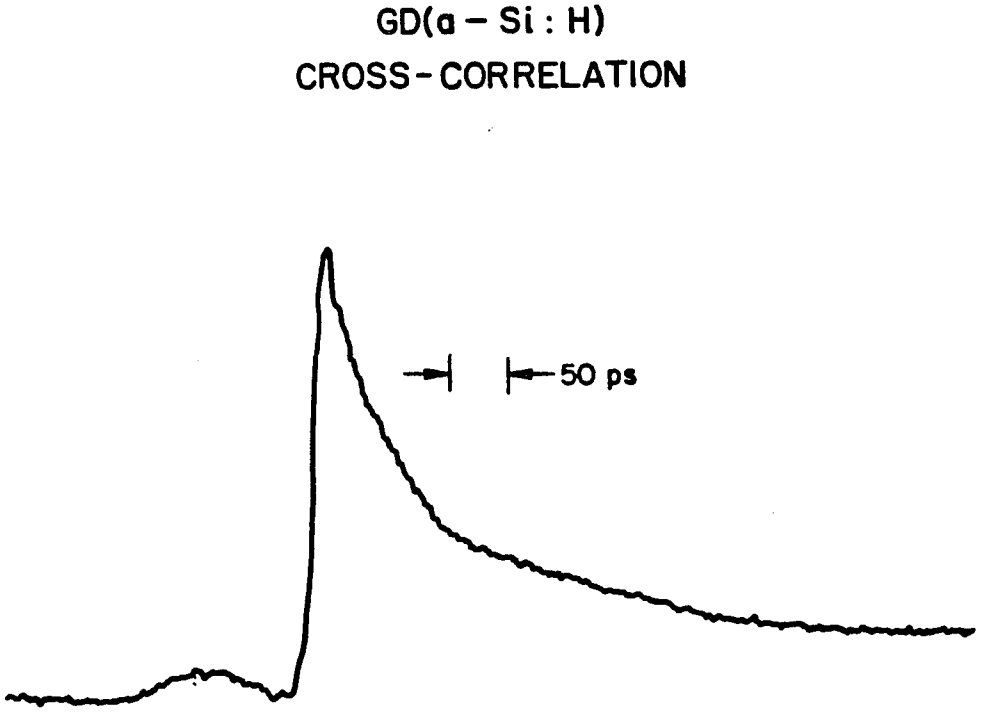

Fig. (4.4-2): Room Temperature Pulsed-Bias Electronic Cross-Correlation of RF Glow-Discharge Deposited a-Si:H (GD) and Radiation Damaged Silicon-On-Silicon (SOS)

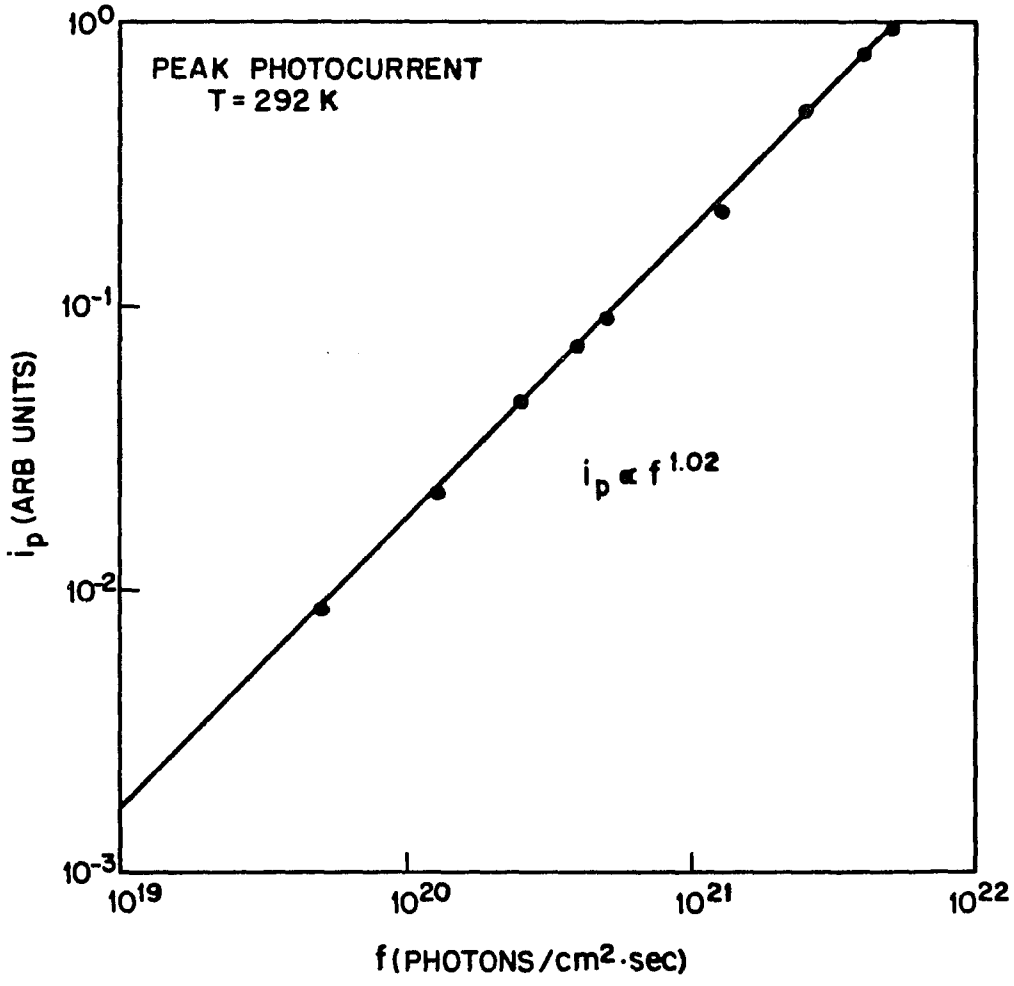

Fig. (4.4-3): Room Temperature Peak Photocurrent as a Function of Photon Flux of RF Glow-Discharge Deposited a-Si:H (GD)

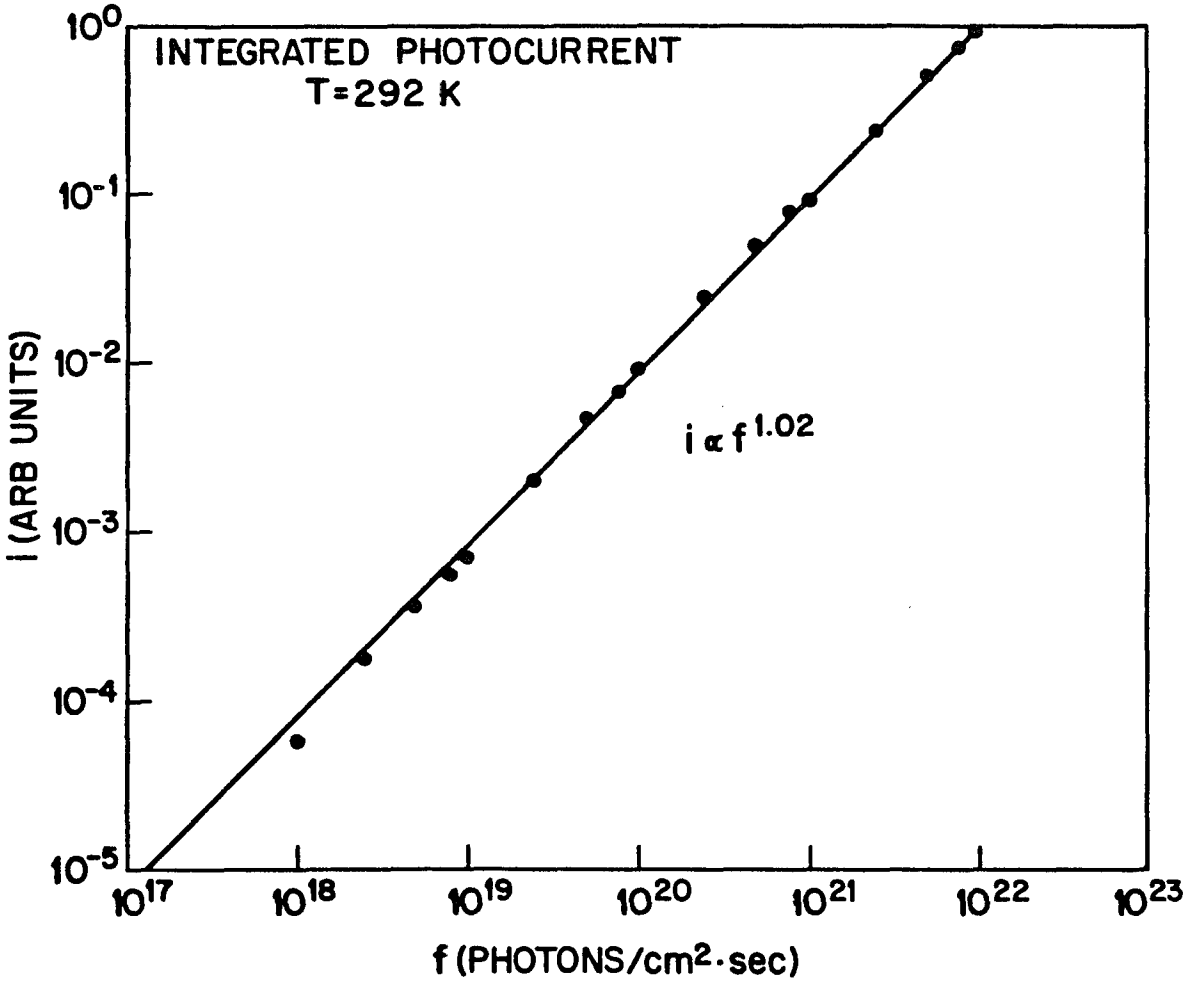

Fig. (4.4-4): Room Temperature Integrated Photocurrent as a Function of Photon Flux of RF Glow-Discharge Deposited a-Si:H (GD)

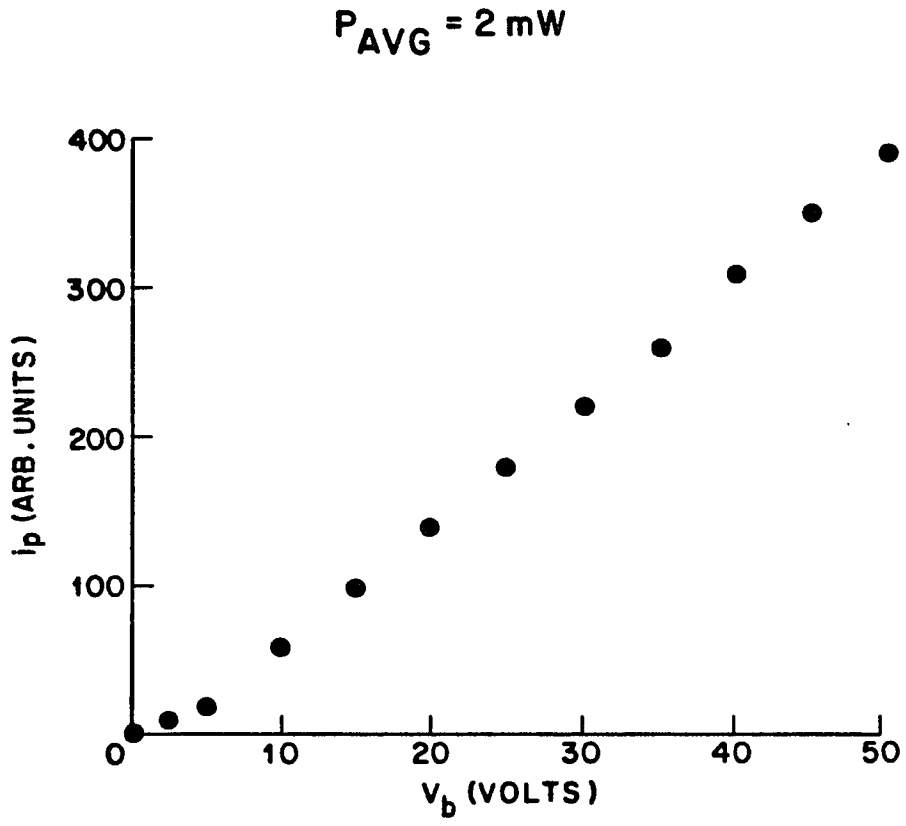

Fig. (4.4-5): Room Temperature Bias Voltage Dependence of the Peak Photocurrent of RF Glow-Discharge Deposited a-Si:H (GD) at an Average Power of 2mW (1.1×10^{21} photons/cm^2s)

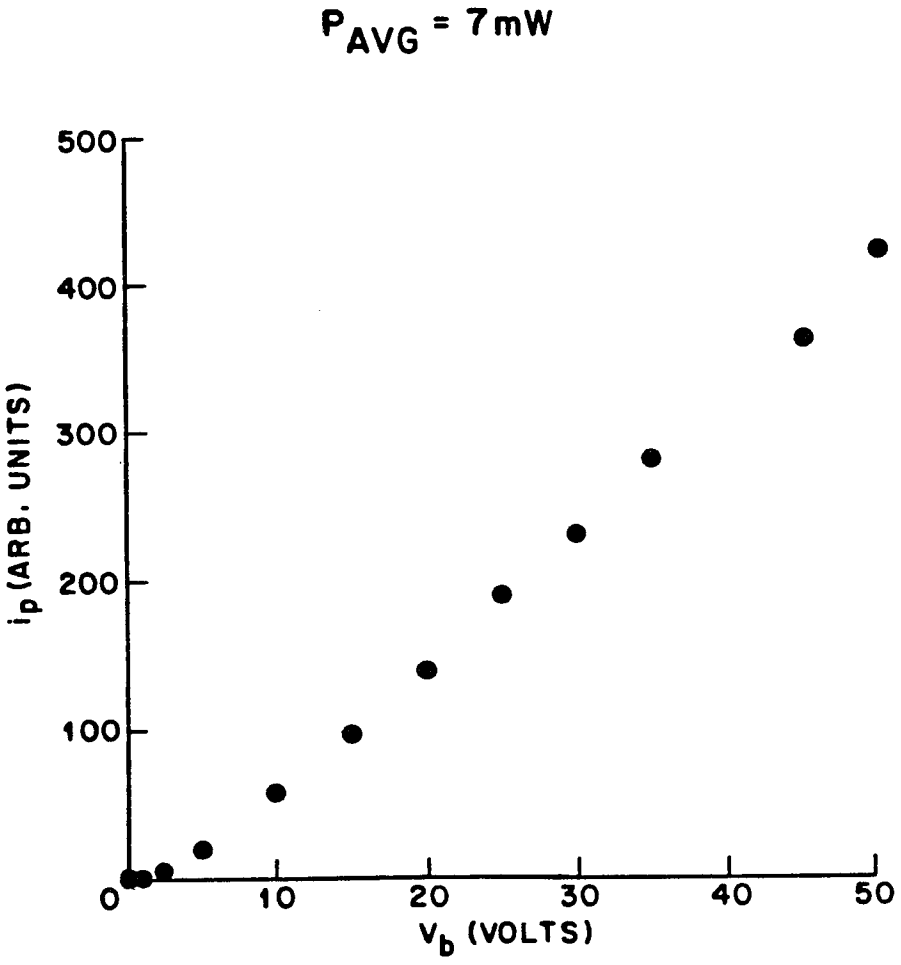

Fig. (4.4-6): Room Temperature Bias Voltage Dependence of the Peak Photocurrent of RF Glow-Discharge Deposited a-Si:H (GD) at an Average Power of 7mW ($4x10^{21}$photons/cm^2s)

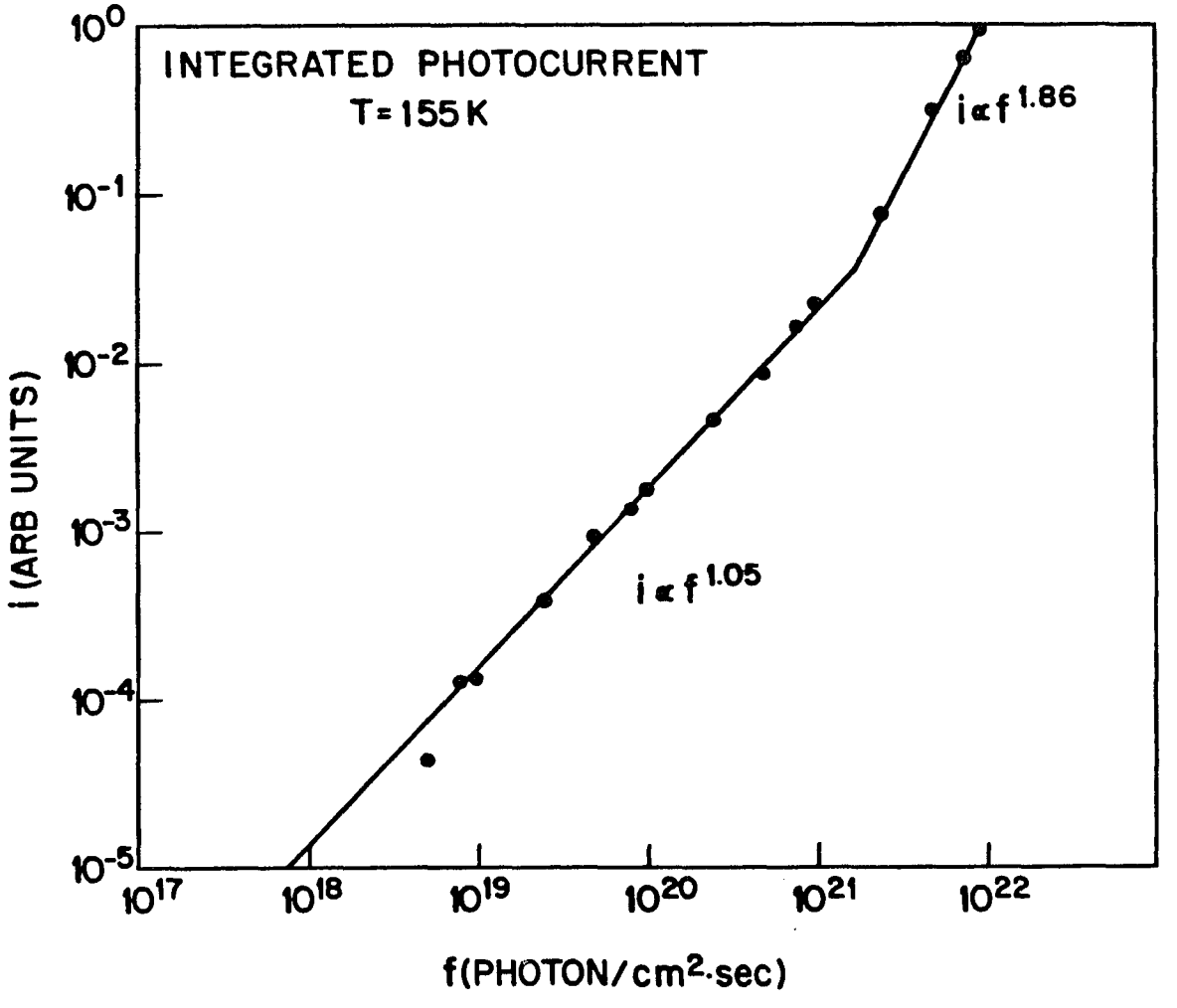

Fig. (4.4-7): Low Temperature (T = 155K) Integrated Photocurrent as a Function of Photon Flux of RF Glow-Discharge Deposited a-Si:H (GD)

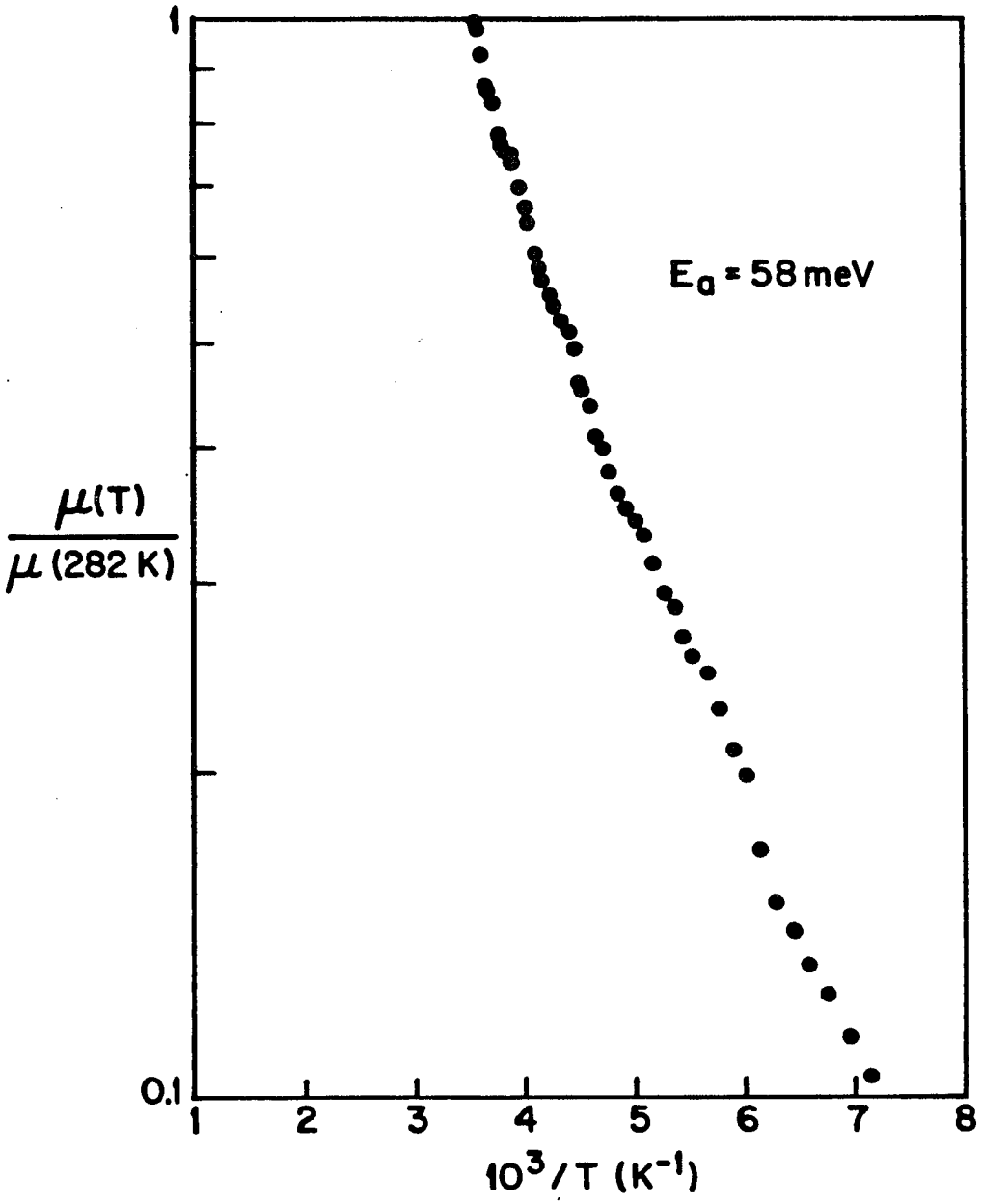

Fig. (4.4-8): Temperature Dependence of the Initial Mobility of RF Glow-Discharge Deposited a-Si:H (GD) Normalized to its Value at 282K

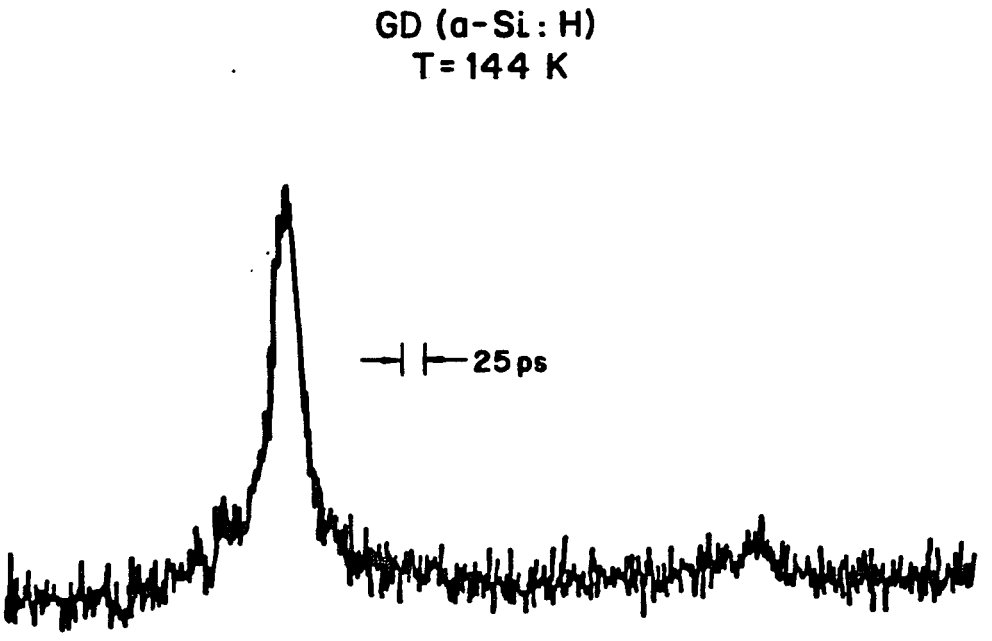

Fig. (4.4-9): Low Temperature (T = 144K) Pulsed-Bias Electronic Cross-Correlation of RF Glow-Discharge Deposited a-Si:H (GD) and Radiation Damaged Silicon-On-Sapphire (SOS)

V. DISCUSSION AND CONCLUSIONS

The extensive work on a-Si and a-Ge and other tetrahedrally bonded materials has shown that the electronic properties of these non-crystalline solids depend critically on the method of preparation and also on the detailed experimental conditions during the specimen deposition (Spear and Le Comber, 1976). For instance, a-Si prepared by two different techniques may well differ in its electrical conductivity by eight orders of magnitude and the optical absorption coefficient at photon energies below the optical gap may differ by a factor of two or more.

These effects, which are not generally met in the other amorphous materials such as Se or the chalcogenides, have complicated the meaningful comparison of results from different laboratories and have proved a serious obstacle in the detailed understanding of the electronic properties of amorphous tetrahedral solids (Spear and Le Comber, 1976). The main problem arises through the defect structure of these materials, which is extremely sensitive to preparation conditions and at the same time has a determining influence on the electronic properties. It is likely that the defects are mainly associated with unsaturated bonds in the random network, situated on internal surfaces of vacancy clusters.

The photoluminescence is also strongly affected by material preparation. The photoluminescence intensity of evaporated a-Si (i.e. EV) is approximately two orders of magnitude lower than silane- decomposed a-Si (i.e. GD a-Si:H) (Engemann, et. al., 1977). They attribute the effect of hydrogen on the luminescence of a-Si: H not to the formation of centers for radiative recombination but to the saturation of defects. The samples prepared in ultra-high vacuum contain much less hydrogen which is able to saturate dangling bonds, and, therefore, exhibits a much higher density of gap states, i.e. centers for radiationless recombination.

In spite of the large variation of the electronic and optical properties of a-Si with

preparation, there is experimental information that supports a model of a-Si that is independent of sample preparation - i.e. an intrinsic structure of a-Si (Section 2.1). The radial distribution function (RDF), small-angle x-ray scattering (SAXS), and neutron scattering studies suggest that the intrinsic structure of evaporated a-Si (EV) and plasma-deposited a-Si:H (GD) are similar (Barna et. al., 1977; D'Antonio and Konnert, 1979; Postol et. al, 1980). Our results confirm this suggestion and support a model of a-Si having a common intrinsic structure which is the same for all three methods of preparation investigated.

Tables (4-1) and (4-2) indicate a large variation in the spin density, deposition temperature, dark resistivity, mobility-relaxation time product, relaxation time, photosensitivity, photoconductive gain, and mean drift distance of the three forms of a-Si. In spite of these wide variations we find an initial room temperature mobility of approximately 1 cm^2/Vs for all three forms of a-Si. Theoretical estimates of the mobility of extended states at the mobility edge fall in the range of 1-10 cm^2/Vs (Mott and Davis, 1979). The magnitude and invariance of the initial mobility of the photogenerated carriers tends to confirm the often-made suggestion that the free carrier mobility is determined by the influence of shallow localized states associated with the disorder of the continuous random network (CRN), and is an intrinsic property of a-Si which is unaffected by the method of preparation.

Charge conduction entirely by "free-carrier" band transport is the biggest casualty in going from an ordered to a disordered solid (Scher and Lax, 1973). The lack of long-range structural order is the central essence of the problem; this lack of order causes a random potential to exist in the solid. The random potential can give rise to a distribution of localized electronic states as well as the extended bandlike states. Therefore, the nature of electronic transport can either be the more familiar band type (free-carrier motion with occasional scattering from potential fluctuations), with the localized states acting as traps, or there can be transport among the localized states. Our results suggest

the former of these channels - free carrier motion modulated by intrinsic shallow localized states. The nonexponential decay of the photocurrent and the magnitude of the initial mobility in GD is suggestive of dispersive electronic transport -- in particular extended state transport controlled by multiple trapping (Pfister and Scher, 1978; Tiedje and Rose, 1980; Hvam and Brodsky, 1981; Tiedje et. al., 1981; Orenstein and Kastner, 1981).

The observed photocurrent decays are very similar to the current decays observed in time-of-flight experiments that have been used to measure drift mobilities in amorphous materials, including a-Si:H (i.e. GD) (Pfister and Scher, 1978; Le Comber et. al., 1972; Fuhs et. al., 1978). The theory of dispersive non-Gaussian transport by Scher and Montroll (1975) has been very successful in explaining most of the features observed in transport measurements on disordered solids.

Scher and Montroll (1975) proposed that the randomness of microscopic transport parameters can produce significant fluctuations of the transition rates (hopping and/or trap release rates) that characterize the drift of a carrier through the sample (Pfister, 1977; Pfister and Scher, 1978). If the resulting distribution of transition rates is sufficiently broad, the propagation and broadening of the drifting carrier packet becomes non-Gaussian. This leads to features of transport that are distinctly different from non-dispersive transport which can be described in terms of conventional Gaussian statistics. That is, the dispersion σ (σ characterizes the spread of the charge sheet about the mean) of the carrier sheet and the mean displacement ℓ from the illuminated surface do not obey the well-known relations $\sigma \propto t^{1/2}$ and $\ell \propto t$ which are expected from Gaussian statistics. The current traces exhibit a significant spreading of the charge packet as it propagates through the film. In fact, whereas from Gaussian statistics $\sigma/\ell \sim t^{-1/2}$, the observed current traces indicate that the spread σ and the mean displacement ℓ feature the same time dependence, i.e. $\sigma/\ell = \text{const}$. In order to obtain non-Gaussian behavior, the event time distribution has to extend into the time range of

the experimental observation determined by the transit time t_T which measures the transit of an appropriate fraction of the (fastest) injected carriers. Such broad distributions can easily be manifested in hopping transport where small fluctuations in the hopping distance and/or activation energy can introduce significant fluctuations in the nearest neighbor hopping time. This fact, is evident from the expression for the hopping probability

$$p = \nu_{ph} \exp(-2\alpha R) \exp(-W/kT) \tag{5.1}$$

where ν_{ph} is an attempt frequency which cannot be greater than the maximum phonon frequency, R the hopping distance (appears as an exponent in the tunneling factor), α is a quantity which is representative of the rate of fall-off of the wavefunction at a site, and W is the hopping energy or height of the potential barrier between sites (Nagels, 1979). Similarly, in the case of multiple trapping transport, broad release time distributions can be obtained for small fluctuations of mobility - limiting traps of sufficient depth.

Scher and Montroll (1975) showed that in the non-Gaussian case the distribution function $\psi(t)$ which describes the probability for an event to happen at time t after the preceding event is a slowly decaying function of time. The distribution function $\psi(t)$ can be approximated by the slowly varying power dependence

$$\psi(t) \sim t^{-(1+\alpha)}$$

where the disorder parameter α assumes a value between zero and unity. This distribution function sharply contrasts with the exponential time dependence

$$\psi(t) \sim \exp(-t/\tau)$$

which is associated with a single event time τ and is sufficient (but not necessary) to describe the Gaussian case.

Scher and Montroll (1975) use the formalism of continuous-time random-walk (CTRW) which describes a carrier (walker) hopping at random time intervals on a periodic lattice under the influence of an applied electric field. The fluctuations of the

transition rates in the real material are incorporated in a hopping time distribution function for the walker on the periodic lattice. For the special case of an algebraic $\psi(t)$, they are able to provide a complete mathematical description of the transport properties in terms of a single parameter α the value of which depends upon the detailed microscopic transport process and has been calculated for the cases of hopping at fixed activation energy and extended state transport with multiple trapping by a distribution of traps. The general equivalence of multiple trapping and CTRW was established by Noolandi (1977) and Schmidlin (1977 a,b).

The major predictions of Scher and Montroll (1975) for the current shape i(t) for non-Gaussian transport are expressed in the following equations:

$$i(t) \sim t^{-(1-\alpha)}, \; t < t_T \tag{5.2}$$
$$i(t) \sim t^{-(1+\alpha)}, \; t > t_T \tag{5.3}$$

where $0 < \alpha < 1$ is defined by the time dependence of the distribution function. Thus, the rate of current decay increases at a characteristic time t_T (transit time). At this time the rate of carrier loss at the collecting electrode begins to dominate the rate of temporary carrier immobilization in the bulk of the sample. Thus, t_T approximately characterizes the time when the leading edge of the carrier packet reaches the absorbing substrate. In accordance with the predictions of Eqns. (5.2) and (5.3), the transient current can be described by two distinct power law time dependences where the power exponents can be obtained from the slopes of the tangents approximating log i(t) versus log t at early ($t < t_T$) and late ($t > t_T$) times of propagation.

Dispersive transport is generally associated with three types of mechanisms: multiple trapping, hopping, and trap-controlled hopping.

Multiple Trapping: Here, a distribution of the energies of the trapping levels accounts for the non-Gaussian behavior (Nagels, 1979). The injected carrier moves in a band of extended states, but occasionally will be trapped for some time. Since the time a carrier stays at a trapping site is closely related to the energy distance between this level and

the band and furthermore to the temperature, a distribution in this distance can be responsible for transit time dispersion to occur. The *dispersion will be temperature dependent,* i.e., the shape of i(t) will change with temperature. For extended state transport with trapping in a distribution of trapping levels α, the dispersion parameter, increases with increasing temperature (Pfister and Scher, 1978). One finds $\alpha = T/T_o$ for a trap distribution of the form $N(\epsilon) \sim \exp(-\epsilon/kT_o)$.

Hopping Between Localized States: This accounts for the *temperature independent dispersion* of the transit time observed in some amorphous semiconductors. In this model the temperature independent hopping distance R is assumed to fluctuate. The reason that such a fluctuation can cause strong dispersion is directly seen from the expression which relates this hopping distance to the hopping probability p (Eqn. 5.1)

$$p = \nu_{ph} \exp(-2\alpha R)\, exp(-W/kT).$$

Since R appears as an exponent in the tunneling factor, a small change in R may cause an amplified change of p and, hence, of the release time. Physically this means that an injected carrier moves toward the collecting electrode by hopping with a constant hopping energy W, but this carrier occasionally will meet a hopping site in which it stays for a rather long time. Therefore, only a small fraction of the injected carriers, i.e., the fastest ones, will reach the electrode without passing a "difficult" hopping site, while most of the other carriers are delayed by a different number of such hops.

Trap-Controlled Hopping: In some experiments a rather high activation energy of the drift mobility has been observed, which is difficult to associate with the hopping energy. In order to explain this observation, Pfister and Scher (1977) presented a modification of the hopping model in the way that the presence of traps is incorporated in the system. This new model includes features of the hopping model such as the temperature independence but also offers the possibility of carrier capture by isolated trapping sites. Thus, one can relate the observed activation energy to a trap depth, while maintaining a

temperature independent dispersion originating from the hopping-distance fluctuations.

Some recent transport measurements in a-Si:H support a mode of electronic conduction in extended states controlled by multiple trapping in an exponential distribution of trapping states. Hvam and Brodsky (1981), in a transient photoconductivity measurement (20 ns resolution), in phosphorus - doped a-Si:H, measured an approximate linear variation of the dispersion parameter α with temperature ($\alpha = T/T_o$) and determined the e^{-1} width of the exponential trap distribution to be $kT_o = 40$ meV. Electron and hole time-of-flight measurements were performed in a-Si:H by Tiedje et al., (1981). The approximate linear temperature dependence of the dispersion parameter α resulted in widths of 27 meV and 43 meV for the exponential electron and hole trap distributions respectively.

We believe that our results are suggestive of extended-state transport controlled by multiple trapping. Let us first concentrate on the room temperature results (Table (4-1), Figures (4.1-1), (4.2-2), (4.3-1), and (4.4-2)). The multiple trapping model is illustrated schematically in Fig. (5-1). In a multiple trapping picture photoexcited carriers thermalize to the conduction band edge and proceed to make transitions to a distribution of trapping states. The thermalization of the hot carriers is believed to occur on a time scale of 1ps or less (Vardeny and Tauc, 1981). It is generally assumed that all of the traps have the same capture cross-section. Thus the initial capture process can be described by a single time constant. Therefore, as is usual for non-dispersive transport, we can use an exponential law for the probability that a free carrier will be trapped (Silver and Cohen, 1977)

$$\psi_{trap}(t) \sim exp(-t/\tau).$$

Thus upon creation and thermalization the carriers are subject to capture at all the trapping levels. However, after capture the time spent in a given level will depend strongly upon the depth of the trap. Carriers must be thermally released from these zero mobility traps into the conduction band in order to contribute to the photocurrent. The

thermal release rate is given by

$$t^{-1} = \nu \exp(-\epsilon/kT)$$

where ν is an attempt-to-escape frequency ($\nu \sim 10^{11} - 10^{13}\,Hz$) and ϵ is the energy difference between the trap level and the conduction band edge (E_c). It is this fluctuation in the release rates with trap depth that is responsible for the dispersive nature of the transport. Deep traps are slow to release carriers into the conduction band because of the higher activation energy whereas shallow traps will have faster release rates.

If one had sufficient time resolution, one would probably observe a photocurrent transient of the type indicated in Fig. (5-2). The fast initial rise of the photocurrent would be due to the essentially instantaneous generation of free carriers by a short optical pulse. The thermalizing hot carriers also contribute to the initial rise and leveling off of the photocurrent peak since these carriers are in extended states. The initial exponential decay of the photocurrent would represent the initial capture of the free carriers into zero mobility traps. If all of the traps had the same capture cross-section the initial trapping would have a single exponential time constant. In crystals this trapping time is given by

$$\tau = (N_t\ \sigma\ \nu_{th})^{-1} \tag{5.4}$$

where N_t is the trap density, σ is the capture cross-section, and ν_{th} is the thermal velocity. After this initial capture process the trapped carriers are thermally released into the conduction band at rates that depend upon trap depth. The conduction process at this point cannot be characterized by a single release rate, but must be characterized by distribution of release rates. The resulting dispersion is of the Scher and Montroll (1975) type and results in a multiple trapping tail with a power law dependence

$$i(t) \sim t^{-(1-\alpha)}.$$

Scher and Montroll (1975) gave two expressions for the current decay (Eqns. (5.2) and (5.3)) that depended upon the transit time in a drift experiment. Since the contact separation in our experiments (25 μm) corresponds to very long (essentially infinite)

transit times, on the time scale of our measurements, we expect the photocurrent decays to approximate

$$i(t) \sim t^{-(1-\alpha)}, \tag{5.2}$$

asymptotically as a function of time. The above expression does not take into account the very early time history of the photoexcited carriers and does not include the initial trapping process. This expression actually diverges at $t \rightarrow 0$.

The magnitudes of the initial room temperature mobilities for the three forms of a-Si ($1\ cm^2/Vs$), are consistent with extended state transport controlled by multiple trapping and therefore we rule out hopping and trap-controlled hopping. As discussed in Section (2.2) hopping mobilities are expected to have magnitudes in the range $10^{-2} - 10^{-3}\ cm^2/Vs$.

The photocurrent decay of CVD appears to have a multi-component character (Fig. 4.1-1). The initial decay is very nearly exponential and the tail non-exponential (power law). This suggests, as in Fig. (5-1), that we have sufficient time resolution to investigate the initial capture of the photo-excited carriers by the distribution of localized states in the gap. In this material, the density of deep states is so great that in the initial capture process only a relatively small fraction of the photo-excited carriers are captured by shallow tail states. The result is a small nonexponential multiple trapping tail, relative to the peak of the photocurrent pulse. Thus, in the case of CVD we believe the first component of the photocurrent decay is the initial capture of the photoexcited carriers and the tail represents the thermal release of carriers from a distribution of shallow localized tail states. The approximate exponential decay of the photocurrent in EV is also indicative of an initial capture of photoexcited carriers by the localized states. It is more difficult to comment about the tail in this material because of the presence of a low-level background signal to due a finite dark conductivity. (The time resolution of the electronic-autocorrelation experiments in EV and CVD was $\lesssim$ 10ps).

The time resolution of the room temperature GD electronic-cross-correlation measurement (Fig. 4.4-2) was ~ 20ps, due to a matched attenuator between photoconductors. The non-exponential decay of the photocurrent in GD (Fig. 4.1-1) has no obvious multi-component character. However, upon careful scrutinization of Fig. (4.4-2) there is some evidence of a "kink" in the decay of the photocurrent. We would like to suggest that the first component represents the initial capture in addition to thermal release and re-capture in very shallow states. This would lead to some dispersion but perhaps not enough to completely obscure the initial capture process. In addition to this possibility is the fact that the density of states in the gap is smaller in this material thus reducing the probability for capture. The carriers remain free for a longer period of time because of the reduced density of final states to make transitions to. This accounts for the larger photosensitivity, (this actually represents a time averaged photosensitivity, since infinite time resolution would result in a single photosensitivity for all forms of a-Si) photoconductive gain, and drift distance. Thus there is the possibility that during the early time history a large fraction of the carriers may have been captured but a small fraction may have remained free - leading to some dispersion in the initial decay. By the time we reach the tail all or most of the carriers have been captured at least once and proceed to execute multiple trapping transport. The fact that the multiple trapping tail is a considerable fraction of the peak photocurrent is consistent with a low density of deep states.

The multi-component nature of the photocurrent decay is much more evident in the low temperature (144°K) cross-correlation of GD (~25 ps time resolution) in Figs. (4.1-1) and (4.4-9). The relaxation time decreases from its room temperature value of 200 ps to our low temperature resolution limit of 25 ps. It is not clear, however, why the initial transient is so much faster at lower temperatures. It is possible that this fast component arises from the initial capture process and the small tail could be due to multiple trapping. It was speculated above that the initial room temperature decay

consisted of a combination of the initial capture process and the very early stages of multiple trapping. The initial low temperature transient may represent a "pure" initial capture process with multiple trapping delayed by a smaller release rate (due to lower temperature). The fact that the initial mobility is thermally activated on this time scale is consistent with a very rapid capture process. With better time resolution we would observe pure extended-state transport and expect a 1/T temperature dependence for the initial mobility (Section 2.2). The fact that the tail is a smaller fraction of the peak photocurrent is consistent with the fact that the probability of thermal release is reduced at lower temperatures.

The temperature dependence of the initial mobility of GD (Fig. 4.4-8) yields a mobility of the form

$$\mu = 8\ exp(-0.058/kT).$$

The preexponential factor $\mu_o = 8\ cm^2/Vs$ is consistent with estimates of extended state conduction at the mobility-edge. A possible explanation for the activated temperature dependence of the initial mobility is in the context of several recent papers on a physical interpretation of dispersive transport in disordered semiconductors (Tiedje and Rose, 1980; Tiedje et. al., 1981; Orenstein and Kastner, 1981). In this model the principal results of the statistical theory of Scher and Montroll (1975) are derived from physical arguments, based on the progressive thermalization of electrons in an exponential distribution of traps.

The model proceeds in the following manner. At the beginning of a time-of-flight experiment a packet of electrons is introduced at one end of a sample, by a flash of light. Within one trapping time ($\sim 10^{-11}\ s$) all of the carriers will be trapped with a distribution that runs parallel with the density of localized states, if all the states have the same capture cross-section (Fig. (5-3)). The immobilization time of a trapped electron is equal to the thermal release time t, which is,

$$t = \nu^{-1} \exp(\epsilon/kT) \tag{5.5}$$

where ν is the attempt-to-escape rate ($\sim 10^{12}\, s^{-1}$) and ϵ is the depth of electron traps below the conduction band mobility edge. A number of trapping times after the injection pulse the electrons that were initially trapped in the shallow states will have had a chance to be thermally emitted and retrapped many times and the population in the shallow traps will approach an equilibrium Boltzmann distribution. Similarly, there will be electrons in the deep states that have remained frozen in the same traps since the initial injection. We note from Eqn. (5.5) that the energy

$$\epsilon(t) = kT\ ln(\nu t) \tag{5.6}$$

separates those states above $\epsilon(t)$ for which the most probable number of release events in the time t is greater than unity, from the deeper states where an electron is unlikely to be thermally released in time t. The energy $\epsilon(t)$ that separates the equilibrium fraction from the frozen part sinks steadily deeper into the trap distribution with time, as the frozen part progressively thermalizes. Tiedje and Rose (1980) assume a density of states that decreases exponentially below the conduction band edge as (Fig. 5-3)

$$N_t(\epsilon) = N_o \exp(-\epsilon/kT_c) \tag{5.7}$$

where the subscript t refers to traps and T_c is a characteristic temperature that describes the steepness of the rate of decline of the trap density with increasing energy. After a large number of trapping times (ν^{-1}), the charge will be localized in energy around $\epsilon(t)$, as shown in Fig. (5-4). This concentration of the injected charge at a well-defined energy $\epsilon(t)$, suggests that the drift mobility be treated as a single trap level problem where the depth of the level increases with time and the density of levels decreases with time. This leads to a drift mobility of the form

$$\mu(t) = \mu_0 \frac{N_c kT}{N_t(\epsilon(t))(kT_c + \frac{kT}{1-\alpha})} \exp(-\epsilon(t)/kT) \tag{5.8}$$

where N_c is the density of states at the conduction band mobility edge, μ_o is the free carrier mobility, and α is the dispersion parameter (Scher and Montroll, 1975)

($\alpha = T/T_c$). A crucial assumption of this model is the existence of a mobility edge which separates localized states with zero mobility from finite mobility band states, such that the trap distribution joins on smoothly to the extended state distribution at the conduction band mobility edge (i.e. $N_c = N_o$). Insertion of $N(\epsilon(t))$ from Eqn. (5.7) and use of $N_c = N_o$, yields

$$\mu(t) = \mu_o \frac{N_o kT}{N_o \exp(-\epsilon(t)/kT_c)\ (kT_c + \frac{kT}{1-\alpha})} \cdot \exp(-\epsilon(t)/kT)$$

$$\mu(t) = \mu_o \frac{T}{T_c + \frac{T}{1-\alpha}} \exp(\frac{\epsilon(t)}{kT_c} - \frac{\epsilon}{kT})$$

Using $\alpha = T/T_c$ yields

$$\mu(t) = \mu_o \frac{1}{\frac{1}{\alpha} + \frac{1}{1-\alpha}} \exp(\frac{\epsilon}{kT}(\frac{T-T_c}{T_c}))$$

$$\mu(t) = \mu_o\ \alpha(1-\alpha)\exp\ (\frac{\epsilon}{kT}(\alpha-1))$$

Insertion of $\epsilon(t)$ from Eqn. (5.6) yields

$$\mu(t) = \mu_o \alpha(1-\alpha)\ (\nu t)^{\alpha-1} \tag{5.9}$$

Since $i(t)\ \alpha\ \mu(t)$, Eqn (5.9) reproduces the first branch of the Scher-Montroll log $i(t)$ vs log t curve (Eqn. 5.2).

With sufficient time resolution an experiment could be performed in which the thermalized injected charge packet would be localized around an energy $\epsilon(t)$ that was only a few kT from the conduction band mobility edge. With the assumption that the trap distribution joins on smoothly to the conduction band, high temporal resolution implies that $\epsilon(t)$ is shallow enough to make the approximation (see Eqn (5.7))

$$N_t(\epsilon(t)) = N_0 = N_c.$$

With this approximation Eqn. (5.8) reduces to

$$\mu(t) = \mu_o\, \alpha(1-\alpha)\, \exp(-\epsilon(t)/kT).$$

Since $0 < \alpha < 1$ (Scher and Montroll, 1975)

$$\mu(t) = \mu_o\, \exp(-\epsilon(t)/kT) \tag{5.10}$$

As noted previously Eqn. (5.10) as well as Eqn. (5.2) neglect the initial trapping. Time dependent mobilities have been assumed as a direct consequence of the dispersive nature of electronic transport in $a-As_2Se_3$ (Orenstein and Kastner, 1979,1981), in phosphorus-doped a-Si-H (Hvam and Brodsky, 1981), and in a-Si:H (Tiedje et al., 1981).

We believe that we have sufficient time resolution in these picosecond photoconductivity measurements to warrant an expression of the form of Eqn. (5.10) in the case of GD. As mentioned earlier, the measured temperature dependence of the mobility of GD in Fig. (4.4-8) was of the form

$$\mu = 8\, \exp(-0.058/kT).$$

Both the small activation energy and the magnitude of the preexponential factor are consistent with the injected charge distribution being thermalized to a very shallow trap depth (with respect to the conduction band mobility edge) and a free carrier mobility well within the theoretically predicted range of mobilities at the mobility edge ($1-10\ cm^2/Vs$), respectively.

In photoconductivity measurements, one measures a mobility that is the sum of electron and hole mobilities. However, it is generally assumed, in a-Si:H, that the holes are quickly trapped (how fast is not known) due to the high density of valence band tail states, and that the dominating carriers are electrons (LeComber, et. al., 1972; Fuhs, et. al., 1978). By fitting their time-of-flight data to the above dispersive transport model, Tiedje, et al., (1981) derived the electron and hole free carrier mobilities of $13cm^2/Vs$ and $0.67cm^2/Vs$, respectively. This lends further support to the notion that electrons dominate transport in undoped a-Si: H. Thus, as is evident from the discussion, we have assumed that our experiments reflect electron transport.

The temperature dependence of the electron drift mobility in a-Si:H has been measured by several groups, resulting in an activation energy in the range 0.13-0.25 eV (LeComber et. al., 1972; Moore, 1977; Allan, 1978; Fuhs et al., 1978; Moustakas, 1979; Tiedje, et al., 1981). The discrepancy between these activation energies and our measured activation energy of 0.058 eV can be explained in terms of the time-dependent mobility model discussed above. This difference in activation energies, is due to the relatively "poor" time resolution (generally ns resolution) of the time-of-flight techniques. To illustrate this point we will invert

$$\epsilon(t) = kT\ ln(\nu t) \tag{5.6}$$

in order to obtain the attempt-to-escape frequency ν,

$$\nu = t^{-1} \exp(\epsilon(t)/kT). \tag{5.11}$$

Substituting our activation energy of 0.058 eV for $\epsilon(t)$, our time resolution of 25 ps for t (low temperature limit), and 300°K for T results in

$$\nu = 3.8 \times 10^{11}\ s^{-1}$$

This agrees very well with the estimated attempt rate of $\nu = 4.6 \times 10^{11}\ s^{-1}$ estimated from the recent time-of-flight measurements of Tiedje et al., (1981). Now, if we solve for the demarcation energy $\epsilon(t)$ (Eqn. (5.6)) with our value of the attempt rate (assuming energy independence) $\nu = 3.8 \times 10^{11}\ s^{-1}$ and a time resolution of 5 ns for t (typical time-of-flight time resolution), the result is $\epsilon(t) = 0.20$ eV which is consistent with the range of activation energies given above.

Unfortunately, at the present time, we have not been able to determine the temperature dependence of the dispersion parameter α. To accurately determine α, one has to view the photocurrent decay on a log i(t) versus log t plot (Scher and Montrol, 1975) over several decades in time. Though we believe we have the range in time delay, we do have the problem of reflections at the microstrip-to- coaxial connector interface. These reflections, not shown in Fig. (4.4-2) (delayed further in time) but evident in the sampling oscilloscope trace (Fig. 4.4-1), in the tails can result in

uncertainty in the determination of α. Experiments are in progress to reduce these reflections and expand further the "window of observation" to make accurate measurements of the dispersion parameter.

Prior to picosecond transient photoconductivity, some three orders of magnitude in response time was inaccessible to both time-of-flight and transient photoconductivity measurements. As we have seen, quite a bit of information can be obtained on a picosecond time scale. There are several discrepancies in the literature that may be due to insufficient time resolution. Pfister and Scher (1977), in the case of a-As_2Se_3, and Fuhs et al., (1978), in the case of a-Si:H, measured temperature independent α's and concluded that hopping transport was the origin of the dispersion. Orenstein and Kastner (1981) claim the range of time and temperature accessible to the time-of-flight technique was insufficient to reveal the weak (linear) dependence of α on the temperature consistent with a model of multiple trapping in $a-As_2Se_3$. Orenstein and Kastner (1981) used photoconductivity to observe the dependence of α on T. Similarly, Hvam and Brodsky (1981) (photoconductivity) and Tiedje et al. (1981) (time-of-flight) measured a linear dependence of α on T in phosphorus doped a-Si:H and a-Si:H, respectively, resulting in extended state transport controlled by multiple trapping. An additional complication can arise in nanosecond time scale photoconductivity measurements. In addition to multiple trapping, recombination of electrons and holes is believed to occur in the nanosecond range (photoluminescence decays have been reported with time constants down to 20 ns (Engemann and Fischer, 1976). The competing channels of multiple trapping and recombination may result in an erroneous determination of α. Without measuring the temperature dependence of α, the time resolution of our measurement enables us to measure a drift mobility whose magnitude is consistent with extend state transport controlled by multiple trapping and inconsistent with hopping in localized states.

The activated nature of the initial mobility could also result from a gap in the density of states. Perhaps there is no tailing of the conduction band into the "forbidden zone". The activation energy would be consistent with a sharp band edge separated by approximately 58 meV from a distribution of localized states. To test this possibility we would have to improve our time resolution. With the improved time resolution the temperature dependence of the initial mobility would be characteristic of the extended states ($\mu_c \propto 1/T$). This temperature dependence resulting from the fact that the trapped carriers wouldn't have sufficient time to be thermally emitted into the conduction band.

Another possibility that could result in a gap in the density of states is a direct consequence of an electron inducing sufficient lattice relaxation to produce a small-polaron band (Section 2.2). Of the two polaronic states illustrated in Fig. (2.2-5) the purely polaronic system of Fig. (2.2-5c) is not consistent with our experimental results. In this system one has small-polaron hopping transport. We believe that our measured initial mobilities are too large for this type of electronic transport. Assuming small-polarons are formed instantaneously the magnitude and the temperature dependence of the initial mobility may be consistent with Fig. (2.2-5b) though. Consider the following: photoexcited carriers thermalize rapidly ($\sim 10^{-12}s$) to the bottom of the conduction band. These free carriers are quickly trapped by the distribution of localized tail states and the relatively small distribution of deep states. The electron-lattice interaction is sufficiently strong to reduce the barrier to small-polaron formation to the point that a small-polaron band of binding energy, $E_b = 58$ meV could be produced. The thermally activated mobility observed would not be due to small-polaron hopping, but thermal activation of the "self-trapped" electrons back into the conduction band. In this case the small-polaron band is functioning effectively as a single trap level of depth 58 meV. The nonexponential decay, at room temperature, of the photocurrent could possibly result from a distribution of times for the formation of small-polarons. The low

temperature photocurrent decay in Fig. (4.4-9) could also be explained in this model. The initial fast 25 ps decay could be due to the initial fast trapping and lattice deformation to produce a small polaron band and the long, flat, small amplitude tail due to emission into the conduction band from this single small-polaron level. As discussed earlier, the test of a gap in the density of states is to watch for a change in the activation energy as one increases the time resolution of the measurement.

The temperature dependence could also be an intrinsic property of the extended states arising, for example, from a nonsharp mobility edge. Redfield (1971,1972) explained the temperature dependence of the conductivity in heavily doped GaAs by using a gradual mobility transition in the band-tails, with the hope of using this concept in the band-tails of amorphous semiconductors. We expect that a more definitive answer to these questions will be provided by further measurements with more precise time resolution.

The measured room temperature mobilities listed in Table (4-1) assume a unit quantum efficiency (η=1). A recent paper by Mort et al., (1981) suggests that geminate recombination may reduce the quantum efficiency to 0.5 in a-Si:H. In this event the mobility would be underestimated by a factor of 2. Surface recombination should make a minimal contribution to the fast decays observed because of the negligible diffusion expected on this time scale. Also, we do not expect bulk recombination to be important on this time scale. We estimate the mobilities to be accurate to within a factor of 2.

In conclusion, we find a relatively large initial mobility ($\sim$1 cm^2/Vs) in all samples of a-Si and a thermally activated ($\sim$ 58 meV) initial mobility in a-Si:H resulting in a free carrier mobility of 8 cm^2/Vs (consistent with estimates of the free carrier mobility at the mobility edge). The magnitude and invariance of the mobility provides strong support for the existence of a mode of conduction in extended states associated with

the disorder of the random atomic network, an intrinsic property of a-Si. The strong dependence of the carrier relaxation rate on the defect density suggests that the photo-current decay in the higher defect-density material (i.e., CVD and EV) is due to the trapping of carriers in deeper states formed by isolated defect sites which are introduced during the sample preparation.

MULTIPLE TRAPPING MODEL

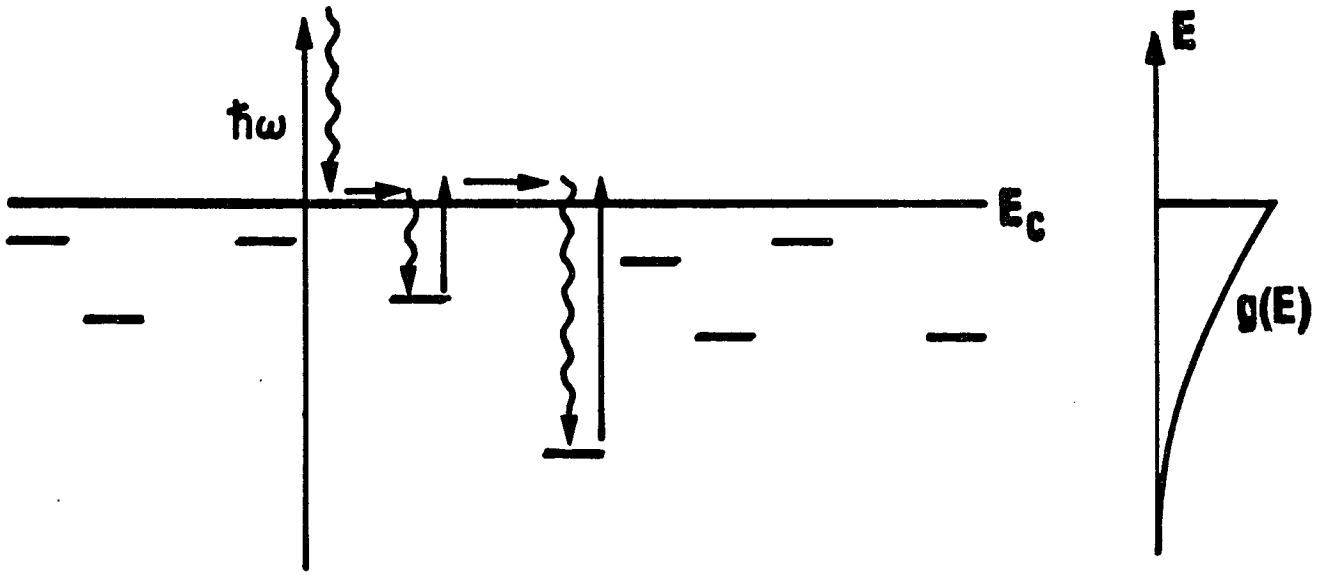

Fig. (5-1)

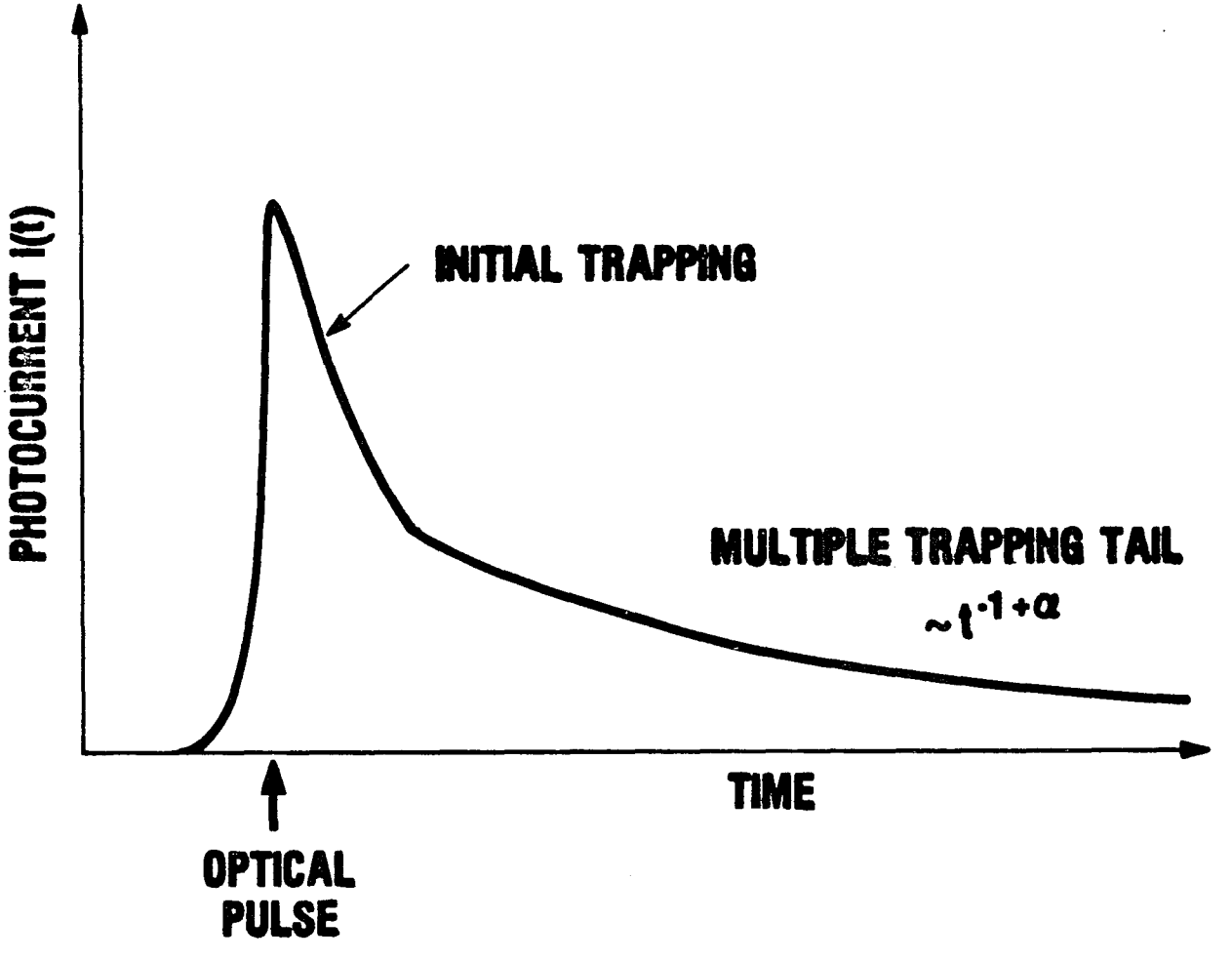

Fig. (5-2): Transient Photocurrent Response Indicating Initial Decay Due to Initial Capture and a Multiple Trapping Tail

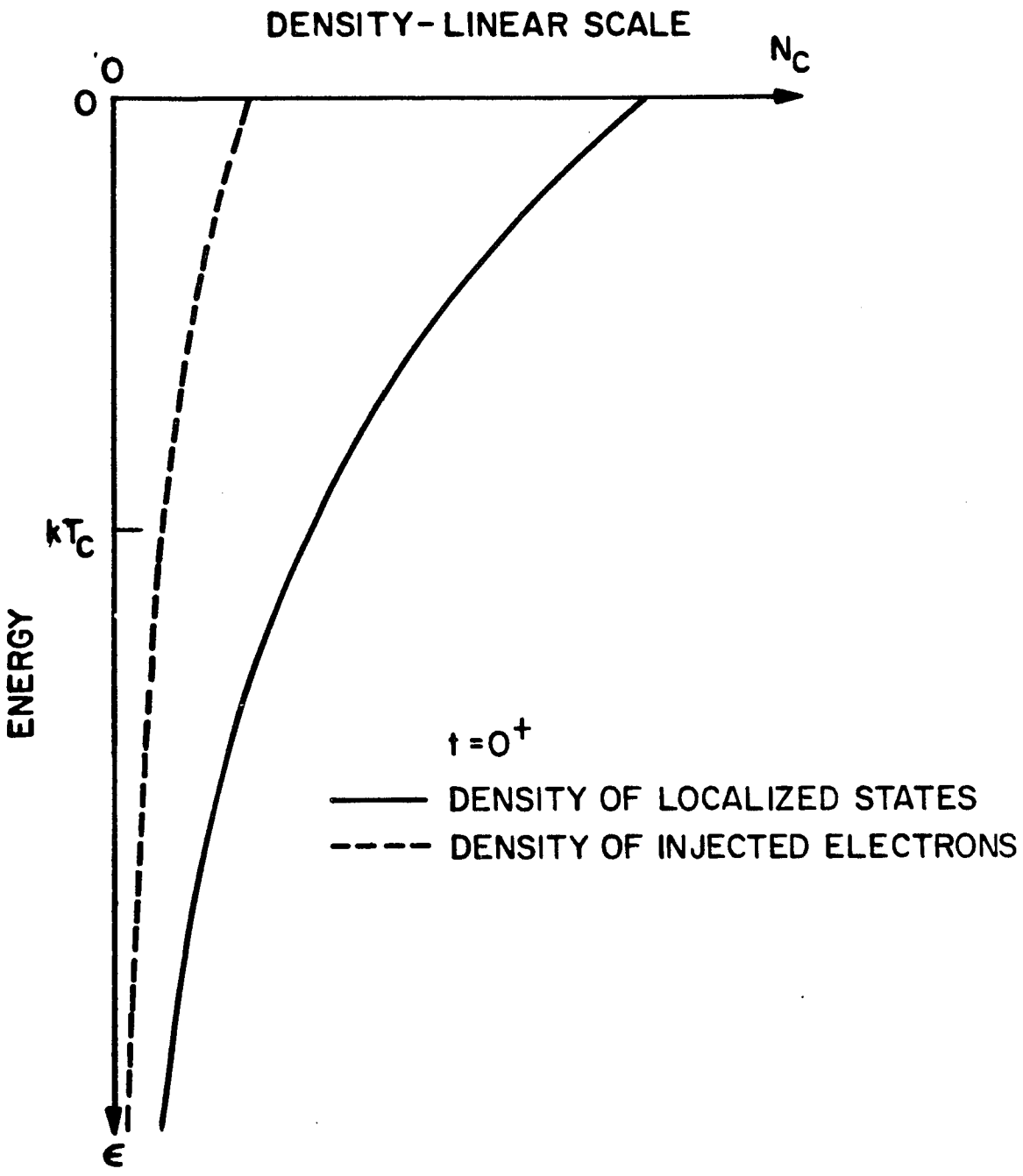

Fig. (5-3): Distribution of injected electrons in traps after one trapping time, plotted on a linear scale. The zero of energy is the conduction band mobility edge.
From: Tiedje and Rose (1980)

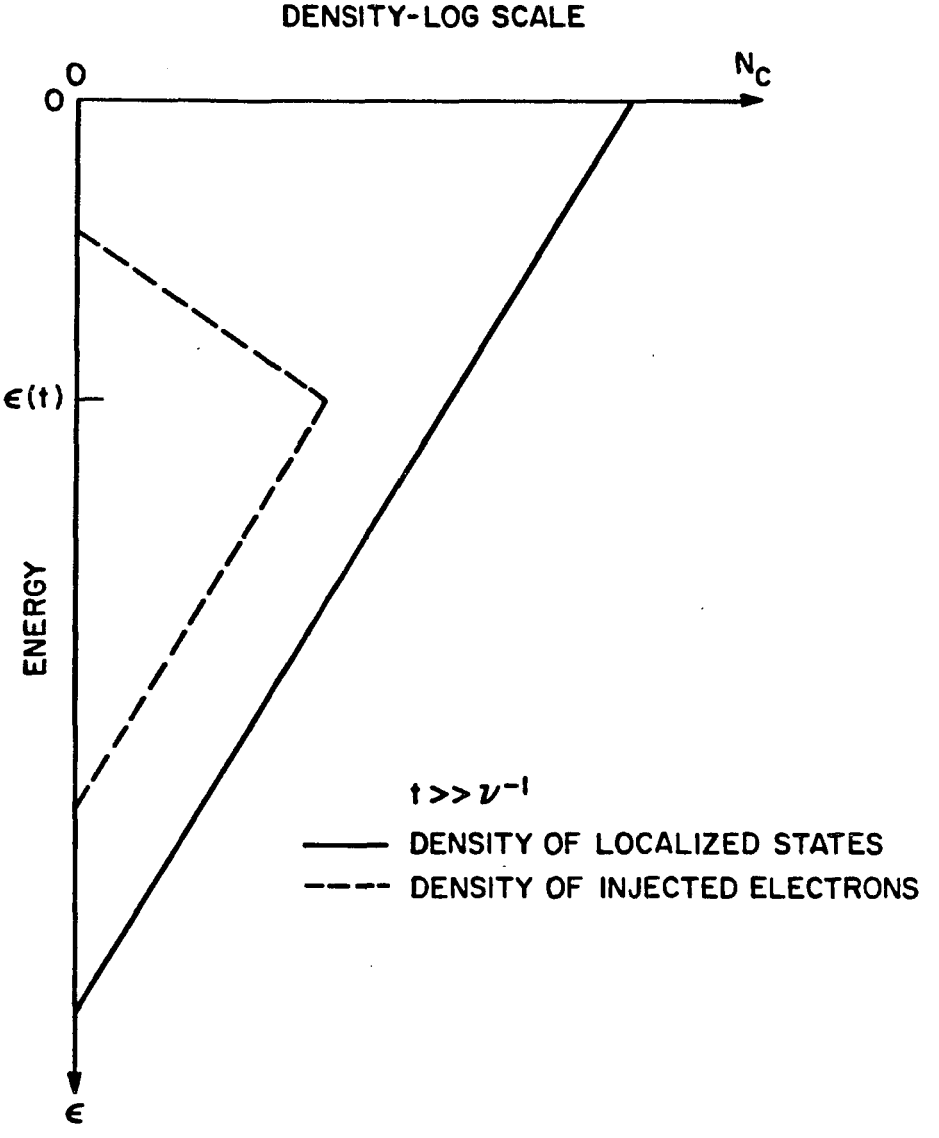

Fig. (5-4): Distribution of electrons at time t, on a log scale, many trapping times after the injection pulse.
From: Tiedje and Rose (1980)

VI. SUMMARY AND FUTURE DIRECTIONS

The early time history of electronic transport in amorphous silicon (a-Si) has been investigated with the development of a new, high-speed electronic measurement capability that has enabled the direct observation of the transient photoresponse of a-Si with a time resolution of $\lesssim$ 10ps. We have used this technique to measure the initial mobility of photogenerated (2.1eV) free carriers in three types of a-Si having widely different densities of structural defects (i.e., as prepared by: (1) RF glow discharge, (2) chemical vapor deposition, and (3) evaporation in ultra-high vacuum). These three forms of a-Si span a range of some 4 to 5 orders of magnitude in the density of structural defects susceptible to electron spin resonance (ESR). The early time history is especially interesting since it relates more closely to the transport properties of the extended and localized states associated with the intrinsic disorder of the random atomic network, whereas the slower events tend to be influenced by the deeper states associated with structural defects and depend on the method of preparation. All three forms of a-Si were found to have the same initial mobility of 1 cm^2/Vs at room temperature and different carrier relaxation times ranging from 200 to 4ps. These results tend to confirm the often-made suggestion that the free carrier mobility is determined by the influence of shallow states associated with the disorder of the random atomic network, and is an *intrinsic* property of a-Si which is unaffected by the method of preparation. The observed strong dependence of the carrier relaxation rate on the defect density suggests that the photocurrent decay in the higher defect density material is due to the trapping of carriers in deeper states formed by the isolated defect sites which are introduced during the same preparation (*extrinsic* disorder).

The temperature dependence of the initial mobility of the RF glow discharge sample (a-Si:H) was found to be of the form

$$\mu = 8exp(-0.058/kT).$$

The preexponential factor $\mu_o = 8$ cm^2/Vs is consistent with theoretical estimates of the free carrier mobility at the mobility edge. The nonexponential decay of the photocurrent and the magnitude of the initial mobility in a-Si:H (room temperature) is suggestive of extended state transport controlled by multiple trapping. In the multiple trapping picture, it is possible that within our time resolution (approximately 25ps for the low temperature measurement) the initial capture is very fast and not completely resolved, and thermal emission from the continuum of localized tail states is already in progress. This could give an apparent activated behavior with a characteristic energy comparable to the first few kT below the mobility edge.

The power law decays of photocurrent transients in disordered solids were given asymptotically as a function of time by Scher and Montrol (1975). This formalism does not take into account the very early time history of the photoexcited carriers and does not include the initial trapping process. A multiple trapping theory that included generation, thermalization, initial capture, and multiple trapping of photoexcited free carriers would complement picosecond electronic transport measurements.

The temperature dependence of the dispersion parameter α needs to be determined in the samples discussed in this thesis. The improvement of some two to three orders of magnitude in temporal resolution will enhance the spectroscopy of the density of localized states immensely by observing the initial capture process.

The recent electroreflectance and Raman scattering investigation of a-Si:F:H by Tsu, Izu, Ovshinsky, and Pollak (1980) indicates the possibility of "microcrystallinity" or some other intermediate range order. We would expect to observe a greatly enhanced initial mobility, using picosecond photoconductivity, if microcrystallites were formed. An interesting experiment would be to measure the initial mobility as a function of *H* and *F* concentration.

With improvements in time resolution experiments could be performed to confirm

or contradict the predicted $1/T$ temperature dependence of "pure" extended state transport at the mobility edge (no trapping). Thus one could observe the transition from free carrier motion to trap-modulated free carrier motion and perhaps draw some conclusions about the nature of the mobility edge.

The chalcogenides would be an interesting group of materials to study with this technique. The large sample dependent variation in electronic properties observed in a-Si does not occur in these materials.

APPENDIX I

Photoconductivity Equation

The fast photocurrent transients observed are due to the short relaxation times of the photo-excited carriers upon being captured by localized states (traps). These short relaxation times are not due to the transit time for carriers to drift from the generation point to the electrodes. In amorphous semiconductors the carrier mobilities are so low, that in a typical situation the carriers may only drift ($<X> = \mu\tau E$) a few tens to hundreds of angstroms during their lifetime compared to a typical gap spacing of 250,000 Å, so that most of the carriers never reach the electrodes. It is not necessary, however, for the carriers to reach the electrodes to produce a current signal in the external circuit.

In an early paper, Shockley (1938) used Green's reciprocation theorem of electrostatics to derive an expression for the induced currents which flow in the external circuit connecting a system of conductors when a point charge is moving among the conductors. For our particular geometry (Figures 3.1.2-1a,b), with the assumption of space charge free conditions, the potential between the electrodes can be obtained from Laplace's equation. The left electrode is biased ($V=V_b$) and the right electrode is grounded. The coordinate system is defined in (a) of Fig. (3.1.2-1b).

$$\frac{d^2}{dx^2} V = 0$$

$$V = C_1 x + C_2$$

The boundary conditions are

(1) $V = V_b \quad ; \quad x = -\ell/2$

(2) $V = 0 \quad ; \quad x = \ell/2$

The potential function is therefore

$$V = -V_b \frac{x}{\ell} + \frac{V_b}{2} \tag{I-1}$$

(We have assumed that the singularity in the field at the electrodes is smoothed by the finite conductivity of the amorphous film. This assumption has been tested by scanning a tightly focussed light beam across the gap and observing no enhancement of the photocurrent at the electrodes. Further studies are being undertaken to determine the precise field dependence in the gap.) Green's reciprocation theorem states that if charges $Q_1, Q_2, \ldots, Q_n$ on the conductors of a system give rise to potentials $V_1, V_2, \ldots, V_n$ and if charges $Q_1', Q_2', \ldots, Q_n'$ give rise to potentials $V_1', V_2', \ldots, V_n'$, then

$$\sum_{i=1}^{n} Q_i V_i' = \sum_{i=1}^{n} Q_i' V_i \, .$$

We will use Green's reciprocation theorem to determine the charge induced on the electrodes by an electron-hole pair generated between the electrodes. Under the influence of the applied electric field each carrier begins to move towards the respective electrode with opposite polarity. We will define the variables x_n and x_p as the distance between the generated carrier and the electrode it is drifting towards for the electron and hole, respectively. Let us call the biased electrode conductor 1 and the grounded electrode conductor 4. Let us imagine two vanishingly small conductors placed at a distance x_n from conductor 1 and x_p from conductor 4 and numbered 2 and 3, respectively. Let us define two problems:

Problem (1). Let conductor 1 be at potential V_b, conductors 2 and 3 be uncharged, and conductor 4 be at zero potential. The potentials and charges will satisfy the equations:

$$V_1 = V_b \qquad ; Q_1$$
$$V_2 = -\frac{V_b}{\ell}\left(x_n - \frac{\ell}{2}\right) + \frac{V_b}{2} \qquad ; Q_2 = 0$$
$$V_3 = -\frac{V_b}{\ell}\left(\frac{\ell}{2} - x_p\right) + \frac{V_b}{2} \qquad ; Q_3 = 0$$
$$V_4 = 0 \qquad ; Q_4$$

Problem (2). Let conductors 1 and 4 be grounded and conductor 2 possess charge -e and conductor 3 possess charge e. The potentials and charges will satisfy the equations:

$$V_1' = 0 \; ; Q_1'$$
$$V_2' \quad ; Q_2' = -e$$
$$V_3' \quad ; Q_3' = e$$
$$V_4' = 0 \; ; Q_4'$$

Green's reciprocations theorem yields

$$0 = Q_1' V_b + e\,\frac{V_b}{\ell}\left(x_n - \frac{\ell}{2}\right) - e\,\frac{V_b}{2} - e\,\frac{V_b}{\ell}\left(\frac{\ell}{2} - x_p\right) + e\,\frac{v_b}{2}$$

The induced charge is therefore given by

$$Q_1' = Q(\text{induced}) = e - \frac{e}{\ell}(x_n + x_p) \tag{I-2}$$

This result is intuitively satisfying in that one would expect the induced charge to increase as the separation between the carrier and the electrode decreased. As the charge in the gap moves under the influence of the bias field, the magnitude of the induced charge in the electrodes change and it is the rate of change of this induced charge that produces the current signal.

$$i(t) = \frac{d}{dt} Q(\text{induced})$$
$$= \frac{d}{dx}\left[e - \frac{e}{\ell}(x_n + x_p)\right]\frac{dx}{dt}$$
$$= -\frac{e}{\ell}(v_n + v_p)\,, \tag{I-3}$$

where v_n and v_p represent the electron and hole velocities, respectively. The velocities of the electrons and holes are given by

$$v_n = \mu_n E \quad ,$$

$$v_p = \mu_p E \quad , \tag{I-4}$$

where μ_n and μ_p are the electron and hole mobilities respectively and E is the electric field strength. The moving charges induce a current $\iota(t)$ in the external circuit which is proportional to their velocity. Thus, after a separated electron-hole pair is produced, there is induced an instantaneous current that is independent of the location of the electron or hole between the electrodes. The current remains constant until the carriers are immobilized or disappear by trapping or by discharge at the electrode. The sign of the current is such that it reduces (discharges) the stored charge of the electrode capacitance. N electron-hole pairs yield,

$$\iota(t) = - Ne(\mu_n + \mu_p) \frac{\mathrm{E}}{\ell} \tag{I-5}$$

Let us define an average mobility that includes contributions from both the electrons and the holes,

$$\mu \equiv \mu_n + \mu_p \quad , \tag{I-6}$$

therefore,

$$\iota(t) = - Ne\mu \frac{\mathrm{E}}{\ell} \tag{I-7}$$

For the potential function given in Eqn. (I-1)

$$\iota(t) = Ne\mu \frac{\mathrm{V_b}}{\ell^2} \tag{I-8}$$

In determining the induced charge on the electrodes we have used a theorem of electrostatics. This electrostatic approximation, which neglects retardation, is valid if the electromagnetic transit time associated with the charge distribution is much less than the duration of the generated signal. The electromagnetic phase velocity of the microstrip transmission line ($\epsilon_r = 3.78$; $w = 0.55$mm; $h = 0.25$mm; see Section (3.1.2)) is approximately 1.7×10^{10}cm/sec (Saad, 1971). For the 25 μm gap-width the electromagnetic transit time is 0.15 ps which is much smaller than the duration of any of the generated signals. We have also assumed that the electric field in the gap is uni-

form (no fringing effects) and is uniquely determined by the charge on the electrodes (i.e., $q = V_b C_g$) and is not directly influenced by the free charge within the gap.

We must now determine the number of carriers generated by the optical pulse. First we will examine the intensity of excitation. The decrease in intensity for light passing through a medium of thickness z is given by Bouguer's Law:

$$\frac{d}{dz} I = -\alpha I \quad , \tag{I-9}$$

where α is the absorption constant. We correct this expression for reflection at the top surface for highly absorbed radiation:

$$\frac{d}{dz} I = -\alpha(1-R)I \quad , \tag{I-10}$$

where R is the reflectivity. Thus, the diminishment of the incident intensity, I_0, as a function of depth into the medium is

$$I(z) = (1-R)I_0 e^{-\alpha z} \tag{I-11}$$

The change in the generated carrier density per unit time may be described phenomenologically as

$$\frac{\partial n}{\partial t} + \frac{n}{\tau} = \eta \frac{\alpha I}{\hbar\omega} \quad . \tag{I-12}$$

The R.H.S. represents the source of freed carriers by optical excitation with η representing the quantum efficiency for generation. The quantity n/τ is a damping term with τ representing a time constant for the relaxation of the freed carriers into localized states. In our special case of picosecond excitation ($t_p = 3.5$ps) we approximate the initial intensity incident upon the active region of the photodetector to be a delta function,

$$I_0 = \frac{\epsilon_p}{(\pi\ell^2/4)} \delta(t) \quad . \tag{I-13}$$

ϵ_p is the optical pulse energy absorbed in the active region. Therefore we have,

$$\frac{\partial n}{\partial t} + \frac{n}{\tau} = \eta \frac{\alpha}{\hbar\omega} (1-R) \frac{\epsilon_p}{(\pi\ell^2/4)} e^{-\alpha z} \delta(t) \tag{I-14}$$

Integrating yields,

$$n(t) = e^{-t/\tau}\eta \frac{\alpha}{\hbar\omega}(1-R)\frac{\epsilon_p}{(\pi\ell^2/4)}e^{-\alpha z}$$

$$\cdot \int \delta(t')e^{t'/\tau}dt'$$

$$n(t) = \eta \frac{\alpha}{\hbar\omega}(1-R)\frac{\epsilon_p}{(\pi\ell^2/4)}e^{-\alpha z}e^{-t/\tau} \tag{I-15}$$

To obtain the number of optically excited carriers we must integrate the carrier density over the illuminated volume,

$$N(t) = \int_0^{\ell/2} 2\pi r dr \int_0^d dz\{n(t)\}$$

where d is the film thickness.

Therefore

$$N(t) = \eta \frac{\alpha}{\hbar\omega}(1-R)\frac{\epsilon_p}{(\pi\ell^2/4)}\int_0^{\ell/2} 2\pi r dr$$

$$\cdot \int_0^d e^{-\alpha z}dz$$

$$= \eta \frac{\alpha}{\hbar\omega}(1-R)\frac{\epsilon_p}{(\pi\ell^2/4)}(\pi\ell^2/4)\left[\frac{1-e^{-\alpha d}}{\alpha}\right].$$

Finally

$$N(t) = \eta \frac{\epsilon_p}{\hbar\omega}(1-R)(1-e^{-\alpha d})e^{-t/\tau} \tag{I-16}$$

Substitution into eqn. (I-8) yields

$$\iota(t) = \eta \frac{e}{\hbar\omega}(1-R)(1-e^{-\alpha d})\frac{V_b}{\ell^2}\mu\epsilon_p e^{-t/\tau} \tag{I-17}$$

Equation (I-17) is the starting point for two expressions utilized to measure the initial mobility of photoexcited carriers, that is dependent upon how fast the carriers relax to localized states. In a material with a relatively long carrier relaxation time (i.e. GD), the relevant quantity is the time resolved peak amplitude of the photocurrent, ι_p. In this case

$$\iota_p = \iota(t = t_{peak})$$

where $\tau >> t_{peak}$ and thus $e^{-t_{peak}/\tau} \approx 1$ and we obtain the expression

$$\iota_p = \eta \frac{e}{\hbar\omega} (1-R)(1-e^{-\alpha d}) \frac{V_b}{\ell^2} \mu \epsilon_p \quad . \tag{I-18}$$

In material in which the carrier relaxation time is sufficiently fast (i.e., CVD and EV) that the peak amplitude of the photocurrent cannot be time resolved the photocurrent (Eqn. (I-17)) is integrated to obtain the charge in the photocurrent pulse,

$$Q = \int_0^\infty \iota(t) dt$$

and results in

$$Q = \eta \frac{e}{\hbar\omega} (1-R)(1-e^{-\alpha d}) \frac{V_b}{\ell^2} \mu \tau \epsilon_p \quad . \tag{I-19}$$

Equations (I-18) and (I-19) represent the idealized case of a rectangular beam (spatial dependence) of circular cross-section focussed to a radius of $\ell/2$. We would like to consider the more realistic situation of the optimum focussing of a Gaussian beam of beam waist W_o to yield the maximum photocurrent (Auston, 1981).

For a rectangular beam, the optical pulse energy density is

$$\epsilon_o(x,y) = \epsilon_o(r,\phi) = \begin{cases} \dfrac{\epsilon_p}{(\pi\ell^2/4)} & ; r \leq \ell/2 \\ 0 & ; r > \ell/2 \end{cases}$$

The carrier density from Eqn. (I-15) is

$$\begin{aligned} n_o(x,y,z) &= n_o(z) \\ &= \eta \frac{\alpha}{\hbar\omega} (1-R) \frac{\epsilon_p}{(\pi\ell^2/4)} e^{-\alpha z} \end{aligned}$$

For the Gaussian beam, the optical pulse energy density is

$$\epsilon(x,y) = \frac{2\epsilon_p}{\pi W_o^2} \exp\left\{-2(x^2+y^2)/W_o^2\right\}$$

$$\cdot \exp(-\alpha z)$$

The corresponding carrier density is

$$n(x,y,z) = \eta \frac{\alpha}{\hbar\omega} (1-R) \frac{2\epsilon_p}{\pi W_o^2}$$

$$\cdot \exp\left\{-2(x^2+y^2)/W_o^2\right\} \exp(-\alpha z)$$

For a meaningful comparison, the total energy in each of the optical pulses should be identical and any differences should be reflected in the focusing properties, i.e. the energy density. For the rectangular beam

$$\epsilon_o = \int_{-\infty}^{\infty} dx \int_{-\infty}^{\infty} dy \ \epsilon_o(x,y)$$

$$= \int_o^{2\pi} d\phi \int_o^{\infty} rdr \ \epsilon_o(r,\phi)$$

$$= 2\pi \int_o^{\ell/2} \mathrm{rdr} \ \frac{\epsilon_p}{(\pi\ell^2/4)}$$

$$= \epsilon_p$$

For the Gaussian beam

$$\epsilon = \frac{2\epsilon_p}{\pi W_o^2} \int_{-\infty}^{\infty} dx \ exp(-2x^2/W_o^2) \int_{-\infty}^{\infty} dy \ \exp(-2y^2/W_o^2)$$

$$= \epsilon_p$$

The conductivity is given by

$$\sigma(x,y,z) = n(x,y,z) \ e\mu$$

$$= \eta \frac{e}{\hbar\omega} \alpha(1-R) \frac{2\mu\epsilon_p}{\pi W_o^2}$$

$$\cdot \exp\left\{-2(x^2+y^2)/W_o^2\right\}$$

$$\cdot \exp(-\alpha z)$$

The conductance per unit distance across a strip of width dx is

$$\frac{dG}{dx} = \int_o^d dz \int_{-\infty}^{\infty} dy \ \sigma(x,y,z)$$

where d is the film thickness.

This yields

$$\frac{dG}{dx} = \eta \frac{e}{\hbar\omega} (1-R)(1-e^{-\alpha d}) \left[\frac{2}{\pi}\right]^{1/2} \frac{\mu \epsilon_p}{W_o}$$

$$\cdot e^{-2x^2/W_o^2}$$

Since the strips, of width dx, are in series with respect to current flow, the net resistance across the gap is

$$R = \int_{-\ell/2}^{\ell/2} \left[\frac{dG}{dx}\right]^{-1} dx$$

$$= \left[\frac{\pi}{2}\right]^{1/2} \frac{\hbar\omega}{e} \frac{W_o}{\eta\mu\epsilon_p} \frac{1}{(1-R)} \frac{1}{(1-e^{-\alpha d})}$$

$$\cdot \int_{-\ell/2}^{\ell/2} dx \ e^{2x^2/W_o^2}$$

The net resistance across the gap when illuminated with a rectangular beam is (using Eqn. (I-18)).

$$R_o = V_b/i_p$$

$$= \frac{\hbar\omega}{e} \frac{\ell^2}{\eta\mu\epsilon_p} \frac{1}{(1-R)} \frac{1}{(1-e^{-\alpha d})}$$

The ratio of the two resistances is given by

$$\frac{R}{R_o} = \left[\frac{\pi}{2}\right]^{1/2} \frac{W_o}{\ell^2} \int_{-\ell/2}^{\ell/2} dx \ e^{2x^2/W_o^2}$$

The minimization of this ratio is equivalent to determining the optimum focussing of the Gaussian beam relative to the rectangular beam. Using the substitution $u = \sqrt{2}\, x/W_o$ we obtain

$$\frac{R}{R_o} = \frac{\sqrt{\pi}}{2}\left[\frac{W_o}{\ell}\right]^2 \int_{-\ell/\sqrt{2}\,W_o}^{\ell/\sqrt{2}\,W_o} du\ e^{u^2}$$

If we expand the exponential we obtain

$$\frac{R}{R_o} = \frac{\sqrt{\pi}}{2}\left[\frac{W_o}{\ell}\right]^2 \int_{-\ell/\sqrt{2}W_o}^{\ell/\sqrt{2}W_o} du\left[1 + u^2 + \frac{u^4}{2} + \frac{u^6}{6} + \frac{u^8}{24} + \frac{u^{10}}{120} + \ldots\right]$$

$$= \frac{\sqrt{\pi}}{2}\left\{\left[\frac{\sqrt{2}W_o}{\ell}\right] + \frac{1}{3}\left[\frac{\ell}{\sqrt{2}W_o}\right] + \frac{1}{10}\left[\frac{\ell}{\sqrt{2}W_o}\right]^3 + \frac{1}{42}\left[\frac{\ell}{\sqrt{2}W_o}\right]^5 + \frac{1}{216}\left[\frac{\ell}{\sqrt{2}W_o}\right]^7 + \frac{1}{1320}\left[\frac{\ell}{\sqrt{2}W_o}\right]^9 + \cdots\right\}$$

Defining $V \equiv \sqrt{2}W_o/\ell$, $\frac{\partial}{\partial V}\frac{R}{R_o} = 0$

yields

$$\frac{\partial}{\partial V}\left\{V + \frac{1}{3V} + \frac{1}{10V^3} + \cdots\right\} = 0$$

$$1 - \frac{1}{3V^2} - \frac{3}{10V^4} = 0$$

$$V^2 = \frac{1}{6} \pm \left\{\left[\frac{1}{6}\right]^2 + \frac{3}{10}\right\}^{1/2}$$

$$V^2 = 0.739$$

$$V = 0.86 \text{ and } W_o = 0.608\ell$$

The ratio becomes

$$\frac{R}{R_o}\,(V = 0.86) = 1.304$$

Substituting a series of values for V, near 0.86, into the expansion of R/R_o yields a

minimum with

$$V_{opt} = 0.96;\ W_o = 0.68\ell;\ \frac{R}{R_o}\Big|_{opt} = 1.29$$

For the same incident energy the resistance across the gap is greater for the Gaussian beam than the rectangular beam since the Gaussian beam overlaps the electrodes ($W_o > \ell/2$). This is consistent with the fact that the maximum photocurrent is obtained when the beam is defocused and overlaps the electrodes. Due to this overlap (in this approximation) only 77% (1/1.29) of the incident optical energy is actually focussed into the gap. The pulse energies used for computation have been adjusted by this factor.

The preceding analysis attempts to account for a nonuniform conductivity resulting from nonuniform (i.e., Gaussian) illumination. In addition, we are not observing the photoconductivity of a single optical pulse but a train of optical pulses. We are observing photocurrent decays due to trapping rather than recombination, so that space charge may persist after the photocurrent decays. At any particular time there may be dielectric relaxation of the field due to the trapped charge of earlier optical pulses. This is consistent with the fact that the maximum signal is obtained when the beam overlaps the electrodes. If the beam were tightly focused between the electrodes more charge would be created near the center of the gap than near the electrodes. After several dielectric relaxation time constants space charge would tend to accumulate near the electrodes reducing the applied field and thus the signal. When the beam overlaps the electrodes the charge distribution is more uniform resulting in space charge neutrality. In this case a space charge field is less likely to form and results in a larger signal. We attempt to account for dielectric relaxation by adjusting our incident power by this factor of 1.29.

APPENDIX II

Electronic Correlation

The essential feature of the electronic correlation technique is to use one photoconductor as a detector and the other as a sampling gate. A variable delay is conveniently introduced by varying the relative timing of the optical pulses absorbed at each photoconductor. The experimental quantity that is measured is the total sampled charge, Q_s as a function of relative time delay. The time resolution of the measurement is determined entirely by the response of the two photoconductors and the interconnecting circuit and does not require any high-speed external circuitry. In the "symmetric gap autocorrelator" of Fig. (3.3.2-3) the photoresponses of each gap are represented by the current sources:

$$i_1(t) = V_b(G_1 + g_1(t))$$

$$i_2(t) = \frac{1}{C_g} q_2(t)(G_2 + g_2(t))$$

where G_1, G_2 and $g_1(t)$, $g_2(t)$ are the dark conductances and photoconductances, respectively, $q_2(t)$ is the charge on the (lower) sampling gap produced by the photocurrent from the first (upper) pulse injecting gap, and C_g is the gap capacitance. The sampled charge $Q_s(\tau)$ can be written in the general form (Auston, 1981):

$$Q_s(\tau) = \frac{V_b Z_o}{2}\left\{G_2 \int_{-\infty}^{\infty} dt\ g_1(t) + G_1 \int_{-\infty}^{\infty} dt\ g_2(t) + \int_{-\infty}^{\infty} dt \int_{-\infty}^{t} dt' g_2(t) g_1(t'+t_{12}) K(\tau = t - t')\right\}$$

where

$$K(t) = \gamma_1\gamma_2\left\{\frac{e^{-\gamma_1 t} - e^{-\gamma_2 t}}{\gamma_2 - \gamma_1}\right\}; t \gtrsim 0$$

$$\gamma_1 = (2Z_o C_g)^{-1}$$

$$\gamma_2 = (Z_o C_g)^{-1}$$

and t_{12} is the electrical propagation delay between the two gaps. For our case the two photoconductors are identical, so that

$$g_2(t) = g_1(t+\tau) .$$

This case is illustrated in Fig. (II-1) in which the autocorrelation function of an exponentially-decaying photoconductance

$$g(t) = g_o e^{-t/\tau_r}$$

is plotted for the "symmetric gap autocorrelator" of Fig. (3.3.2-3). The circuit time constant, $Z_o C_g$, was assumed to be 1ps (i.e., $Z_o = 50\Omega$, $C_g = 0.02$pF). As seen in the figure, when the decay time of the photoconductance is very short, the autocorrelation function approaches the limiting circuit response. In spite of the geometrical symmetry of this circuit, a delay is observed due to the discharging of the first gap and charging of the second gap. The value of this delay is

$$\tau_D = \begin{cases} 1.39 Z_o C_g \; ; \; \tau_r \ll Z_o C_g \\ 2.00 Z_o C_g \; ; \; \tau_r \gg Z_o C_g . \end{cases}$$

As demonstrated for the case of ultra-high vacuum evaporated a-Si (EV), this delay can be readily measured by interchanging the bias and sampling electrodes, and can be used to estimate the gap capacitance and hence determine the circuit response function.

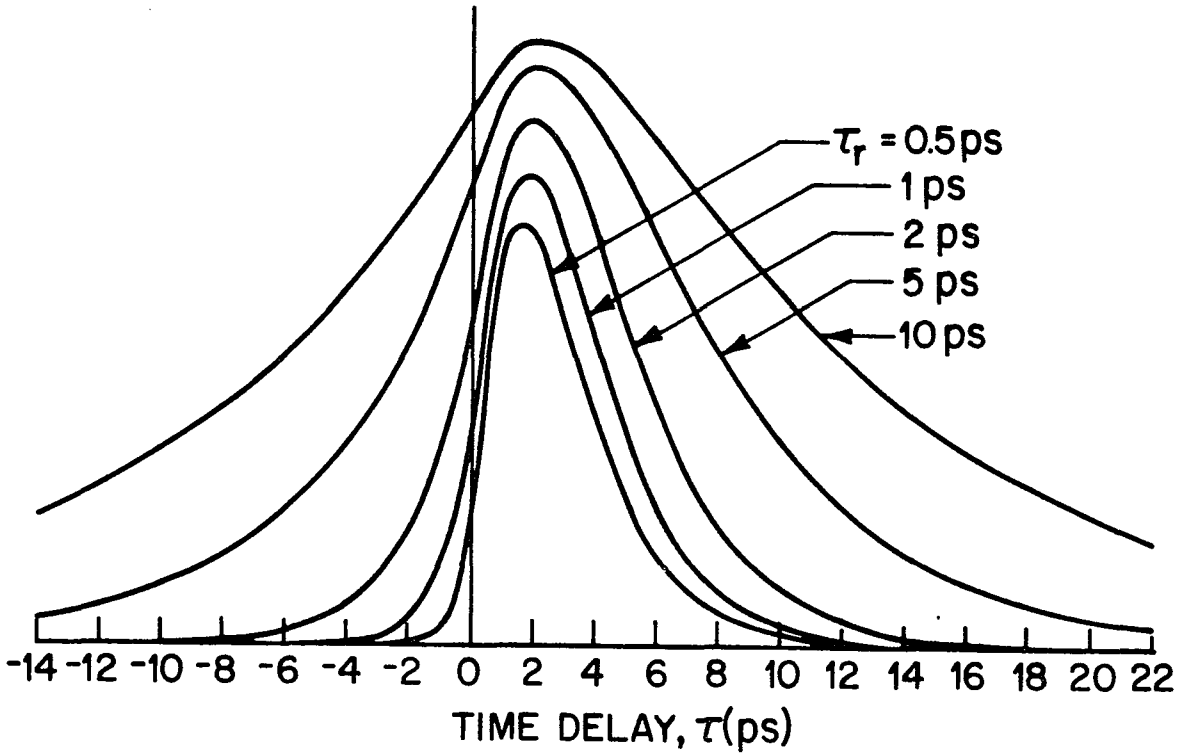

Fig. (II-1): Autocorrelation Response of the "Symmetric Gap" Circuit in Fig. (3.3.2-3) for Different Values of the Photoconductance Relaxation Time, τ_r. The Circuit Time Constant, $\frac{3}{2}Z_o C_g$, is 2-ps and the Optical Pulses are Assumed Infinitesimally Short. From: Auston(1981)

APPENDIX III

Estimate of Laser-Induced Temperature Rise

We will concentrate our attention on sample GD (a-Si:H). The sample consists of 0.9μm of a-Si:H deposited on a 254μm fused silica (a-SiO_2) substrate. The sample is silver pasted onto a copper cold-finger. Some of the relevant tabulated material parameters are the absorption constant, α (2.1 eV), the reflectivity, R (2.1 eV), and the density, ρ: $\alpha = 5\times10^4 cm^{-1}$ (Mott and Davis, 1979); $R = 0.4$ (Weiser, et al., 1980); $\rho = 2\ g/cm^3$ (Carlson, 1980). In general, in order to ascertain the thermal properties of a material the following thermal parameters are requisite: the thermal conductivity, K, the thermal diffusivity, k, and the specific heat, c. We are interested in the magnitudes of these parameters at the extremes of our measurement: T=300K and T=140K. These thermal parameters are available for crystalline silicon (c-Si), c-SiO_2, and a-SiO_2, but have not been measured, to date, for a-Si. One possible means of estimating the magnitude of the variation (if any) of these parameters in the crystalline and amorphous phases is to compare the variation of the tabulated thermal parameters of c-SiO_2 and a-SiO_2.

The trend is a decrease in the thermal conductivity of SiO_2 with decreasing temperature in going from the crystalline to the amorphous phase (Touloukian, et al., 1970a). The thermal conductivity of c-SiO_2 is anisotropic:

K (300K, // to c-axis) = 0.1 W/cmK

K (300K, $\perp$ to c-axis) = 0.06 W/cmK

K (140K, // to c-axis) = 0.25 W/cmK

K (140K, $\perp$ to c-axis) = 0.15 W/cmK

The thermal conductivity of a-SiO_2 is:

K (300K) = 0.014 W/cmK

$$K\ (140K) = 0.009\ W/cmK$$

The thermal diffusivity is given by

$$k = K/\rho c \qquad \text{(III-1)}$$

where ρ is the density and c is the specific heat per unit mass. The density of SiO_2 (Touloukian, et al., 1970a) is:

$$c\text{–}SiO_2 : \rho = 2.6 g/cm^3$$

$$a\text{–}SiO_2 : \rho = 2.2 g/cm^3$$

The specific heat of c-SiO_2 and a-SiO_2 is nearly identical for the temperature range of interest (Touloukian, et al., 1970b):

$$c(300K) = 0.75 J/gK$$

$$c(140K) = 0.38 J/gK.$$

Since it is clear from the above example that the thermal conductivity decreases with disorder we will use the larger of the two crystalline thermal conductivities for comparisons and computation of thermal diffusivities to emphasize the decrease. Therefore, the thermal diffusivity of c-SiO_2 is:

$$k\ (300K) = 0.051\ cm^2/s$$

$$k\ (140K) = 0.25\ cm^2/s.$$

The thermal diffusivity of a-SiO_2 is:

$$k\ (300K) = 0.0085\ cm^2/s$$

$$k\ (140K) = 0.011\ cm^2/s.$$

The above example seems to indicate (at least in the case of SiO_2) that disorder decreases the thermal conductivity, leaving the density and specific heat relatively intact. Specifically, the thermal conductivity decreased by factors of 7.1 and 27.8 at 300K and 140K, respectively. The thermal diffusivities decreased by factors of 6 and

22.7 at 300K and 140K, respectively.

The thermal conductivity of c-Si (Albany and Vandevyver, 1967) is:

$$K\ (300K) = 1.4\ W/cm\ K$$

$$K\ (140K) = 4.2\ W/cm\ K$$

Albany and Vandevyver (1967) irradiated the above sample of c-Si with fast neutrons at a maximum dose of $3.4 \times 10^{18}\ n/cm^2$. The thermal conductivity decreased with increasing dose, as expected from the SiO_2 example above. At this maximum dose the thermal conductivity was:

$$K\ (300K) = 0.7\ W/cm\ K$$

$$K\ (140K) = 0.8\ W/cm\ K.$$

The thermal conductivity curves had not begun to level off at this dose indicating that the thermal conductivities could be further depressed with higher doses. We will estimate the thermal conductivity and thermal diffusivity of a-Si by depressing the crystalline values by comparable factors encountered in SiO_2. The thermal conductivity and thermal diffusivity of c-Si are (Albany and Vandevyver, 1967; Touloukian, et al., 1973):

$$K\ (300K) = 1.4\ W/cm\ K$$

$$K\ (140K) = 4.2\ W/cm\ K$$

$$k\ (300K) = 0.88\ cm^2/s$$

$$k\ (140K) = 4.5\ cm^2/s.$$

We estimate the thermal conductivity and the thermal diffusivity of a-Si by depressing the crystalline values by factors of 10 and 35 at 300K and 140K, respectively:

a-Si (Estimate)

$$K(300K) = 0.14 W/cmK$$

$$K(140K) = 0.12 W/cmK$$

$$k(300K) = 0.088 cm^2/s$$

$$k(140K) = 0.13 cm^2/s$$

An expression for the laser-induced temperature rise, ΔT, has been given, by Bartoli, et al. (1973), for a semi-infinite isotropic solid, uniformly illuminated by an optical pulse of duration t_p at the surface, $z = o$:

$$\Delta T = \frac{(1-R)E_o}{\alpha K t_p} \left[\left(\frac{4\alpha^2 k t_p}{\Pi} \right)^{1/2} - 1 + \exp(\alpha^2 k t_p) erfc(\alpha^2 k t_p)^{1/2} \right]$$

where E_o is the energy per unit area of radiation incident on the crystal and erfc (X) is the complementary error function. Using Eqn. (III-1) $k = K/\rho c$ and defining

$$t_o \equiv \frac{4}{\Pi \alpha^2 k},$$

the above expression for ΔT becomes:

$$\Delta T = \frac{(1-R)\alpha E_o}{\rho c} \left(\frac{\Pi t_o}{4 t_p} \right) \left[\frac{4}{\Pi} \left(\frac{t_p}{t_o} \right)^{1/2} - 1 + \exp\left(\frac{4 t_p}{\Pi t_o} \right) erfc\left(\frac{4 t_p}{\Pi t_o} \right)^{1/2} \right]$$

Physically, t_o gives an order of magnitude estimate of the time required for the heat to diffuse one absorption depth ($1/\alpha$). Using the estimates of the thermal diffusivity of a-Si t_o is:

$$t_o(300K) = 5.8 ns$$

$$t_o(140K) = 3.9 ns.$$

The optical pulsewidth (FWHM) is,

$$t_p = 3.5ps$$

resulting in

$$t_p/t_o\ (300K) = 6\times10^{-4}$$

$$t_p/t_o\ (140K) = 9\times10^{-4}.$$

In the limit $t_p/t_o \ll 1$ the temperature rise reduces to

$$\Delta T = \frac{(1-R)\alpha E_o}{\rho c}$$

or using Eqn. (III-1) $k = K/\rho c$

$$\Delta T = \frac{(1-R)\alpha k E_o}{K} \qquad \text{(III-2)}$$

The use of the semi-infinite approximation for the absorption of a single picosecond optical pulse is justified by the fact that $t_p/t_o \ll 1$.

The room temperature sampling oscilloscope measurement (Section 3.3.1) was performed with the following parameters:

$$P_{avg} = 21\ mW$$

$$P_p = 73\ W$$

$$\epsilon_p = 0.26\ nJ$$

$$E_o = 52\mu J/cm^2$$

The temperature dependence of the mobility was performed in the electronic cross-correlation mode (Section 3.3.2) with the following parameters:

$$P_{avg} = 1\ mW$$

$$P_p = 3.5W$$

$$\epsilon_p = 12pJ$$

$$E_o = 2.5\mu J/cm^2$$

The incident power was reduced in the low temperature measurement because of the

observed super-linear dependence (Fig. 4.4-7) of the integrated photocurrent on photon flux (at T=155K) for average powers of 4mW. Substitution of the appropriate parameters into Eqn. (III-2) yields

$$\Delta T\ (300K) = 0.98\ K$$

$$\Delta T\ (140K) = 0.081\ K$$

Thus a single picosecond optical pulse results in negligible heating.

We will now consider the more relevant case of a quasi-continuous source of picosecond optical pulses. Let us consider the role of the a-Si film relative to the a-SiO_2 substrate.

$$1/\alpha = 0.2\mu m$$

$$d = 0.9\mu m$$

All of the transmitted radiation is absorbed in the a-Si film. We can use the Fourier law for linear heat flow to estimate the contribution of the a-Si film in the dissipation of heat:

$$\frac{dQ}{dt} = -KA\frac{dT}{dZ}$$

where dQ/dt is the time rate of heat transfer across the area A and dT/dZ is the temperature gradient. This can be approximated by

$$\frac{dQ}{dt} = KA\frac{T_2-T_1}{d} \qquad \text{(III-3)}$$

where T_2 and T_1 are the temperatures of the outer surfaces of the a-Si film and d is the film thickness. The illuminated area is

$$A = 5\times10^{-6}cm^2\ .$$

The rate of heat transfer can be approximated by

$$\frac{dQ}{dt} = (1-R)(1-e^{-\alpha d})\, P_{avg}$$

but

$$(1-e^{-\alpha d}) \sim 1$$

therefore,

$$\frac{dQ}{dt} = (1-R)P_{avg} \ .$$

The temperature differential between the two surfaces of the film is given by:

$$(T_2-T_1) = \frac{(1-R)P_{avg}\ d}{KA} \qquad \text{(III-4)}$$

The temperature differentials for the two cases of interest are:

$$(T=300K) : (T_2-T_1) = 0.077\ K/mW$$

$$(T=140K) : (T_2-T_1) = 0.09\ K/mW$$

Thus the heat is uniformly distributed throughout the illuminated volume and must be dissipated through the a-SiO_2 substrate. The radiation is absorbed in the a-Si film but the heat is deposited in an infinitesimal layer at the a-SiO_2 surface. In steady state, to a first approximation, the thin a-Si film can be ignored since it merely serves as a means of transferring the heat to the a-SiO_2 substrate. The substrate has a thickness, d', of 254μm (10mil).

The temperature rise induced, in a semi-infinite solid, by a laser beam with a Gaussian intensity distribution ($I_o \exp(-r^2/\omega^2)$) of beam waist ω and average power P_{avg} is given by M. Lax (1977, 1978). The temperature rise can be written as a product of two terms

$$\Delta T = \Delta T_{max}\, N(R,Z,W)$$

where $R = r/\omega$, $Z = z/\omega$, and $W = \alpha\omega$. ΔT_{max} describes the maximum temperature rise at the beam center ($R=O$) and the surface ($Z=O$) when the beam attenuation is

so great ($W \rightarrow \infty$) that the heat is all generated in a surface layer. For a Gaussian intensity profile this can be expressed as

$$\Delta T_{max} = \frac{P_{avg}}{2\Pi^{1/2} K \omega}$$

Correcting for the reflectivity this expression becomes

$$\Delta T_{max} = \frac{(1-R)P_{avg}}{2\Pi^{1/2} K \omega} \qquad \text{(III-5)}$$

The term $N(R,Z,W)$ accounts for a reduction in the maximum temperature rise due to reduction in the intensity as a function of the radial distance from beam center, depth of penetration beneath the surface, and finite absorption constant. For convenience we will restate the thermal parameters of a-SiO_2:

$$a\text{-}SiO_2$$

$$K\ (300K) = 0.014\ W/cmK$$

$$K\ (140K) = 0.009\ W/cmK$$

$$k\ (300K) = 0.0085\ cm^2/s$$

$$k\ (140K) = 0.011\ cm^2/s$$

For a beam waist of $\omega = 12\mu m$, Eqn. (III-5) yields

$$\Delta T_{max}\ (300K) = 10\ K/mW$$

$$\Delta T_{max}\ (140K) = 16\ K/mW$$

for the temperature rise at beam center ($R=O$) on the surface ($Z=O$). We will check the validity of the semi-infinite approximation by determining the temperature rise at the back surface of the substrate ($z=d'$) and one beam waist from beam center ($r=\omega$). If the semi-infinite approximation is valid the temperature rise should approach zero:

$$\Delta T_{max}\ N(\omega/\omega, d'/\omega, \infty) \rightarrow O$$

For a Gaussian intensity profile in the limit $R \gg 1/W$

$$N(R,Z,W) = \frac{1}{\Pi^{1/2}} \frac{1}{(R^2+Z^2)^{1/2}} \qquad \text{(III-6)}$$

Substituting ω=12μm and $d' = 254\mu m$ into Eqn. (III-6) yields

$$N(1,21.2,\infty) = 0.027$$

resulting in

$$(T=300K) : \Delta T(1,21.2,\infty) = 0.27\ K/mW$$

$$(T=140K) : \Delta T(1,21.2,\infty) = 0.43\ K/mW$$

The temperature differential between the front and back surfaces is considerable indicating some reasonable validity in utilizing the semi-infinite approximation here. On the other hand these small but finite values indicate a finite rate of heat transfer to the back surface which then diffuses into the copper cold-finger. (All of the heat must eventually go into the copper cold-finger.) This approximation doesn't take into account convection of heat through the air (zero in cryostat vacuum) or of probably major consequence radial diffusion into the aluminum electrodes. The relatively high thermal conductivity and thermal diffusivity of aluminum can provide a path of low thermal resistance (Touloukian, et al., 1970c; 1973):

Aluminum

$$K(300K) = 2.37\ W/cmK$$

$$K(140K) = 2.5\ W/cmK$$

$$k(300K) = 0.97\ cm^2/s$$

$$k(140K) = 1.4\ cm^2/s$$

Another means of obtaining an estimate of the laser-induced temperature rise in a-Si is through an observed bolometric effect in EV a-Si. Evaporated a-Si films have much higher conductivities than glow-discharge samples deposited at the same temperature. Due to the large density of states in the gap of evaporated a-Si electrical transport normally occurs by variable range hopping (Section 2.2) at the Fermi level as evidenced by an (approximately) $T^{-1/4}$ dependence of the logarithm of the dark conductivity

(Mott and Davis, 1979). Figure (III-1) is the temperature dependence of the dark conductivity of an evaporated sample deposited at room temperature. For a 70V bias the dark current was:

$$i_d = 52\mu A$$

When this sample is connected to the 50-Ω sampling oscilloscope (Section 3.3.1) and irradiated with the dye laser ($P_{avg} = 21mW$) two electrical responses are observed. The first is the scope-limited transient photoresponse of EV. The second response is a constant dc level background shift of ~ 1 mV -- this is what we refer to as a bolometric effect. This light activated dc level shift corresponds to a current of

$$i_\ell = 20\mu \text{A} \ .$$

We will assume that the electronic contribution of the light is confined to the transient photoresponse and that the dc level shift is due to light induced heating. Given this assumption the total dc component of the photoresponse can be used to determine the light induced temperature rise of the sample. The advantage of this approach is that it already takes into account all the possible thermal conducting paths. The total bolometric current is given by

$$i_b = i_d + i_\ell$$

For an average power of 21mW at T=292K

$$i_b = 72\mu A$$

Figure (III-1) indicates three possible extrapolations of the conductivity data. The straight line corresponds to the $T^{-1/4}$ dependence expected for variable range hopping. We believe that these three curves correspond to the largest spread in temperature at this value of the current. The straight line extrapolation yields a sample temperature of 296K or ΔT=4K (R.T.=292K). The central curve resulted in a temperature of 312K (ΔT=20K). The curve on the extreme left yields a maximum temperature of 323K

(ΔT=31K). The bolometric effect tends to indicate that the laser-induced heating is minor and is consistent with the room temperature linear variation of peak photocurrent versus photon flux (Fig. (4.4-3)) and integrated photocurrent versus photon flux (Fig. (4.4-4)). This measurement also seems to indicate the importance of the contacts in dissipating heat.

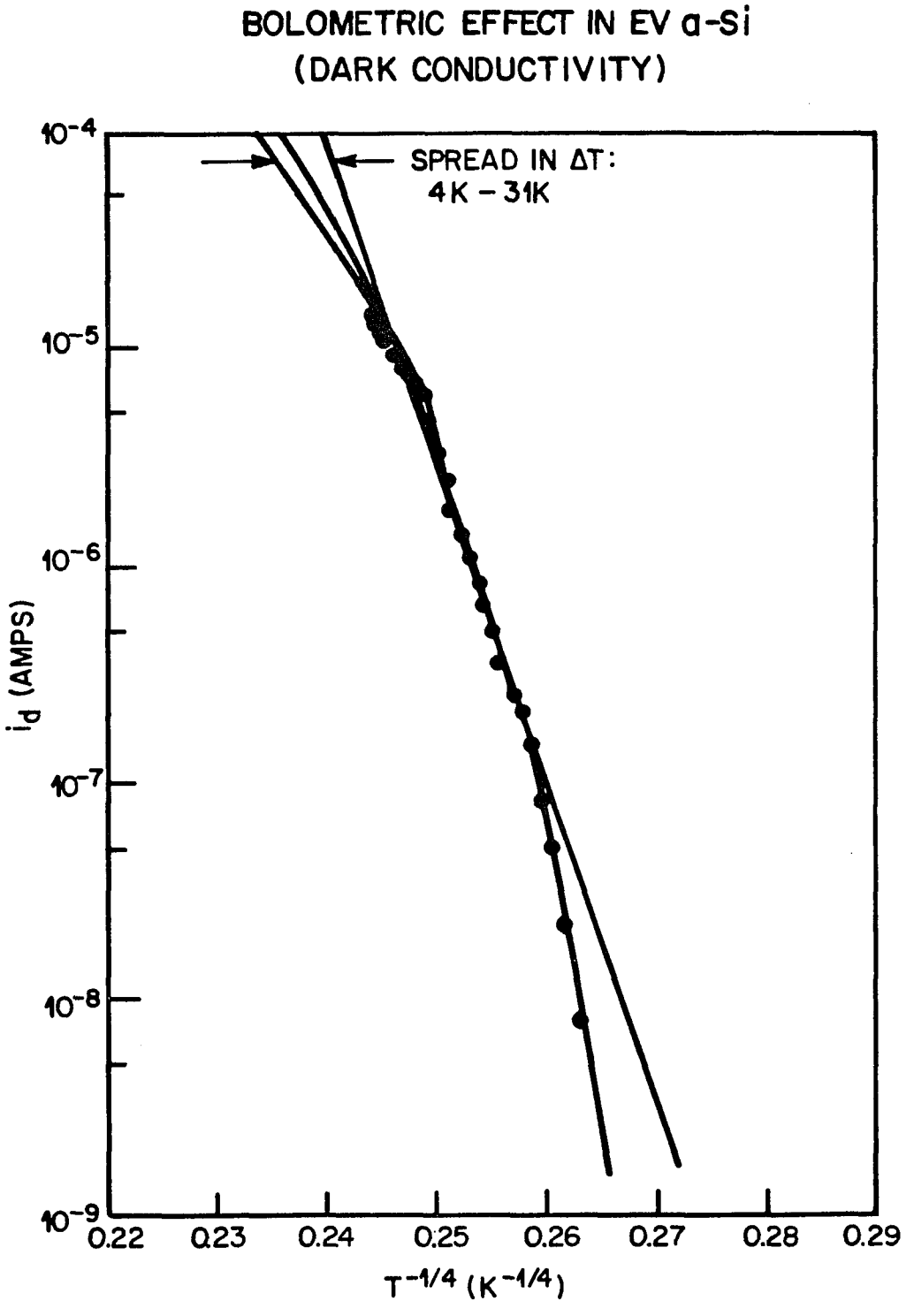
BOLOMETRIC EFFECT IN EV a-Si
(DARK CONDUCTIVITY)
SPREAD IN ΔT:
4K - 31K
10^{-4}
10^{-5}
10^{-6}
10^{-7}
10^{-8}
10^{-9}
i_d (AMPS)
0.22
0.23
0.24
0.25
0.26
0.27
0.28
0.29
$T^{-1/4}$ ($K^{-1/4}$)

Fig. (III-1)

REFERENCES

Adler, D. (1980): *J. Non-Cryst. Solids* **42**, 315.

Albany, H. J. and Vanderyver, M. (1967): *J. Appl. Phys.* **38**, 425.

Allan, D. (1978): *Phil. Mag.* **38**, 381.

Anderson, P. W. (1958): *Phys. Rev.* **109**, 1492.

Ausschnitt, C. P., Jain, R. K., and Heritage, J. P. (1979): *IEEE J. Quantum Electron* **QE-15**, 912.

Auston, D. H. (1975): *Appl. Phys. Lett.* **26**, 101.

Auston, D. H., Lavallard, P., Sol, N., and Kaplan, D. (1980a): *Appl. Phys. Lett.* **36**, 66.

Auston, D. H., Johnson, A. M., Smith, P. R., and Bean, J. C. (1980b): *Appl. Phys. Lett.* **37**, 371.

Auston, D. H., Smith, P. R., Johnson, A. M., Augustyniak, W. M., Bean, J. C., and Fraser, D. B. (1980c): *Picosecond Phenomena II*, ed. by R. M. Hochstrasser, W. Kaiser, and C. V. Shank (Springer-Verlag, Berlin), p. 71.

Auston, D. H., Johnson, A. M., Smith, P. R., Augustyniak, W. M., Bean, J. C., Harbison, J. P., and Kaplan, D. (1980d): *Digest of the XI International Quantum Electronics Conference* (Boston, June), p. 605.

Auston, D. H. (1981): to be published.

Barna, A., Barna, P. B., Radnoczi, G., Toth, L., and Thomas, P. (1977), *Phys. Stat. Sol. (A)* **41**, 81.

Bartoli, F., Kruer, M., Esterowitz, L., and Allen, R. (1973): *J. Appl. Phys.* **44**, 3713.

Bean, J. C. and Poate, J. M. (1980a): *Appl. Phys. Lett.* **36**, 59.

Bean, J. C. (1980b): *Appl. Phys. Lett.* **36**, 741.

Bean, J. C. (1981): (to be published) Growth of Doped Silicon Layers by Molecular Beam Epitaxy. In *Impurity Doping Processes in Silicon*, ed. by F. F. Y. Wang (North Holland).

Bloom, A. L. (1974): *J. Opt. Soc. Amer.* **64**, 447.

Brenig, W. (1974): *Proceedings of the Fifth International Conference on Amorphous and Liquid Semiconductors, Garmisch-Partenkirchen, FDR, 1973*, ed. by J. Stuke and W. Brenig (Taylor and Francis, London), p. 31.

Brodsky, M. H. and Title, R. S. (1969): *Phys. Rev. Lett.* **23**, 581.

Brodsky, M. H. (1979): Introduction. In *Amorphous Semiconductors, Topics in Applied Physics* **36**, ed. by M. H. Brodsky (Springer-Verlag, New York).

Bube, R. H. (1978): *Photoconductivity of Solids* (Robert E. Krieger Publishing Co., N.Y.).

Carlson, D. E. (1977): *IEEE Trans. Electron Devices* **24**, 449.

Carlson, D. E. (1980): Amorphous Thin-Film Devices. In *Polycrystalline and Amorphous Thin Films and Devices*, ed. by L. L. Kazmerski (Academic Press, N.Y.).

Chan, C. K. and Sari, S. O. (1974): *Appl. Phys. Lett.* **25**, 403.

Cohen, M. H., Fritzsche, H. and Ovshinsky, S. R. (1969): *Phys. Rev. Lett.* **22**, 1065.

Cohen, M. H. (1970): *J. Non-Cryst. Solids* **4**, 391.

Connell, G. A. N. (1979): Optical Properties of Amorphous Semiconductors. In *Amorphous Semiconductors, Topics in Applied Physics* **36**, ed. by M. H. Brodsky (Springer-Verlag, N.Y.).

D'Antonio, P. and Konnert, J. H. (1979): *Phys. Rev. Lett.* **43**, 1161.

Davis, E. A. and Shaw, R. F. (1970): *J. Non-Cryst. Solids* **2**, 406.

Davis, E. E. (1979): States in the Gap and Defects in Amorphous Semiconductors. In *Amorphous Semiconductors, Topics in Applied Physics* **36**, ed. by M. H. Brodsky (Springer-Verlag, N.Y.).

Economou, E. N., Cohen, H. H., Freed, K. F., and Kirkpatrick, E. S. (1974): Electronic Structure of Disordered Materials. In *Amorphous and Liquid Semiconductors*, ed. by J. Tauc (Plenum Press, London).

Emin, D. (1973): Aspects of the Theory of Small-Polarons in Disordered Materials. In *Electronic and Structural Properties of Amorphous Semiconductors*, ed. by P. G. LeComber and J. Mort (Academic Press, London).

Emin, D. (1976): Localized States in Semiconducting Noncrystalline Solids. In *Physics of Structurally Disordered Solids*, ed. by S. S. Mitra (Plenum Press, N.Y.).

Emin, D. (1980a): Electrical and Optical Properties of Amorphous Thin Films. In *Polycrystalline and Amorphous Thin Films and Devices*, ed. by L. L. Kazmerski (Academic Press, N.Y.).

Emin, D. (1980b): *J. Non-Cryst. Solids* **35-36**, 969.

Engemann, D., and Fischer, R. (1976): *Structure and Excitations in Amorphous Solids*, ed. by G. Lucovsky and F. L. Galeener (A.I.P. No. 31, N.Y.) p. 37.

Engemann, D., Fischer, R., and Mell, H. (1977): *Proceedings of the Seventh International Conference on Amorphous and Liquid Semiconductors*, ed. by W. Spear University of Edinburgh, Edinburgh), p. 387.

Friedman, L. (1971): *J. Non-Cryst. Solids* **6**, 329.

Frigo, N. J., Daly, T., and Mahr, H. (1977): *IEEE J. Quantum Electron.* **QE-13**, 101.

Fritzsche, H. (1971): *J. Non-Cryst. Solids* **6**, 49.

Fritzsche, H. (1974): Electronic Properties of Amorphous Semiconductors. In *Amorphous and Liquid Semiconductors*, ed. by J. Tauc (Plenum Press, London).

Fritzsche, H. and Tsai, C. C. (1979): *Solar Energy Mater.* **1**, 471.

Fröhlich, H. (1947): *Proc. R. Soc. A* **188**, 521.

Fuhs, W., Milleville, M., and Stuke, J. (1978): *Phys. Stat. Sol. (B)* **89**, 495.

Grigorovici, R. (1974): Structure of Amorphous Semiconductors. In *Amorphous and Liquid Semiconductors*, ed. by J. Tauc (Plenum Press, London).

Gunston, M. A. R. (1972): *Microwave Transmission Line Impedance Data* (Van Nostrand Reinbold Co., London).

Hargrove, L. E., Fork, R. L., Pollack, M. A. (1964): *Appl. Phys. Lett.* **5**, 4.

Harris, J. M., Chrisman, R. W., and Lytle, F. E. (1975): *Appl. Phys. Lett.* **26**, 16.

Hayama, H., and Matsumura, M. (1980): *Appl. Phys. Lett.* **36**, 754.

Heritage, J. P., and Jain, R. K. (1978): *Appl. Phys. Lett.* **32**, 101.

Hindley, N. K. (1970): *J. Non-Cryst. Solids* **5**, 17.

Hirose, M., Taniguchi, M., and Osaka, Y. (1977): *Proceedings of the Seventh International Conference on Amorphous and Liquid Semiconductors*, ed. by W. Spear (University of Edinburgh, Edinburgh), p. 352.

Hitchman, M. L., Kane, J., and Widmer, A. E. (1979): *Thin Solid Films* **59**, 231.

Hughes, R. C. and Emin, D. (1978): *The Physics of SiO_2 and its Interfaces*, ed. by S. Pantelides (Pergamon Press, Oxford), p. 14.

Hvam, J. M. and Brodsky, M. H. (1981): *Phys. Rev. Lett.* **46**, 371.

Ioffe, A. F. and Regel, A. R. (1960): *Prog. Semicond.* **4**, 237.

Ippen, E. P., and Shank, C. V. (1975): *Appl. Phys. Lett.* **27**, 488.

Ippen, E. P. and Shank, C. V. (1977): Techniques for Measurement. In *Ultrashort Light Pulses, Topics in Applied Physics* **18**, ed. by S. L. Shapiro (Springer-Verlag, N.Y.).

Johnson, A. M., and Auston, D. H. (1975): *IEEE J. Quantum Electron.* **QE-11**, 283.

Johnson, A. M., Auston, D. H., Harbison, J. P., Bean, J. C., Kaplan, D., and Smith, P. R. (1980a): *Bull. Am. Phys. Soc.* **25**, 384.

Johnson, A. M., Auston, D. H., Smith, P. R., Bean, J. C., Harbison, J. P., and Kaplan, D. (1980b): *Picosecond Phenomena II*, ed. by R. M. Hochstrasser, W. Kaiser, and C. V. Shank (Springer-Verlag, Berlin), p. 285.

Johnson, A. M., Auston, D. H., Smith, P. R., and Harbison, J. P. (1981a): *Bull. Am. Phys. Soc.* **26**, 454.

Johnson, A. M., Auston, D. H., Smith, P. R., Bean, J. C., Harbison, J. P., and Adams, A. C. (1981b): *Phys. Rev. B* **23**, 6816.

Johnson, A. M., Auston, D. H., Smith, P. R., Bean, J. C., Harbison, J. P., and Adams, A. C. (1981c): *Tetrahedrally Bonded Amorphous Semiconductors*, ed. by R. A. Street, D. K. Biegelsen, and J. C. Knights (A.I.P. No. 73, N.Y.), p. 248.

Kogelnik, H. W., Ippen, E. P., Dienes, A., and Shank, C. V. (1972): *IEEE J. Quantum Electron,* **QE-8**, 373.

Knights, J. C. (1976): *Structure and Excitations in Amorphous Solids*, ed. by G. Lucovsky and f. L. Galeener (A.I.P. No. 31, N.Y.), p. 296.

Knights, J. C. (1980): *J. Non-Cryst. Solids* **35-36**, 159.

Lax, M. (1959): *J. Phys. Chem. Solids* **8**, 66.

Lax, M. (1960): *Phys. Rev.* **119**, 1502.

Lax, M. (1977): *J. Appl. Phys.* **48**, 3919.

Lax, M. (1978): *Appl. Phys. Lett.* **33**, 786.

Leadbetter, A. J., Rashid, A. A. M., Richardson, R. M., Wright, A. F., and Knights, J. C. (1980): *Solid State Commun.* **33**, 973

LeComber, P. G. and Spear, W. E. (1970): *Phys. Rev. Lett.* **25**, 509.

LeComber, P. G., Madan, A., and Spear, W. E. (1972): *J. Non-Cryst. Solids* **11**, 219.

LeComber, P. G. (1979): *Sci. Prog. (Oxf.)* **66**, 105.

Lewis, A. J., Connell, G. A. N., Paul, W., Pawlik, J. R., and Temkin, R. J. (1974): *Tetrahedrally Bonded Amorphous Semiconductors*, ed. by M. H. Brodsky, S. Kirkpatrick, and D. Weaire (A.I.P. No. 20, N.Y.), p. 27.

Loveland, R. J., Spear, W. E., and A. Al-Sharbaty (1973): *J. Non-Cryst. Solids* **13**, 55.

Lucovsky, G., and Hayes, T. M. (1979): Short-Range Order in Amorphous Semiconductors. In *Amorphous Semiconductors, Topics in Applied Physics*, **36**, ed. by M. H. Brodsky (Springer-Verlag, N.Y.).

Madelung, O. (1978): *Introduction to Solid-State Theory* (Springer-Verlag, Berlin).

Maeda, M. (1972): *IEEE Trans. Microwave Theory Tech.* **MTT-20**, 390.

Maier, M., Kaiser, W., and Giordmaine, J. A. (1966): *Phys. Rev. Lett.* **77**, 1275.

Malley, M. M. and Mourou, G. (1974): *Opt. Commun.* **10**, 323.

Miller, A. and Abrahams, E. (1960): *Phys. Rev.* **120**, 745.

Moore, A. R. (1977): *Appl. Phys. Lett.* **31**, 762.

Mort, J., Troup, A., Morgan, M., Grammatica, S., Knights, J. C., and Lujan, R. (1981): *Appl. Phys. Lett.* **38**, 277.

Moss, S. C. and Graczyk, J. F. (1970): *Proc. Tenth Intern. Conf. Phys. Semicond.* (U.S.A. E.C., Washington) p. 658.

Mott, N. F. (1967): *Adv. Phys.* **16**, 49.

Mott, N. F. (1969): *Phil. Mag.* **19**, 835.

Mott, N. F. (1970): *Phil. Mag.* **22**, 7.

Mott, N. F. and Davis, E. A. (1979): *Electronic Processes Non-Crystalline Materials*, 2nd Ed. (Oxford University Press, Oxford).

Moustakas, T. D. (1979): *J. Elect. Mat.* **8**, 391.

Nagels, P. (1979): Electronic Transport. In *Amorphous Semiconductors, Topics in Applied Physics*, **36**, ed. by M. H. Brodsky (Springer-Verlag, N.Y.).

Noolandi, J. (1977): *Phys. Rev. B* **16**, 4474.

Orenstein, J. and Kastner, M. (1979): *Phys. Rev. Lett.* **43**, 161.

Orenstein, J. and Kastner, M. (1981): *Phys. Rev. Lett.* **46**, 1421.

Pfister, G. (1977): *Phil. Mag.* **36**, 1147.

Pfister, G. and Scher, H. (1977): *Phys. Rev. B* **15**, 2062.

Pfister, G. and Scher, H. (1978): *Adv. Phys.* **27**, 747.

Phillips, J. C. (1979): *Phys. Rev. Lett.* **42**, 1151.

Phillips, J. C. (1980): *J. Non-Cryst. Solids* **35-36**, 1157.

Polk, D. E. (1971): *J. Non-Cryst. Solids* **5**, 365.

Postol, T. A., Falco, C. M., Kampwirth, Schuller, I. K., and Yelon, W. B. (1980): *Phys. Rev. Lett.* **45**, 648.

Rahmat-Samii, V., Itoh, T., and Mittra, R. (1974): *IEEE Trans. Microwave Theory Tech.* **MTT-20**, 372.

Redfield, D. (1971): *Phys. Rev. Lett.* **27**, 730.

Redfield, D. (1972): *J. Non-Cryst. Solids* **8-10**, 602.

Rhoderick, E. H. (1978): *Metal-Semiconductor Contacts* (Clarendon Press, Oxford).

Rose, A. (1951): *RCA Rev.* **12**, 362.

Saad, T. S. (1971): *Microwave Engineers Handbook*, Vol. 1 (Bedham, Mass.).

Sakurai, T. and Hagstrum, H. D. (1975): *Phys. Rev. B* **12**, 5349.

Scher, H. and Lax, M. (1973): *Phys. Rev. B* **7**, 4491.

Scher, H. and Montroll, E. W. (1975): *Phys. Rev. B* **12**, 2455.

Schmidlin, F. W. (1977a): *Solid-State Commun.* **22**, 451.

Schmidlin, F. W. (1977b): *Phys. Rev. B* **16**, 2362.

Schneider, M. V. (1969): *Bell Syst. Tech. J.* **48**, 1421.

Shank, C. V. (1975): *Rev. Mod. Phys.* **47**, 649.

Shimizu, I., Komatsu, T., Saito, K., and Inoue, E. (1980): *J. Non-Cryst. Solids* **35-36**, 773.

Shockley, W. (1938): *J. Appl. Phys.* **9**, 635.

Silver, M. and Cohen, L. (1977): *Phys. Rev. B* **15**, 3276.

Smith, P. R., Auston, D. H., Johnson, A. M., and Augustyniak, W. M. (1981a): *Appl. Phys. Lett.* **38**, 47.

Smith, P. R., Auston, D. H., and Johnson, A. M. (1981b): *Rev. Sci. Instrum.* **52**, 138.

Smith, R. A. (1978): *Semiconductors* 2nd Ed. (Cambridge University Press, Cambridge).

Smith, R. W. and Rose A. (1955): *Phys. Rev.* **97**, 1531.

Sol, N. Kaplan, D., Dieumegard, D., and Dubreuil, D. (1980): *J. Non-Cryst. Solids* **35-36**, 291.

Solomon, I. (1979): Spin Effects in Amorphous Semiconductors. In *Amorphous Semiconductors, Topics in Applied Physics,* **36**, ed. by M. H. Brodsky (Springer-Verlag, N.Y.).

Spear, W. E., Loveland, R. J., and Al-Sharbaty, A. (1974): *J. Non-Cryst. Solids* **15**, 410.

Spear, W. E. and LeComber, P. G. (1975): *Solid-State Commun.* **17**, 1193.

Spear, W. E., LeComber, P. G., Kinmond, S., and Brodsky, M. H. (1976a): *Appl. Phys. Lett.* **28**, 105.

Spear, W. E. and LeComber, P. G. (1976b): Amorphous Tetrahedrally Bonded Solids. In *Photoconductivity and Related Phenomena*, ed. by J. Mort and D. M. Pai (Elsevier, Amsterdam).

Theye, M. L. (1976): Optical Properties of Tetrahedrally Bonded Amorphous Semiconductors: Absorption Spectra and Absorption Edge. In *Physics of Structurally Disordered Solids*, ed. by S. S. Mitra (Plenum Press, N.Y.).

Tiedje, T., Abeles, B., Morel, D. L., Moustakas, T. D., Wronski, C. R. (1980): *Appl. Phys. Lett.* **36**, 695.

Tiedje, T. and Rose, A. (1980): *Solid-State Commun.* **37**, 49.

Tiedje, T., Cebulka, J. M., Morel, D. L., and Abeles, B. (1981): *Phys. Rev. Lett.* **46**, 1425.

Touloukian, Y. S., Powell, R. W., Ho, C. Y., and Klemens, P. G. (1970a): *Thermal Conductivity, Nonmetallic Solids* (Plenum, N.Y.).

Touloukian, Y. S. and Buyco, E. H. (1970b): *Specific Heat, Nonmetallic Solids* (Plenum, N.Y.).

Touloukian, Y. S., Powell, R. W., Ho, C. Y., and Klemens, P. G. (1970c): *Thermal*

Conductivity, Metallic Elements and Alloys (Plenum, N.Y.)

Touloukian, Y. S., Powell, R. W., Ho, C. Y., and Nicolaou, M. C. (1973): *Thermal Diffusivity* (Plenum, N.Y.).

Tsu, R., Izu, M., Ovshinsky, S. R., and Pollak, F. H. (1980): *Solid State Commun.* **36**, 817.

Vardeny, Z. and Tauc, J. (1981): *Phys. Rev. Lett.* **46**, 1223.

Weiser, G., Ewald, D., and Milleville, M. (1980): *J. Non-Cryst. Solids* **35-36**, 447.

Wronski, C. R., Carlson, D. E., and Daniel, R. E. (1976): *Appl. Phys. Lett.* **29**, 602.

Yonezawa, F. and Cohen, M. H. (1981): Theory of Electronic Properties of Amorphous Semiconductors. In Fundamental Physics of Amorphous Semiconductors, ed. by F. Yonezawa (Springer Verlag, Berlin, 1981).